ELECTROCHEMICAL ENZYMATIC BIOSENSING OF NEOTAME IN SWEETENERS BY EXPERIMENTAL AND COMPUTATIONAL METHODS

By

Matshidiso Lephalala

(Reg No: 21533647)

Submitted in fulfilment of the requirements of the degree of Master of Applied

Science in Chemistry in the Faculty of Applied Sciences at the Durban

University of Technology

September 2020

DECLARATION

I **Matshidiso Lephalala** hereby declare that the thesis submitted for the degree of Master of Applied Science (M.App.Sci.): Chemistry at the Durban University of Technology is the result of my investigation and has not already been accepted in substance for any degree and is not being concurrently submitted for any other degree. All the work was done by the Author.

Student Name: Ms. Matshidiso Lephalala

Signature: Date:

Supervisor Name: Prof Krishna Bisetty

Signature Date:

Co-Supervisor Name: Dr. Suvardhan Kanchi

Signature: Date:

Co-Supervisor Name: Dr Myalowenkosi I Sabela

Signature Date:

DEDICATION

"Gratitude makes sense of your past, brings peace for today, and creates a vision for tomorrow"- Melody Beattie.

I dedicate this thesis to my parents (**John and Kate Lephalala**), I have made a promise to myself that one day I would be one of the reasons you kneel to God to thank him for his Grace upon your lives because of the person that I chose to become and the dreams I chose to follow. You have given me love and taught me respect not forgetting to remain humble. Thank you for everything- I love you.

ACKNOWLEDGEMENTS

This study became a success with the support and help of many individuals hence I would like to extend my gratitude to each of them according to their contribution.

Firstly, I would like to thank **God** almighty for the wisdom and the strength that he granted me for me to complete this research, for it says in his word “Rejoice always, pray continually, give thanks in all circumstances; for this is God’s will for you in Christ Jesus”- 1 Thessalonians 5: 16-18/ NIV.

I extend my gratitude and appreciation to my supervisor, **Prof Krishna Bisetty** for his guidance, advice (theoretically and practically), multiple revisions, motivation, and encouragement throughout the work. I am thankful to have him as my academic advisor. I would also like to show my sincere gratitude and appreciation to my co-supervisors **Dr. Suvardhan Kanchi** and **Dr. Myalowenkosi Sabela** for their assistance and patience during difficult times throughout the research. Mrs. Mavis Xhakaza also played a very important role throughout the whole journey hence also extend my appreciation to her.

I would like to extend my gratitude to my family especially my parents, John and Kate Lephalala for their encouragement and support to complete this research, to my siblings, Semakaleng and Amogelang Lephalala who are always by my side whenever I need support.

Many thanks go to Sbusiso Robert Junior Sithole, Tumelo Lephalala, Boikgantšo Lehlohonolo Lephalala, Mpho Zwane, and lastly my late grandmother Agnes Ramatsimela Sebake (May her soul rest in perfect peace). Not forgetting my friends

Senzekile Majola, Nomnotho Jiyane, Phathisanani Hloma, Lyndon Naidoo, Kwanele Kunene, and Ayanda Shabangu for their advice.

I would like to acknowledge the financial support of the **National Research Foundation (NRF)**.

ABSTRACT

An enzymatic biosensor comprises of an enzyme, which recognizes and then reacts with the target analyte producing a chemical signal. In this type of sensor, an electrode is a key component that is employed as a solid support for the immobilization of biomolecules and electron movement. This work focuses on two case studies to assess the signal enhancing strategy that can potentially be used to quantify Neotame (NTM) in food and non-alcoholic beverages.

The first case study involves a highly sensitive electrochemical enzymatic biosensor for the detection of NTM in the soft drinks developed, based on multiwalled carbon nanotubes (MWCNTs) decorated with *aloe vera*-derived gold nanoparticles (AuNPs) and carboxylesterase (CaE) enzyme. This electrochemical biosensor showed high sensitivity with a limit of detection (LOD) and limit of quantification (LOQ) of 27 μg L^{-1} and 83 μg L^{-1}, respectively. The calibration plot revealed a linear dependence of the cathodic peak current on the NTM concentration profile with an R^2 of 0.9829, indicating an improved electrocatalytic property of the glassy carbon electrode. The viability of the proposed strategy was confirmed by assessing the interactions between the enzyme and the analyte using computational methods. The density functional theory (DFT) calculations of NTM showed a HOMO–LUMO energy gap of -0.46618 eV, indicating that NTM can act as a good electron donor. Moreover, adsorption and enzyme-analyte docking studies were carried out to better understand the redox mechanism. These outcomes showed that NTM formed hydrogen bonds with LEU 249, GLU251, and other amino acids of the hydrophobic channel of the binding sites, making it easier for the redox reaction to take place for the detection of NTM. The

results confirmed that the *aloe vera*-derived AuNPs are good platforms for immobilizing CaE because of their high surface area, encouraging an electron transfer from NTM to form a substrate-enzyme complex, contributing to improved biosensing signals.

The second case study deals with an enzymatic biosensor developed, based on graphene oxide (GO) anchored with honey-derived nickel nanoparticles (NiNPs) and alcohol oxidase (AOx) enzyme. The biosensor showed high sensitivity with a limit of quantification (LOQ) of 47 µg L^{-1} and a limit of detection (LOD) of 15 µg L^{-1}, respectively. The calibration curve of the cathodic peak current on the analyte concentration profile showed an improved electrocatalytic property with an R^2 of 0.9926. The interactions between the enzyme and analyte were assessed using computational tools to confirm the viability of the proposed biosensor. A HOMO–LUMO energy gap of -0.46618 eV was confirmed using density functional theory (DFT) calculations, this suggested that NTM has great potential to act as an electron donor. Analyte-enzyme and adsorption docking studies were carried out for a better comprehension of the redox reaction mechanisms. These outcomes indicated that NTM forms hydrogen bonds with TRP 47, ARG 56, VAL 328, PRO 55, and other amino acids, thus assisting the redox reaction for the determination of NTM. The results confirmed that the *honey*-derived NiNPs have a high surface area, which acted as a good platform to immobilize AOx so that the electrons can be transferred from NTM to form a substrate-enzyme composite to give out an improved biosensing signal. Moreover, the magnified catalytic activity of these two biosensors for the determination of NTM in soft drinks showed great potential in the beverage industry.

TABLE OF CONTENTS

Table of Contents

Table of contents

Table of contents

Table of contents

Table of contents

LIST OF TABLES

LIST OF FIGURES

List of Figures

List of Figures

List of Figures

List of Figures

LIST OF SCHEMES

DEFINITIONS

Sweeteners: a substance used to sweeten food or drinks, especially one other than sugar.

NTM: is a non-caloric artificial sweetener.

Voltammetry: is a category of electroanalytical methods in which information about the analyte is obtained measuring the current and as the potential is varied.

Biosensor: a device that uses a living organism or biological molecules especially enzymes or antibodies to detect the presence of chemicals.

Enzymes: a substance produced by a living organism that acts as a catalyst to bring about a specific biochemical reaction.

Carboxylesterase: is an enzyme that catalyzes a chemical reaction of the form carboxylic ester + H_2O → alcohol + a carboxylate.

Alcohol oxidase: is an enzyme that catalyzes a chemical reaction primary alcohol + O_2 → an aldehyde + H_2O_2.

Nanotechnology: the branch of technology that deals with dimensions and tolerances of less than 100 nanometres especially the manipulation of individual atoms and molecules.

Nanoparticle: A nanoparticle or ultrafine particle is usually defined as a particle of matter that is between 1 and 100 nanometres (nm) in diameter.

The term is sometimes used for larger particles, up to 500 nm, or fibers and tubes that are less than 100 nm in only two directions.

Pre-concentration: Pre-concentration is the procedure used to obtain a high local protein concentration at the sensor chip surface. Pre-concentration makes the immobilization of the protein to the sensor chip surface more efficient.

ACRONYMS AND SYMBOLS

AL	Adsorption Locator
AOx	Alcohol Oxidase
AuNPs	Gold Nanoparticles
CaE	Carboxylesterase
CHARMm	Chemistry at Harvard Macromolecular Mechanics
COMPASS	Condensed-Phase Optimized Molecular Potentials for Atomistic Simulation Studies.
CV	Cyclic Voltammetry
DFT	Density Functional Theory
DLS	Dynamic Light Scattering
DMF	Dimethyformamide
DPV	Differential Pulse Voltammetry
FFF	Field Flow Fractionation
FTIR	Fourier Transform Infrared
GCE	Glassy Carbon Electrode
GO	Graphene Oxide
HOMO	Highest Occupied Molecular Orbital

Acronyms and symbols

LOD	Limit of Detection
LOQ	Limit of Quantification
LUMO	Lowest Unoccupied Molecular Orbital
MD	Molecular Docking
MDS	Molecular Dynamic Simulations
MS	Material Studio
MWCNTs	Multiwall carbon nanotubes
NiNPs	Nickel nanoparticles
NTM	Neotame
PSB	Phosphate buffer
PSD	Particle size distribution
spICP-MS	Single-particle inductively coupled plasma mass spectrometry
TGA	Thermogravimetric analysis
TEM	Transmission electron microscopy
UV-Vis	Ultra Violet-Visible spectroscopy

RESEARCH OUTPUTS

Publications

1. Matshidiso Lephalala, Suvardhan Kanchi, Myalowenkosi I Sabela, and Krishna Bisetty. “Electrochemical enzymatic biosensing of NTM supported by computational methods”. *Electroanalysis*, 2020, 32, 1–13, https://doi.org/10.1002/elan.202060208.

Oral presentation

1. 4th interdisciplinary research and innovation conference 2019, Hilton Hotel, Durban, South Africa, 17-20 September 2019. *Electrochemical enzymatic biosensing of NTM in sweeteners using experimental and computational methods*.

CHAPTER 1: INTRODUCTION

This chapter describes sweeteners with emphasis on their regulation according to the food industry standards. This is followed by the aims, objectives, and thesis outline.

1.1. Sweeteners

Sweeteners are additives that are used to substitute sugar and to stimulate a sense of sweetness during consumption. There are two branches of sweeteners, non-nutritive and nutritive sweeteners. The difference is that nutritive sweeteners can be digested by the body and have energy value, while non-nutritive sweeteners cannot be digested by the body and do not have energy value. One of the reasons why sweeteners are suitable sugar substitutes for diabetics is because they contain little or no calories and they do not metabolize.

Sugar-free foods are very popular nowadays because they contain fewer calories. Hence the food and beverage industries use various artificial sweeteners that are low in calorie content. The United States Food and Drug Administration (Authority 2007) has approved aspartame, acesulfame-k, NTM, cyclamate, and alitame use according to the acceptable recommended daily intake value. However, the breakdown products of these sweeteners have metabolic and health effects (Chattopadhyay, Raychaudhuri and Chakraborty 2014). The amount of sweeteners in foodstuffs is limited by the specific regulations as per the country (Zygler, Wasik, and Namieśnik 2009). Consumption of sugar-sweetened beverages has been linked to health problems such as weight gain, cardiovascular diseases, metabolic syndrome, and type 2 diabetes (Swithers 2013). To mitigate the health risks, mentioned above, people have turned to high-intensity sweeteners such as stevia, sucralose, NTM, aspartame, and saccharin.

1.2. Problem statement

The stability of these sweeteners even at high temperatures has increased their applications widely in foodstuff. One of the safety concerns with artificial sweeteners is the risk of carcinoma, which was shown by animal studies (Purohit and Mishra 2018) and one study has linked aspartame consumption with the risk of leukemia and lymphoma in men (Schernhammer *et al.* 2012). The above-mentioned artificial sweeteners are known to reduce caloric intake. However, they might not have any benefit in controlling diabetes when consumed regularly. This is attributed to artificial sweeteners altering sensitivity to insulin when they are consumed daily (Purohit and Mishra 2018). Hence the widespread use of NTM in the food industry needs to be regulated. In this study, NTM will be detected by newly developed electrochemical enzymatic biosensors instead of the traditional analytical methods.

1.3.Aims and objectives

Aims

The study aims to develop two novel and selective electrochemical enzymatic biosensors for the detection of NTM in selected food beverages.

Objectives

- To synthesize gold nanoparticles (AuNPs) and nickel nanoparticles (NiNPs) using greener routes.
- To characterize AuNPs and NiNPs using Transmission Electron Microscopy (TEM), Ultraviolet-Visible Spectroscopy (UV-Vis), Single Particle Inductively

Coupled Plasma Mass Spectrometry (spICP-MS) Thermal methods (TGA; DSC).

- To determine the particle size of AuNPs and NiNPs using the Field-flow fractionation technique (FFF).
- To fabricate a glassy carbon electrode (GCE) with a nanocomposite of MWCNTs/AuNPs/CaE and GO/NiNPs/AOx.
- To perform the chemical interaction studies of NTM to AOx and CaE using molecular docking.
- To calculate adsorption energies using the adsorption locator and to perform docking studies using molecular docking.
- To optimize the experimental parameters for the development of enzymatic biosensors using cyclic voltammetry (CV).
- To quantify NTM in spiked samples by differential pulse voltammetry (DPV).
- To statistically evaluate the efficiency of the enzymatic biosensors using real samples.

This work necessitated the development of highly sensitive electrochemical enzymatic biosensors for the detection of NTM based on a wave strengthening strategy. Electrochemical quantifications using differential pulse voltammetry (DPV) and cyclic voltammetry (CV) were used to investigate and understand the redox mechanism of NTM, computational methods were used to support the experimental results.

1.4. Thesis outline

Chapter 1 provides an overview of sweeteners and their role in the food and beverage industry.

Chapter 2 focuses on the literature review discussing NTM, gold, and nickel nanoparticles specifically their applications and their properties, electrochemical detection, electrochemical enzymatic biosensors, enzymes, and nanotechnology.

Chapter 3 focuses on the basic theoretical principles underpinning the techniques that were used for experimental studies carried out. Furthermore, the equations concerning the operation of the techniques are presented. The role of computational chemistry in biosensors is highlighted. The equations and rigorous foundation of density functional theory (DFT) are included.

Chapter 4 provides the outline of the experimental and computational methodology used in this study, instrumentation, chemical, and reagents, preparation of supporting electrolyte, preparation of standards, electrode modification, computational and real sample preparation.

Chapter 5 This chapter provides experimental outcomes obtained using the CaE/AuNPs/MWCNTs modified GCE and AOx/NiNPS/GO GCE. This chapter is divided into two sections (Sensor 1 and Sensor 2). Computational work was carried out to get a better understanding of the conformational profile of the NTM-CaE enzyme and NTM-AOx enzyme. Furthermore, the interaction studies were helpful to get a better understanding of the interactions between the enzymes, nanomaterials, and NTM. HOMO-LUMO calculations were executed to assess the redox ability of NTM.

Chapter 6 outlines a summary of the conclusions and recommendations of this work.

CHAPTER 2: LITERATURE REVIEW

This chapter focuses on the literature review of NTM, gold, and nickel nanoparticles specifically their applications and their physio-chemical properties, electrochemical detection, electrochemical enzymatic biosensors, enzymes, and nanomaterials.

NTM is a derivative of the dipeptide composed of the amino acids, aspartic acid, and L-phenylalanine (N-[N-(3,3-dimethylbutyl)-L-α-aspartyl]-L-phenylalanine-1-methyl ester). The constituents of NTM are joined to form a uniquely sweet ingredient with unique flavour improvement properties. At estimate discovered levels of use, NTM provides a fully sweet taste in victuals. NTM is a white to off-white powder that has a sweetness factor approximately 7000 to 13000 times greater than sucrose and approximately 30 to 60 times larger than aspartame (Authority 2007).

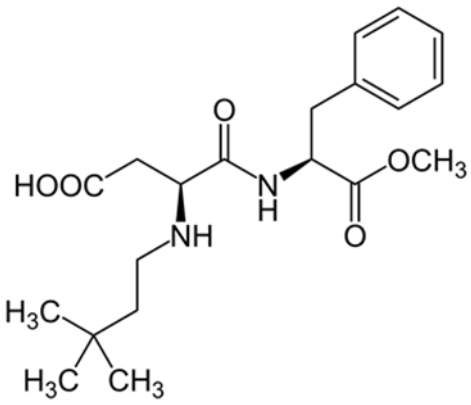

Figure 2-1: a 2D sketch of NTM *(Bathinapatla* et al. *2015b).*

NTM is produced by the reaction of aspartame and 3,3-dimethyl butyraldehyde in methanol for several hours at ambient temperature under hydrogen pressure and the catalyst is separated by a strainer. Nevertheless, sweeteners such as sucralose, NTM, aspartame, and acesulfame have been reported to cause health problems such as DNA damage, insulin sensitivity, chronic fatigue, and brain tumour after entering the human body (Purohit and Mishra 2018).

Applications of NTM

Unnatural high-intensity sweeteners sucralose, NTM, and stevia form an important class of food additives that are commonly used in the pharmaceutical and confectionery, food, and beverage industries. They give the sensation of sweetness and smell, but with little or no intake of food vitality. There are many known intense sweeteners, but only very few can be used in the modern food industry which varies from country to country. Food manufacturing companies are heavily promoting their artificial-sweetened and flavour products by emphasizing their benefits. Little or lessened-calorie food products and beverages can help in the treatment of obesity, management of diabetes, and maintaining body weight (Yang and Chen 2009; Pepino 2015). These days, the common trend in the food industry is to use sweetener blends, because some of the sweeteners impart side tastes and aftertastes that can limit their applications in victuals (Leksrisompong *et al.* 2012).

Unnatural high-intensity sweeteners intensely promoted by the food industry are among the most controversial food additives due to suspicions of unfavourable health ramifications (Thomas and Adegoke 2015). These claims include causing dermatological problems, headaches, behaviour changes, seizures, allergies, cancer, mood variations, and respiratory difficulties (Kroger, Meister, and Kava 2006; Zygler, Wasik and Namieśnik 2009).

1.1. Sensors

Sensors are a category of tools that produce measurable responses to changes in chemical concentrations or physical conditions. Normally a sensor consists of a sensing element and a signal transducer and produces a signal proportional to the

analyte concentration. The sensors continue to make a significant impact in biological and medical applications because of their properties such as high sensitivity, fast response, and low cost.

1.1.1. Biosensors

Biosensors are normally defined as sensors that consist of biological recognition elements and are often called bio-receptors and transducers. The sensing parts of biosensors are biological structures such as enzymes, nucleic acids, or cells (Vo-Dinh and Cullum 2000). The biosensor is used to measure physical changes or biological processes. With the current advances in nanotechnology, nanomaterials have received great interest in the field of biosensors due to their exquisite sensitivity in biological and chemical sensing (Jain 2003).

With dissimilar kinds of signal transducers, the physical or chemical changes that occur during the binding of the analyte to the bio receptors of biosensors can be transformed into output, qualitative, electrical, or optical signals.

Current research on enzyme-based electrochemical biosensors deals essentially with the target analytes as was the focus in the early days of biosensor research, that is those within the clinical/medical, food/agriculture, and environmental fields (Turner, Karube and Wilson 1987; Scheller and Schubert 1991; Wilson and Hu 2000; Dzyadevych *et al.* 2008; Turner 2013).

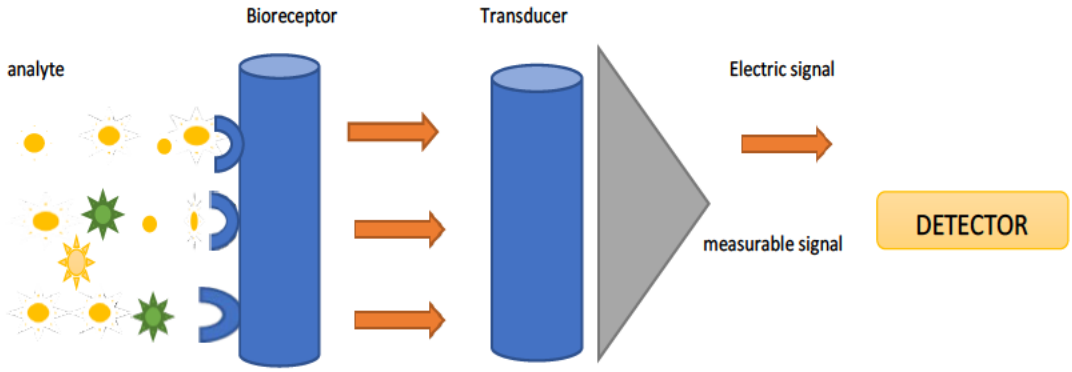

Figure 2-2: A representation of a biosensor (Kumar and Neelam 2016).

2.1.2. Electrochemical enzymatic biosensors

Electrochemical enzymatic biosensors depend on biological identification. For an enzymatic biosensor to work, an enzyme must be present to catalyze a specific biochemical reaction and be stable under the normal operating conditions of the biosensor. The fabrication of biosensors is based on the information about the target analyte, as well as the complications of the matrix in which the analyte was to be quantified (Rocchitta *et al.* 2016). Enzyme-based biosensors in which the production of current is monitored when a fixed potential is applied between the electrodes have been studied as they are easy to be diminished and can work with small sample volumes (D'Orazio 2003; Wilson 2005).

Communication between a redox enzyme and an electrode has been a central theme and continues along with the traditional major electron transfer (ET) routes namely mediated electron transfer and direct electron transfer (Gorton *et al.* 1999; Habermüller, Mosbach and Schuhmann 2000).

1.2. Enzymes

An enzyme is a big composite macromolecule consisting largely of proteins that act as a powerful catalyst to change substrates to products. The enzymes that are used in the biosensor and their mode of action which involve oxidation or reduction, can be detected by electrochemical methods. The key motive for the popularity of bio receptors is their specific binding capacity and the catalytic activity of enzymes. The biosensors use enzymes that are specific to the wanted molecules. Different kinds of enzymes are used for the creation of biosensors. For instance, alcohol oxidase enzyme for alcohol (Hämmerle *et al.* 2011), glucose dehydrogenase for glucose (Liang *et al.* 2013), amino acid oxidase for amino acids (Lata *et al.* 2013), and fructose dehydrogenase for fructose (Trivedi *et al.* 2009). The lifespan of a sensor is limited by the enzyme's stability. The five fundamental techniques of enzyme immobilization are microencapsulation, covalent bonding, cross-linking, adsorption, and entrapment (Eggins 2008).

The catalytic activity of enzymes depends on the pH and the temperature. These contrasts can be attributed to the enzyme itself, substrate, and oxygen (Xu 1997). For instance, past studies (Secchi *et al.* 2013) demonstrated that the optimal working temperature of alcohol oxidase immobilized on a platinum electrode was between 35 °C and 40 °C. The optimum pH ranged between 8.6 to 9.2 and it depends on variable parameters such as temperature, enzyme, and matrix composition (Rangelova, Tsankova, and Dimcheva 2010). At optimum temperature and pH, the biosensor's response is reproducible and has great sensitivity that makes it to be accurate.

Enzymes are biological catalysts with very good prospects for application in chemical industries due to their high activity under mild conditions, high selectivity, and

specificity. The most commonly used strategy to achieve more sensitive and selective enzymes and consequently biosensors are to increase the affinity for the target analyte favouring the accessibility of the active site (Campàs, Prieto-Simón, and Marty 2009).

2.2.1. Alcohol oxidase

Alcohol oxidase (AOx) is an oxidase that contains Flavin which, in the presence of molecular oxygen catalyzes the oxidation of series of short-chain aliphatic alcohols, whereby the corresponding hydrogen peroxide and aldehydes are formed (Johansson *et al.* 1993) :

$$R\text{-}CH_2\text{-}OH + O_2 \longrightarrow R\text{-}CHO + H_2O_2$$

Figure 2-3: A representation of Alcohol Oxidase.

Alcohol oxidase as a bio-identification element for sensing alcohol has triggered interest since the previous decade (Azevedo *et al.* 2005a). Prospective advantages of alcohol oxidase based on the bio-recognition system are identified among which the irreversible catalytic oxidation of alcohols and the avidly bound Flavin-based co-factor to the redox centre of the enzyme are relevant to the biosensor implementations. Furthermore, the comprehension of molecular and functional characteristics of this unexplored group of redox enzymes is quickly growing. AOx catalyzes the oxidation

alcohols using molecular oxygen as the electron acceptor and producing corresponding hydrogen peroxide and carbonyl compound in the reaction. The reaction can be followed by measuring O_2 and H_2O_2 concentration using electrochemical or optical detections (Vijayakumar *et al.* 1996; Patel *et al.* 2001; Razumien *et al.* 2001; Gülce *et al.* 2002; de Prada *et al.* 2003; Raj and Behera 2005; Svensson *et al.* 2005; Carelli *et al.* 2006; Shkotova *et al.* 2006; Yildiz and Toppare 2006; Barsan and Brett 2008; Lee and Tsai 2009; Zhang and Gorski 2011).

2.2.2. Carboxylesterase

An esterase is an α/β- fold hydrolase enzyme that catalyzes the hydrolysis of both endogenous and exogenous esters. Each representative of this group of enzymes carries the same core that is made of an α/β-sheet of eight β-sheets attached by α-helices (Wheelock, Severson, and Hammock 2001). The α/β hydrolase group was first described by Ollis and co-workers cover a broad range of enzymes that share similarities in tertiary and secondary shapes (Ollis *et al.* 1992). These enzymes are linked by different evaluations and include lipases, epoxide hydrolases, esterase, haloalkane dehalogenase, cholinesterase (Quinn, Medhekar and Baker 1999).

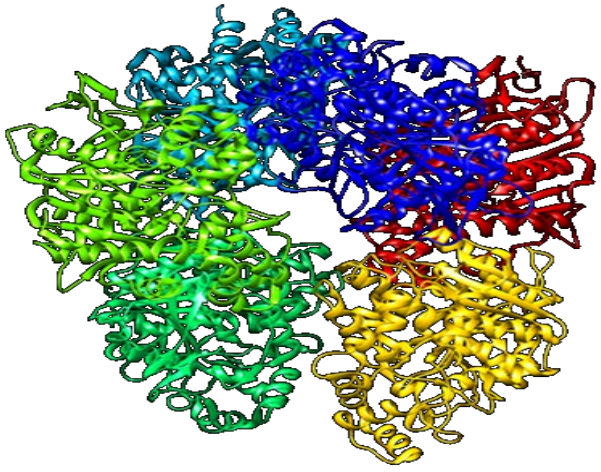

Figure 2-4: Optimized structure of Carboxylesterase at DFT level 6-311+G (d.p).

Carboxylesterases are a subdivision of the α/β- hydrolase family and have very wide substrate selectivity. They are beta-esterase under the nomenclature of Aldridge by their hindrance by organophosphates and are distinguished by their catalysis of the hydrolysis of a carboxyl ester to the matching acids and alcohols (Aldridge 1953). Carboxylesterases are significant in the metabolism of many exogenous compounds including pesticides and pharmaceuticals, but their endogenous function is not stated plainly (Satoh and Hosokawa 1998).

The nature and specificity of their catalytic activity make them excellent tools for chemical analysis. The ability of AOx and CaE enzyme molecules to catalyze the reaction of NTM also provides an amplification effect, which enhances the sensitivity of the analysis (Azevedo *et al.* 2005b). A comprehensive review of how to control the orientation of redox enzymes at planar electrodes was recently published by Lojou and coworkers (Rahman *et al.* 2010). Moreover, also nanomaterials have been used to address enzyme immobilization issues, sometimes increasing enzyme stability (Chopra *et al.* 2007; Wang and Lin 2008; Wujcik, Monty and Nanobiotechnology 2013; Hasanzadeh *et al.* 2014; Izyumskaya *et al.* 2017).

1.3. Nanotechnology

Nanotechnology necessitates the manipulation, research, formation, and utilization of materials, devices, and systems typically with dimensions smaller than 100 nm. Nanotechnology has a major role in the invention of biosensors (Vo-Dinh, Cullum and Stokes 2001; Haruyama 2003; Jain 2003). Sensitivity together with other attributes of biosensors can be improved by using nanomaterials in their fabrication. Nanomaterials, or matrices with at least one of their dimensions ranging in scale from

1 to 100 nm, display unique physical and chemical features because of effects such as macro-quantum effect, quantum size effect, surface effect, and mini size-effect. The utilization of nanomaterials in biosensors enables the use of many new signal transduction technologies in their construction. Nanotechnology is transforming the invention of biosensors and nanomaterials (Jianrong *et al.* 2004).

1.3.1. Nanoparticles in biosensing

Nanoparticles have many possible applications in biosensors, for instance, functional nanoparticles (electronic, magnetic, and optical) bound to biological molecules (enzymes, proteins, nucleic acids, and peptides) have been developed for use in biosensors to detect and increase diverse signals (Mahmoud, Hrapovic and Luong 2008; Ganesana *et al.* 2011; Elshafey *et al.* 2013; Yang *et al.* 2014; Ali *et al.* 2015; Chen *et al.* 2015; Lin *et al.* 2016). Nanoparticle-based sensors include electrochemical biosensors, acoustic wave biosensors, optical biosensors, and magnetic biosensors.

Electrochemical biosensors have been manufactured from mostly metallic nanoparticles. Metal nanoparticles based electro-analysis has been reviewed by Hernández-Santos, González-García, and García (Hernández-Santos, González-García and García 2002). On account of its ultrahigh surface area, colloidal Au has been used to enhance the DNA immobilization on a gold electrode (Au-E), to ultimately lower the detection limit of the fabricated electrochemical DNA biosensor (Cai *et al.* 2001). Metal nanoparticles are utilized to catalyze biochemical reactions and this capability can be usefully employed in biosensor design. Catalysis is the most significant and widely used chemical application of metal nanoparticles. Transition metals show very high catalytic abilities for numerous organic reactions.

Currently, the research field of the development of new protocols for preparing functionalized gold and nickel nanoparticles and using them for biosensing is presently an active research area. Gold and nickel nanoparticles represent an attractive approach for biosensing applications and will continue to be used as a tool for novel future applications (Zeng *et al.* 2011; Başkaya *et al.* 2017b). In this work, we discuss the use of gold and nickel nanoparticles in the detection of NTM.

1.3.2. Gold nanoparticles

Gold nanoparticles are nanomaterials with a wide variety of applications (Lee *et al.* 2014). Therefore diversity of synthetic procedures for the formation of various shapes and sizes of AuNPs have been described (Grzelczak *et al.* 2008). Various isotropic structures including rods, wires, plates, and teardrop structures can be obtained by wet actinic synthesis ways (Shankar *et al.* 2004). Biosynthetic procedures that use biological microorganisms, plants, or plant extracts have emerged as simple and eco-friendly 'green' alternatives to the actinic routes. It was described that inorganic nanoparticles can interact with microorganisms and may exhibit antifungal and antibacterial activity (Hernández-Sierra *et al.* 2008; Eby *et al.* 2009; Panáček *et al.* 2009; Chwalibog *et al.* 2010). Few publications have also shown that AuNPs show notable antimicrobial activity (Kaittanis, Nath and Perez 2008; Park *et al.* 2011). Their widespread antimicrobial activity may be credited to their strong cytotoxicity to various microorganisms. The interaction with the various surface-exposed functional groups present on the bacterial cell surface may lead to bacterium inactivation (Ray *et al.* 2007).

The characteristics of AuNPs are different from their bulk form. The bulk gold is an inert yellow solid, compared to gold nanoparticles (which are antioxidants) that have

a wine-red colour in solution. Gold nanoparticles show diverse sizes ranging from 1 nm to 8 µm and they also exhibit different shapes such as nano triangles, tetrahedral, hexagonal platelets, nanorods, irregular shape, multiple twined, decahedral, octahedral, and spherical (Deb *et al.* 2011).

Amid all the structures, triangular-shaped nanoparticles (NPs) show attractive optical properties as compared to the spherical structured NPs. The utilization of a single active substance from plant extract in the synthesis of AuNPs is an important bio-synthesis technique to purify AuNPs and to investigate their medical applications (MubarakAli *et al.* 2011). AuNPs have been widely used in the field of radiation medicine to strengthen radiation. AuNPs have diverse uses as platform nanomaterials for biomolecular ultrasensitive detection, killing cancer cells by hyperthermal treatment, delivering therapeutic agents within cells, labelling for cells, and proteins (Fernandez-Fernandez, Manchanda, and McGoron 2011; Ganeshkumar *et al.* 2012; Oliveira *et al.* 2019).

Due to the presence of negative charge on AuNPs, they can be easily functionalized by all kinds of biomolecules, such as targeting ligands, drugs, and genes (Fratoddi *et al.* 2015). Noncovalent alterations occur through electrostatic interactions, Van der Waals forces, and hydrophobic entrapment. The benefit of this interaction is that the biomolecule cannot attach to diverse chemical modifications that are likely to compromise its primary, active sites. In biological studies, the binding is not strong enough to yield a stable surface capable of withstanding the necessary washing steps and incubation conditions. It is paramount to consider the impact of the surrounding medium's ionic strength and pH when using this modification. Unlike covalent alterations, which make use of immediate chemical attachments, click chemistry,

provides greater stability and reproducibility and linker molecules (Austin *et al.* 2014). Covalent alterations can resist very high salt concentrations and are extremely stable under the thermal state. The comparative ease of nanoparticle surface modification, through noncovalent and covalent modifications, allows for specific biological targeting and can be used further in biosensing and bio diagnostic applications (Kong *et al.* 2017).

1.3.3. Nickel nanoparticles

Nickel nanoparticles (NiNPs) are very useful for a variety of practical applications namely bio-hydrogen production from dairy wastewater (Gadhe, Sonawane and Varma 2015), construction of gas sensing devices (Tamburri *et al.* 2015), non-enzymatic glucose biosensing (Guo *et al.* 2015), hydrogen adsorption (Giraudet and Zhu 2011), development of efficient and easily recoverable dip-catalyst for pollutants degradation (Kamal, Khan and Asiri 2016), catalysts for aldehydes de-hydrosilylation (Blandez *et al.* 2016), sensitive and reusable detection of glucose (Başkaya *et al.* 2017a), catalysts for hydrogen production (Zhao *et al.* 2017), catalysts for the oxidation reaction of ethanol and methanol (Sharel *et al.* 2016), as the absorbent used for sewage treatment (Zhang *et al.* 2015), desulfurization of thiophene for *in-situ* upgrading of heavy crude oil (Guo *et al.* 2018) and bilirubin biosensing (Rawal *et al.* 2017). To synthesize the NiNPs, many methods have been described namely hydrazine reduction (Wu, Munoz and Montero 2010; Chandra, Kumar and Tomar 2014; Hemalatha, Suriyanarayanan and Prabahar 2014; Kashid, Raut and Malghe 2016), using aqueous cationic surfactant solutions (Chen and Hsieh 2002), by femtosecond laser ablation in liquids (Muñeton Arboleda *et al.* 2015) and lately, the electrodeposition of nickel nanostructures from deep eutectic solvents (DES) as

described by Mernissi Cherigui (Mernissi Cherigui *et al.* 2017). The DES offers many advantages for metal electrodeposition process, such as great stability at higher temperatures (Bund and Zschippang 2007; Abbott *et al.* 2008; Ali, Rahman and Saha 2014; Abbott *et al.* 2017; Urcezino *et al.* 2017). Even the electrochemical deposition allows the growth of the nanostructures through only one step, directly onto the final support without needing further sample preparation thus improving the electron pathway within the nanostructure, substrate and the environment (Aldana-González *et al.* 2018).

Predominantly, bare NiNPs are very unstable and prone to oxidation in the air but they can be stabilized with reduced graphene oxide (rGO) to form a Ni-rGO composite. The rGO surface contains a lot of free electrons which help to stabilize the Ni in its zero-valent state. Because of this kind of environment the metallic NiNPs present on the rGO surface are rarely oxidized to a higher oxidation state(Zhang *et al.* 2005; Jang *et al.* 2012). Even, the high surface area of rGO prevents the NiNPs from agglomerating into bigger particles. In comparison with carbon nanotubes, graphene has a larger surface area, fewer impurities, and superior electrical and mechanical properties (Novoselov *et al.* 2005b; Zhang *et al.* 2005). Graphene oxide has been investigated as a membrane material (Joshi *et al.* 2015) and a mechanical reinforcement (Fan *et al.* 2010). Regardless of its poor electron conductivity, it presents good electrocatalytic properties (Davies, Hyde, and Compton 2005) due to the high density of functional groups and structural defects (Gómez-Navarro *et al.* 2010). Consequently, rGO is a better-balanced material for electrochemical applications (Krishna *et al.* 2016).

Nanoparticles are better supported by either carbon nanotubes or graphene oxide. The surface of GO contains a large number of reactive functional groups (carboxyl

groups, hydroxyl groups, and epoxy groups). These functional groups make GO particularly easy to be modified (Yuan *et al.* 2020). The construction of graphene oxide supported by a nanomaterial and a biomolecule-based electrochemical sensor is discussed in this study. The advantage of using carbon nanotubes in the fabrication of the electrode is to promote different electron transfer reactions, in special those related to biomolecules (Rivas *et al.* 2007). The construction of carbon nanotubes supported by a nanomaterial and a biomolecule-based electrochemical sensor is discussed in this study.

1.3.4. Carbon nanotubes

Carbon is prominent amongst the most copious and most entrancing elements on earth. It appears in a few distinctive structures or allotropes with broadly remarkable properties (Alim *et al.* 2018). Amid these allotropes are amorphous carbon, graphite, and precious stone. The disclosure of novel carbon allotropes or carbon nanostructures has pulled in solemn consideration due to their key and mechanical interests (Dresselhaus, Dresselhaus and Eklund 1996). Carbon nanotubes (CNTs) are found in two types (single-walled CNTs and multi-walled CNTs). SWCNTs possess excellent catalytic properties and low toxicities, which could be explored as a replacement of nanotubes in the electrochemical study. However, SWCNTs tend to aggregate easily, which results in poor distribution (Gao *et al* 2014). Multi-walled carbon nanotubes (MWCNTs) are constituted of more than two layers of a curly graphene sheet and the diameter is at a range of 2-30 nm (Popov 2004).

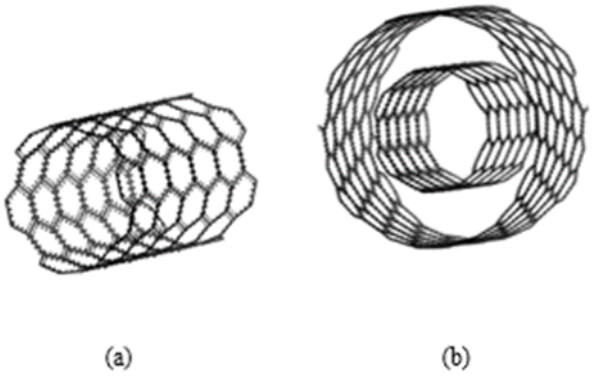

Figure 2-5: (a) sketch of CNTs, (b) sketch of MWCNTs generated using Material Studio (MS).

Attributable to the large inter-tube attraction energy, the structure of CNTs is stable enough which causes their insolubility in diverse solvents. Moreover, the dispersibility of CNTs is the foremost task for the preparation of carbon nanotubes. To develop a biosensor (Yang *et al.* 2015) due to the hydrophobicity of CNTs, guest particles, or sidewall substituents surface, functionalization of polymers is important to enhance the biocompatibility of CNTs (Barsan, Ghica and Brett 2015). Functionalized CNTs have many enhanced attributes like high catalytic efficiency, high surface activity, and a large edge plane. The biosensor that is developed with functionalized CNTs has higher sensitivity, faster response, and a stable wider detection range in comparison with a conventional carbon biosensor. Functionalization of CNTs can be achieved by both physical and chemical methods, whereas physical approaches exploit the mechanical means such as ultrasonic, crushing, milling, and friction to activate CNTs surface by changing their exterior formation (Fujigaya *et al.* 2008). The chemical approach is made up of two methods as covalent and non-covalent modification. Whereas only non-covalent modification can remain the original structure and properties of CNTs and does not damage the system but the covalent alteration is stable (Alim *et al.* 2018).

Covalent alterations result in tip defects as well as a sidewall of CNTs followed by introducing functional groups. More amounts of functional groups can be introduced to the surface of CNTs if they are treated with different types of acids (Pavlidis *et al.* 2012) to a huge number of active sites to formulate the functionalized CNTs with better catalytic activity for biological materials. A bigger surface area was possessed by the hollow tube structure of functionalized CNTs and the carboxyl group on the surface of functionalized CNTs helped the biomolecules to be immobilized by covalent binding (Musameh *et al.* 2012).

1.3.5. Graphene oxide

Graphene is a planar sheet of sp^2-bonded carbon atoms densely packed in a honeycomb crystal lattice (Kuila *et al.* 2012). It's the mother element of some carbon allotropes including carbon nanotubes, fullerenes, and graphite (Geim and Novoselov 2010; Singh *et al.* 2011). Graphene is famous because of its unique mechanical, optical, catalytic, and electrical properties (Novoselov *et al.* 2005a; Zhang *et al.* 2005; Meyer *et al.* 2007; Zhao *et al.* 2010). Graphene is set to surpass all the allotropes in utility for life and material science attributable to its unique properties (Novoselov *et al.* 2004; Balandin *et al.* 2008; Lee *et al.* 2008). Graphene oxide (GO) is soluble in water, it contains both aromatic (sp^2) and aliphatic (sp^3) domains.

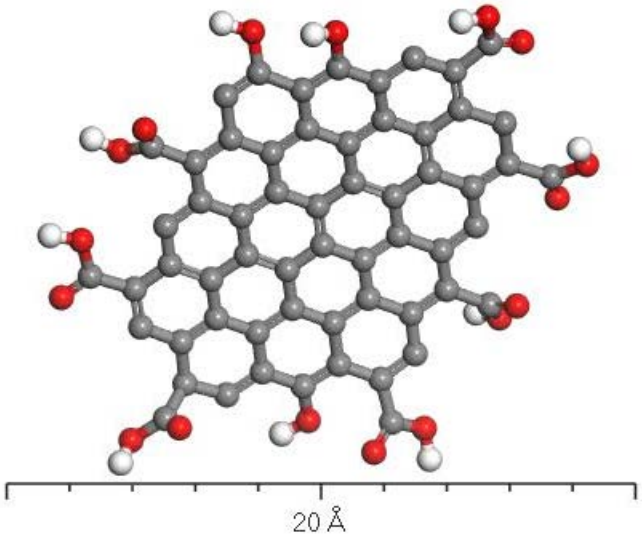

Figure 2-6: A 3D sketch of a graphene sheet generated using Material Studio (MS) whereby H, O, C atoms are denoted in white, red, and grey respectively.

Graphene oxide (GO) gives an excellent platform for the size-controlled deposition of highly dispersed nanoparticles (Georgakilas *et al.* 2016). The use of NPs in diverse applications depends on the multitudes of factors such as surface area, facet order, size, number of facets, and shape (Zhang *et al.* 2005). The GO can act as a substrate for NPs, in many applications where the inherent properties of graphene such as conductivity or anchoring site are very beneficial (Duan *et al.* 2014; Liu *et al.* 2014). A lot of studies have utilized noncovalent functionalized G/GO applications, ranging from cell imaging and biosensing (disease-related diagnostics, human telomerase detection) (Shah *et al.* 2014; Kang *et al.* 2015; Kim *et al.* 2015; Park *et al.* 2015; Tiwari *et al.* 2016).

The principal functional groups in GO are those situated on basal planes: epoxy and hydroxyl groups (Li *et al.* 2013). The residual sp^2 system can also be used for chemical reactions, in the end forming the C-C bonds. A part of C-C bonds in GO can be increased by chemical reduction, and thus reduction methods produce a reduced graphene oxide (Yan and Chou 2010). Furthermore, the study of the chemical

structure of rGO is briefly compared to that of graphene to understand how it reacts chemically. A lot of reactions can be used to functionalize rGO, leading to dispersible rGO. Due to the heterogeneity of GO and rGO, it is very difficult to control their chemistry. The chemical formation of GO depends on the preparation conditions, keeping in mind that the shape of GO has been a matter of discussion for more than a century, hence it makes it difficult to analyze the reaction products after chemical alterations (Xu, Yuan, and Wang 2014).

The formation of GO is highly variable, and the absolute structure depends to some extent on the reaction conditions. NPs can be formed and deposited onto the sheets of GO and rGO to form metal-graphene compounds. Interactions between the rGO and the metal particles are not certain, a metal-C bond may be formed, or the particles may be non-covalently bounded while residual oxygen impurities of rGO can also form metal-O-C bonds.

In this study, AuNPs and MWCNTs are combined to fabricate an AuNPs/MWCNTs nanocomposite and CaE is introduced to the modified glassy carbon electrode for the detection of NTM. NiNPs and GO are combined to fabricate a NiNPs/GO nanocomposite and AOx is introduced to the modified glassy carbon electrode for the detection of NTM. Computational tools are employed for a better understanding of the interaction of the enzymes, analyte, and nanomaterials with the surface modification of the electrode surface.

1.4. Computational Chemistry

Computational chemistry uses computer simulation to help in solving chemical problems. It uses methods such as Density Functional Theory (DFT), Molecular

Dynamic Simulation (MDS), and Molecular Docking to calculate the structures, properties of the molecule, and interactions (Shakerzadeh 2016). Computational chemistry is used to predict models of different enzyme-substrate complexes (Manzetti *et al.* 2003). The implementation of computational software programs helps to obtain results that are difficult to be obtained during experimental studies. The property of molecules is calculated and visualized so that the interactions between the molecules can be seen and understood better. To determine the motion of the electrons within the molecule, we need to look at the electronic structure theory. A basis set was determined based on the calculations while utilizing the mathematical equations, during this process, we can look at the energy of the molecule, predicted experimental structures, and saw the orbitals of the molecule.

CHAPTER 3: THEORETICAL PRINCIPLES

This chapter focuses on the basic theoretical principles underpinning the techniques that were used for experimental studies carried out. Furthermore, the equations concerning the operation of the techniques are presented. The role of computational chemistry in this study is highlighted by explaining the functions of molecular dynamic simulation, molecular docking, and the foundation of density functional theory (DFT).

3.1. Instrumental

3.1.1. UV-Visible Spectroscopy

A UV-Vis spectrometer is the equipment used for measuring absorbance or transmittance of a sample as a function of the wavelength of electromagnetic radiation. The spectrometer is made up of key components which include a source, a dispersion device, a sample area, and a detector as shown in Figure 3-1.

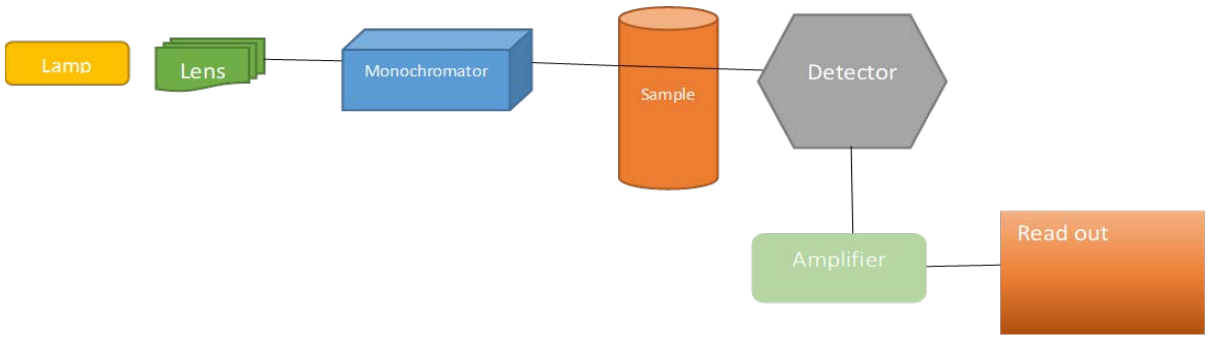

Figure 3-1: A representation of a UV-Vis spectrometer was redrawn from (Pavia *et al.* 2008).

UV-Vis spectroscopy is absorption spectroscopy in which light is absorbed by the molecule and that results in the excitation of electrons. Spectroscopy is associated with the interaction of light with matter so as light is absorbed by matter, the energy content of the atoms and molecules increases. The excitation of electrons from the ground state to a higher state occurs when ultraviolet radiation is absorbed. When the

electrons are easily excited, the wavelength of light that they can absorb will be longer. A chemical compound will absorb ultraviolet light to produce a distinct spectrum which helps to identify the compound. Several processes can occur when radiation interacts with the matter which includes photochemical reaction (absorbance and bond-breaking), absorbance, reflection, scattering, and fluorescence/phosphorescence (absorption and reemission). When light is reflected from a sample, the amount of light absorbed is the difference between the transmitted radiation (I) and the incident radiation (I_0). The light absorbed is expressed as absorbance or transmittance.

Transmittance is expressed in terms of a fraction of I or as a percentage and is used defined as follows:

$T = I/I_0$ or $\% T = (I/I_0) \times 100$ **[Eqn 3.1]**

Where I_0 is the intensity of the incident, I is the intensity of the transmitted light, T is the transmittance.

The absorbance is expressed as follows:

$A = -\log T$ **[Eqn 3.2]**

Where A is the absorbance and T is the transmittance

For many implementations, absorbance values are used since the relationship between absorbance and both concentration and path length is linear. This is proven by Beer-Lambert law, expressed by an equation:

$A = \varepsilon c l$ **[Eqn 3.3]**

Where A is the absorbance, *l* is the length of the light path through the sample,

ε is the molar extinction coefficient.

3.1.2. Single Particle Inductively Coupled Plasma Mass Spectrometry

Single-particle ICP-MS is a technique that can be used to detect particle size, particle distribution, and concentration (Laborda *et al.* 2013). A basic theory of how the detection of a single particle is applied was discussed by Degueldre, Favarger, and Wold (Degueldre, Favarger and Wold 2006) for nanoparticle suspensions continuously introduced through the conventional nebulization process. An analysis in a single particle mode is performed by inductively coupled plasma-mass spectrometry (ICP-MS). The signal induced by the flash of ions due to the ionization of a colloid in the plasma torch is measured for the ions by the mass spectrometer without interferences. The intensity is recorded in a time scan. When an analyte of mass concentration Cm is nebulized into an ICP-MS, the signal R (ions counted per time unit): quantitative detection of the nanoparticle number concentration is based on the linear relationship between the frequency of nanoparticle events and the number of NPs.

The relationship is expressed as:

$$F_{NP} = Q_{NP} = \eta_{neb} Q_{sam} N_{NP} \qquad \textbf{[Eqn 3.4]}$$

Where F_{NP} is the frequency of nanoparticles detected, Q_{NP} is the flux of nanoparticles reaching the plasma, η_{neb} is the analyte transport, Q_{sam} is the flow rate of the sample,

N_{NP} is the nanoparticle number concentration.

3.1.3. Transmission Electron Microscopy

Transmission emission microscopy (TEM) is a microscopy technique in which a beam of the electron is transmitted through a sample to create an image. TEM has three important systems namely, an electron gun, the image-producing system, and the image–recording system. TEM is known as one of the best standard methods for nanoparticle characterization when analyzing particle sizes. Electron microscopy operates by bombarding a sample with a stream of electrons and monitoring the resulting transmission. The detected electrons are converted into magnified images of particles in the sample scattering (Pyrz and Buttrey 2008). The images are analyzed using software to provide information about the morphology of the nanoparticles, such as the particle size data for individual particles and number-based size distributions for the entire dispersion.

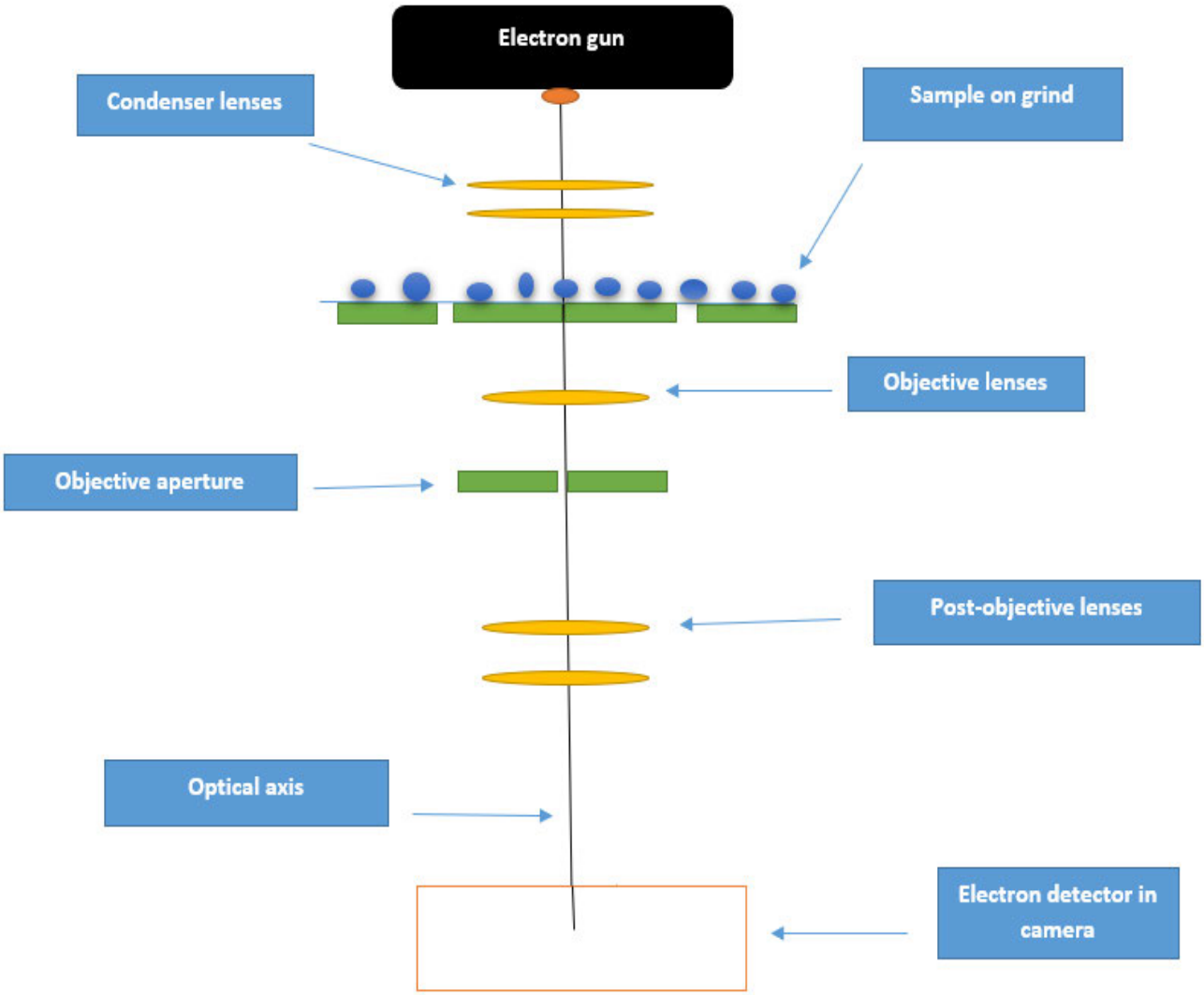

Figure 3-2: A representation of a TEM principle (Marturi 2013).

3.1.4. Thermogravimetric Analysis

Thermogravimetric analysis is a technique of thermal analysis whereby the mass of an analyzed sample is measured as temperature changes over time. This technique provides information about physical phenomena, namely absorption, adsorption, and desorption, and phase transitions. It also provides information about chemical phenomena, namely thermal decomposition, solid-gas reactions, and chemisorption (Corazzari *et al.* 2015; Ünveren *et al.* 2017). After doing a thermogravimetric experiment, you can plot a graph of mass as a function of time or temperature. The

thermogravimetric analysis consists of a sample pan that resides in a furnace that heats and cools it during an experiment. It is important to purge the gas during the experiment to control the environment. The gas used may be an inert gas or reactive gas. During a TGA experiment, six operating variables contribute to reproducibility namely calibration, furnace cleanliness, sample preparation, temperature range, sample atmosphere, and temperature scanning rate.

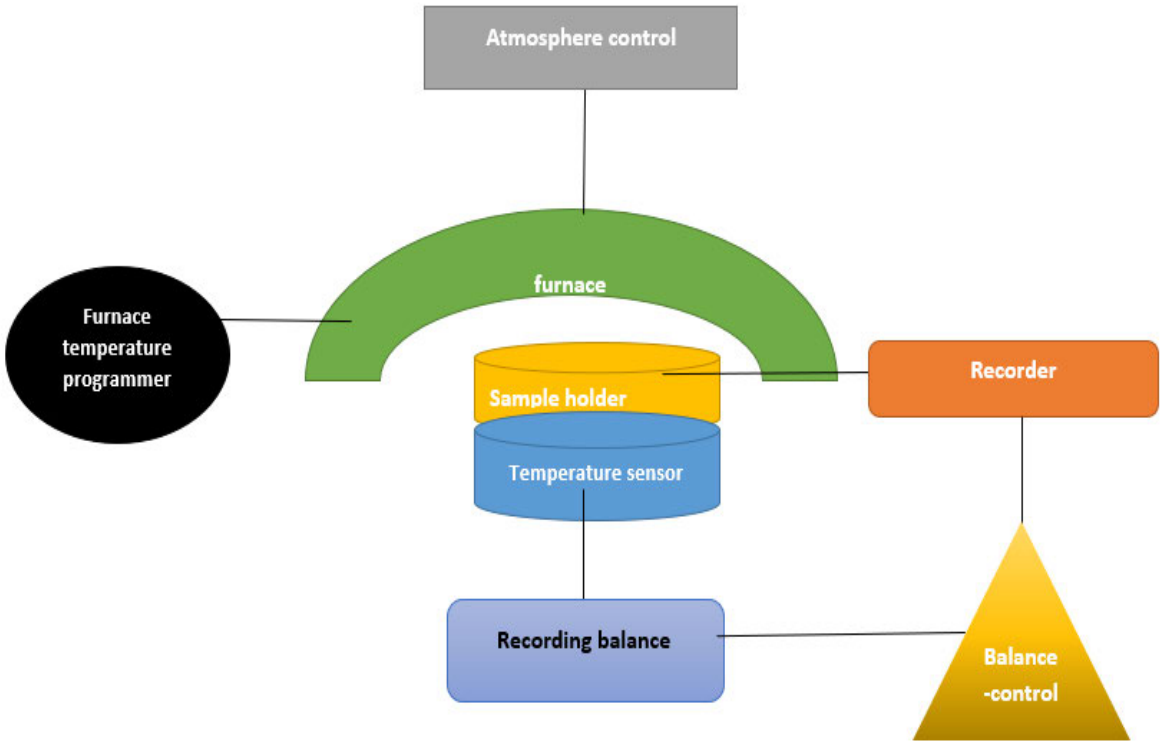

Figure 3-3: A representation of a Thermogravimetric Analysis was redrawn from *(Yang, Teng, and Seetharaman 2012).*

3.1.5. Field-Flow Fractionation

Field-Flow Fractionation (FFF) is a high-resolution technique that can separate NPs and colloids. The separation is based on the forces instead of chemical interactions as compared to chromatography. Different modes of the FFF can be chosen to achieve optimal separations results depending on the type of analysis that is being

performed. Thermal, sedimentation, and flow are the three FFF techniques that are commonly used. FFF is an elution based chromatography-like method in which the separation is carried out in a single liquid phase. FFF is characterized by the use of an external field applied perpendicularly to the direction of sample flow through an empty, thin ribbon-like channel. Due to the high aspect ratio of the FFF channel a laminar parabolic flow profile develops, with flow velocity increasing from near zero at the channel walls to a maximum at the centre of the channel. The perpendicularly applied force drives the sample toward the accumulation wall. A counteracting diffusive force develops due to the concentration build-up at the wall and drives the analyte back towards the centre of the channel. When the forces balance, steady-state equilibrium is reached, and an exponential analyte concentration profile is built up. Retention occurs when analytes reside in inflow velocity zones slower than the average flow velocity of the carrier liquid passing through the channel. Separation occurs because different analytes reside in different flow velocity zones (Messaud *et al.* 2009). It is versatile for a range of both manufactured and natural nanoparticles (Dubascoux *et al.* 2008; Dubascoux *et al.* 2010; Baalousha, Stolpe, and Lead 2011). The balance of these forces depends on the spacer thickness and the flow conditions hence due to interactions between the analyte and the membrane, the balance can also be affected by the membrane composition.

Asymmetric flow field-flow fractionation (AF4) is a type of fractionation that is based on hydrodynamic radius and can be coupled to concentration and MALS detectors. The advantages of using AF4 include wide separation and concentration range, lack of interactions between the analyte and the stationary phase, more mobile phase options and minimizes shear degradation. This technique allows the determination of the root mean squared radius (of gyration), molar mass, etc.

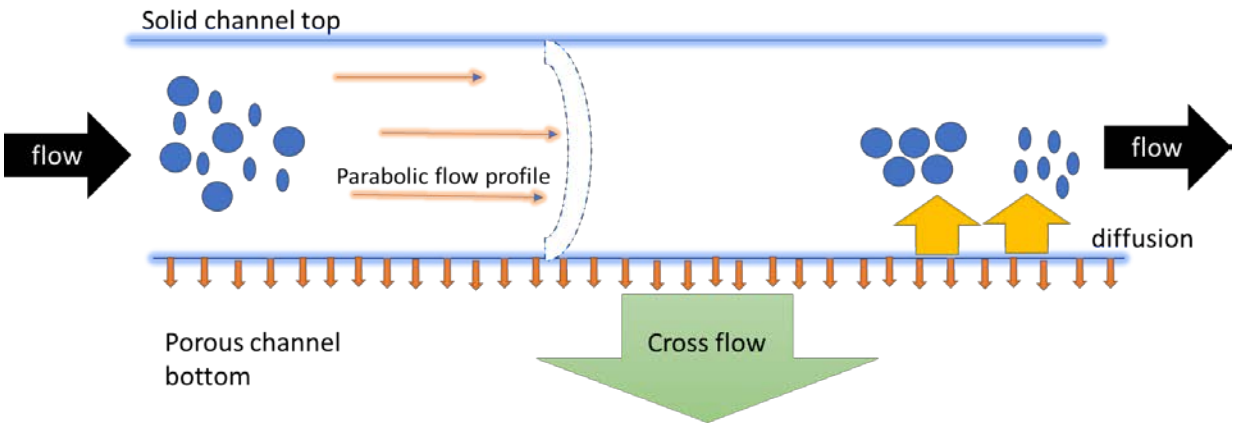

Figure 3-4: Principle of Asymmetric Field-Flow Fractionation was redrawn from *(Messaud et al. 2009).*

3.1.6. Cyclic Voltammetry

Cyclic Voltammetry (CV) is a widely used electroanalytical technique in chemistry. It is mostly used for quantification studies, but it is also used for the study of redox processes, for obtaining the stability of reaction products, and for understanding reaction intermediates. This method is based on changing the applied potential at a working electrode in both forward and reverses directions (at a certain scan rate) in the process of observing current (Bhattacharyya *et al.* 2012; Aristov and Habekost 2015). For instance, the initial scan could be in the negative direction to the reverse potential. In that position, the scan rate would be reversed and run in the positive route. A response that you get from a CV can be very simple for a reversible redox reaction, as shown in Figure 3.5 for a reversible redox reaction. A CV has important parameters which are the peak currents (i_{pa}, i_{pc}) of the anodic and cathodic peaks, respectively, and the peak potentials (E_{Pa}, E_{pc}). The relationship between the peak current and the concentration is described by the Randles-Sevcik equation at 25 ℃. The peak current is directly proportional to the concentration of the analyte as shown below.

$$i_p = 2.686 \times 10^{5} n^{3/2} A C_0 D^{1/2} v^{1/2} \qquad \textbf{[Eqn 3.5]}$$

Where i_p is the anodic or cathodic peak current in amps, A is the surface area of the electrode in cm^{-2}, D is the diffusion coefficient in cm^2. s^{-1}, C_0 is the concentration of the analyte in mol cm^{-3}, V is the scan rate in $V.s^{-1}$ and n is the stoichiometric number of electrons involved in the electrode redox reaction,

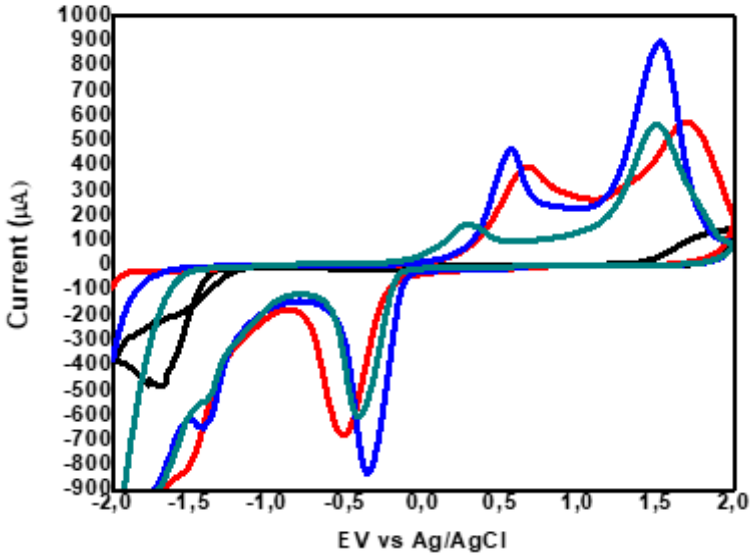

Figure 3-5: A CV response of a reversible redox reaction.

3.1.9 Differential Pulse Voltammetry

Differential pulse voltammetry can give greater sensitivity, differentiation of many species, and more efficient resolution. The peak current is studied at two points from each pulse, just before the application of the pulse and at the end of the pulse. The dissimilarity between the current measurements at these points for each pulse is determined and plotted against the potential. The peak current is shown as a symmetric peak after the analysis is performed. DPV is suitable for reversible and irreversible system and provides a high sensitivity during the analysis. A response of

a staircase-shaped increasing direct potential is expected when performing an analysis using the DPV. For reversible reaction there is a directly proportional relationship between the analyte concentration and the peak height in the DP polarograms, the relationship is expressed by the Ilkovic equation:

$$id = knFD^{1/2}mr^{2/3}t^{1/6}c \qquad \textbf{[Eqn 3.6]}$$

Where, *i*d is the diffusion current, k is the constant which includes the π and the density, n is the number of electrons exchanged during the reaction, F is the Faraday constant, D is the diffusion coefficient of the depolarizer in the medium, m_r is the mass flow rate, t is the drop time in seconds, c is the concentration of the depolarizer

3.2. Computational Chemistry

3.2.1. Density Functional Theory

Density Functional Theory (DFT) is an important tool used by scientists for studying the behaviour of electrons to measure the performance of the materials in application fields. Various experimental studies in inorganic and organic chemistry routinely include such calculations using a standard basis set (Casely *et al.* 2011). The same transformation is underway in material science whereby improvement in both hardware and codes have made it easier to perform systematic comparisons with experiments across large ranges of materials, learning which approximations work and why, and allowing for true first-principles predictions of properties. (Burke 2012). The Born-Oppenheimer approximation is used, and modern calculations and theories are always within a generalization and spin-DFT (von Barth and Hedin 1972). In this case, the Born-Oppenheimer approximation was considered from the electron transfer

point of view. This approximation makes it possible to separate the motion of the nuclei and the motion of the electrons (Essén 1977).

Thomas-Fermi theory is an approximate method for determining the electronic structure of the atom by using one electron ground state density (Thomas 1927; Thomas and Umeda 1957). Kohn-Sham (KS) DFT approximate method is used today and it defines self-consistent equations that must be solved for a set of orbitals whose density is assumed to be of the real system (Kohn and Sham 1965). Chemistry of nanoscience is more understood, for instance when a molecule is absorbed on a surface and considering that areas of material research related to energy need input from electronic structure methods. The transport gap is I - A where A is the electron affinity and I is the ionization potential hence the KS gap (the difference between the KS LUMO and HOMO energies is not equal to this value (Perdew *et al.* 1982). Kohn–Sham (KS) and Hartree–Fock (HF) determinants were used as the true many-body wave functions for calculations of molecular energies, vibrational frequencies, and excited electronic states. The results justified common practice, encountered in the sum over states theories, in which these two determinants are used as the first-order approximation of the wave function (Bouř 2000). The Kohn–Sham (KS) determinant is often used as an approximation to the molecular wave function density functional theory (DFT) studies (Filippi, Umrigar and Gonze 1997). Also, the determinant may be taken as a reference point for further configuration interaction instead of the usual Hartree–Fock (HF) function (Jamorski, Casida and Salahub 1996).

3.2.2. Molecular Dynamics Simulation

Molecular Dynamic Simulations provides the methodology for detailed microscopic modelling on a molecular scale. MD Simulations follows a constructive approach in

that it tries to reproduce the behaviour using model systems (Rapaport 2004). MD Simulations have shown to be indispensable in explaining the mechanical, chemical, structural, and electrical properties of manifold sets of matter. For instance, molecular dynamics simulations have been used to study the bulk solid, diffusion, liquid state, phase transformations, polymers, protein dynamics, and wetting phenomena. It can be shown that MD simulations represent the future of theoretical endeavours in the fields of molecular biology, chemistry, and physics (Berne and Straub 1997). When examining molecular dynamic simulations of a biomolecule, one would ideally like to carry out a quantum mechanical calculation based on the density functional theory approach (Sagui, Darden, and structure 1999).

3.2.3. Molecular Docking

Molecular docking is a computational technique used for placing small particles into the binding site of their receptors. Docking scoring functions and algorithms can generate structures of ranking compounds, estimate binding affinities/energies, and generate structures of receptor-ligand complexes. Automated docking is one of the most important tools that allow the prediction of ligand binding poses and also provides an estimate of how well small molecules fit in the binding site of a protein. The scoring function is also used to evaluate, and rank docking poses according to their potential binding affinities. Molecular docking and scoring is computationally fast and allows virtual screening of millions of ligands within a reasonable timeframe for practical applications.

MD technique tells us more about the behaviour of small molecules in the binding site of a target protein or enzyme. Molecular docking against homology-modelled targets also becomes possible for proteins that have unknown structures. An affinity function

ΔG is used to show the sum of Van der Waals and electrostatic energies. The important forces for these specific interactions in biological systems aim toward complementarities between the shape and electrostatic of the ligands, substrates, and binding site surfaces. The sum of Van der Waals interactions, the addition of coulombic interactions, and the hydrogen bonds are approximated by a docking score which shows the binding potential (Pagadala, Syed, and Tuszynski 2017).

In a standard docking methodology, ligands are freely docked into a receptor, the side chain flexibility plays a vital role in ligand-protein and ligand- enzyme complexes. A functional group/ligand in a (6+ N) –dimensional space of rotational, conformational, and translational variables in the anisotropic surface of the receptor (Moon, Howe and Bioinformatics 1991; Nishibata and Itai 1993; Rotstein and Murcko 1993; Jackson, Gabb and Sternberg 1998). A docking protocol of high-resolution is needed to understand the basic principles to detect the mechanism of protein-protein interactions with other proteins and enzyme-enzyme interactions with other enzymes.

CHAPTER 4: MATERIALS AND METHODS

This chapter outlines, instrumentation, chemicals and reagents, preparation of supporting electrolyte, methods of preparation of standard solutions, methods of electrode modification, real sample preparation, and computational protocols used in this study.

4.1. Experimental

4.1.1. Chemicals and reagents

A standard solution of NTM (98.0% purity, Cas no. 165450-17-9), 20-30% MWCNTs basis with 0.D X l 7-12 nm x 0.5-10 µm (Cas no. 308068-56-6), a solution of graphene oxide 2 $mgmL^{-1}$, dispersion in H_2O (Mean sheet diameter: 22 µm, 90% below 50 µm by laser diffraction), gold (III) chloride hydrate (99.99% purity, Cas no. 27988-77-8), nickel nitrate hexahydrate (99.99% purity, Cas no 13478-00-7), an oxidase solution from Pichia pastoris (CAS no. 9073-63-6) and Carboxylesterase from porcine liver – lyophilized (Cas no. 9016-18-6) were obtained from Sigma Aldrich, South Africa (SA). The analytical grade dimethylformamide, methanol sodium hydrogen phosphate, and sodium dihydrogen orthophosphate were bought from Merck, SA. High-quality sodium hydroxide and hydrochloric acid were purchased from Capital Lab Supplies CC (Durban, SA). An alumina powder ≤ 3.0 µm was supplied by Metrohm, SA. Nitrogen gas of 99.9% purity was supplied by AFROX (Durban, SA). Fanta orange cool drink (The Coca Cola Company, Atlanta, Georgia), red grape juice, and apple juice (The Rhodes Food Group, Western Cape, South Africa) were purchased from a local supermarket. All samples and solutions were prepared with deionized distilled water from an aqua MAXTM-Basic 360 series water purification system supplied by TRILAB

SUPPORT Durban (SA). All standard solutions were kept in the refrigerator at 4° C for stability.

4.1.2. Instrumentation

All electrochemical quantifications were executed using a 797 VA Computrace from Metrohm (Herisau, Switzerland) equipped with the Computrace 1.3.1 software. The data of voltammograms were recorded at room temperature using a three electrodes system consisting of a modified glassy carbon electrode (GCE) with 3.0 mm diameter as a working electrode, the platinum wire as an auxiliary electrode, and the Ag/AgCl (3 M KCl) as a reference electrode. The examined solutions were initially purged for 10 min with 99.9% pure nitrogen gas. The pH was adjusted using a CRISON micro pH 2000 digital meter. The UV-Vis spectra of the biosynthesized nanoparticles were characterized using Varian Cary 50 UV-Vis Spectrometer. The particle size of the biosynthesized nanoparticles was detected using the Perkin Elmer NexION 2000 ICP-MS equipped with the Syngistix Nano module software. The geometric diameter of the biosynthesized nanoparticles was determined using the Asymmetric Flow (AF4) with a model AF2000 Multiflow supplied by Postnova Analytics equipped with the AF2000 software. The morphology studies of biosynthesized nanoparticles were carried out using the transmittance electron microscope model JEM 2100 equipped with a LaB_6 emitter (MAX OXFORD instruments). The STAR^e system of the TGA/DSC 1 SF/1346 model was supplied with STAR^e software version 9.20 by METTLER TOLODO (Johannesburg, SA) for thermogravimetric analysis. A Labcon 5019 U ultrasonic bath was used to sonicate all solutions.

4.1.3. Methodology

4.1.3.1. Biosynthesis of AuNPs

An aqueous *aloe vera* extract was used as a reductant. To prepare the extract, 2.0 g of *aloe vera* was soaked into 20 mL of deionized water overnight and it was then crushed into small pieces while it is still in the deionized water to extract its juice from the leaf. The deionized water containing the *aloe vera juice* was boiled for 10-15 min at 70-80 °C. The extract was left to cool so that 15 mL of the extract can be centrifuged for 15 min at 5000 rpm, the standard sterilized filtration method was applied during the filtration of the collected supernatant. The *aloe vera* extract was stored in the refrigerator at 4 °C for future use. The *aloe vera* aqueous extract was added to a 1 mM $HAuCl_4$ aqueous solution at three different concentrations using a v/v ratio (1:1, 5:1, 10:1) while stirring at 200 rpm at room temperature for 1 h during optimization. The solution changed from yellow to grey within 5 min, indicating the formation of gold nanoparticles.

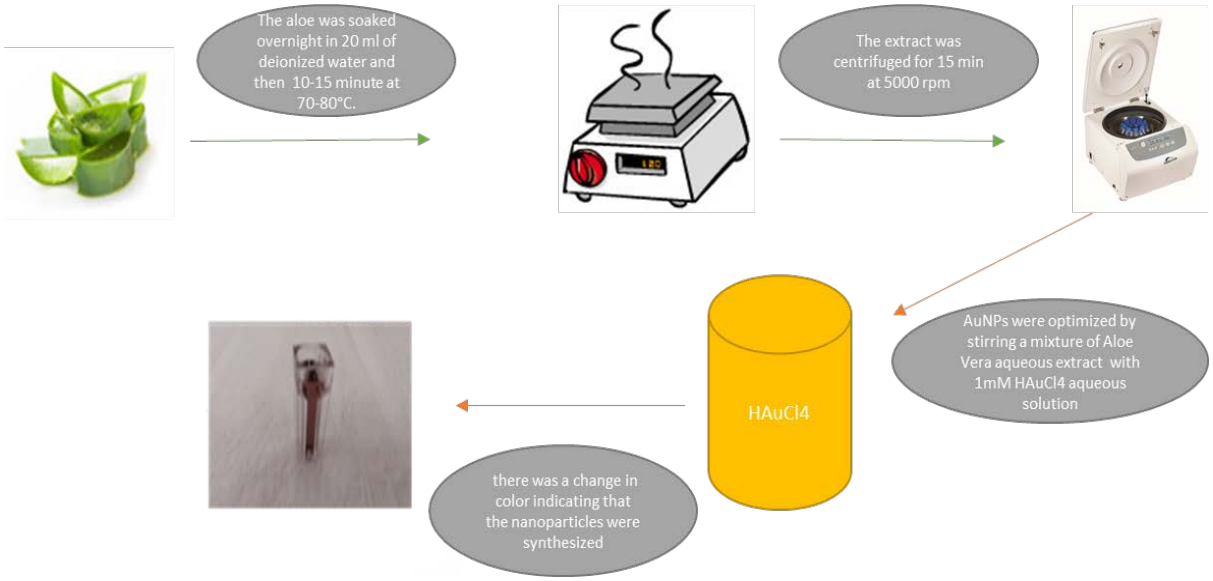

Figure 4-1: A representation of the hydrothermal synthesis of gold nanoparticles capped with aloe-vera extract was redrawn from (Muralikrishna et al. 2014).

4.1.3.2. Biosynthesis of NiNPs

An aqueous *honey* extract used as a reducing agent was prepared by weighing 20 g of honey into 80 mL of deionized water. The mixture was boiled for 15 min at 70 ° C. A clear yellowish solution was formed, and the solution was left to cool at room temperature. The extract was stored at 4 °C for future use. The honey aqueous solution was mixed with 1 mM nickel nitrate hexahydrate aqueous solution using a v/v ratio (1:1, 5:1, 10:1) and was left to stir at 200 rpm at room temperature for 1 h. Within a few minutes, the solution changed from yellow-green to a light lime colour indicating that the formation of NiNPs.

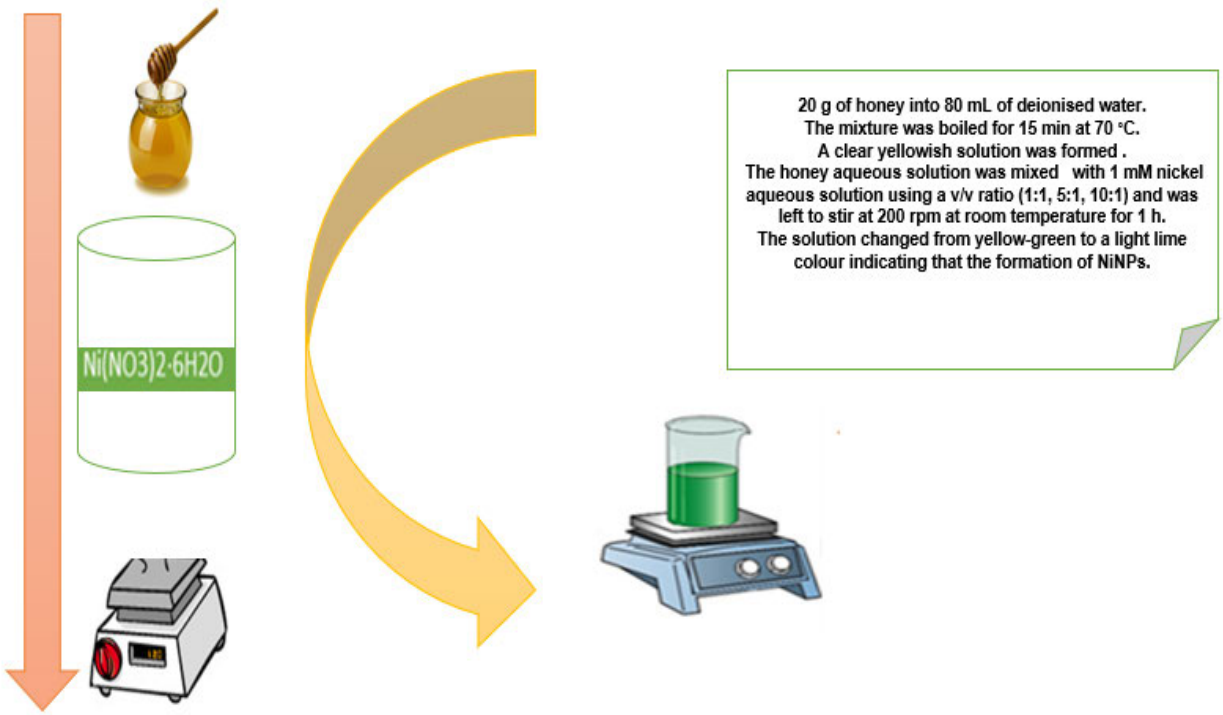

Figure 4-2: A representation of the hydrothermal synthesis of nickel nanoparticles capped with a honey solution was redrawn from (Beshkar and Salavati-Niasari 2015).

4.1.3.3. Characterization of the biosynthesized nanoparticles

This section involves theoretical principles of characterization methods and techniques that were employed for the characterization of the nanomaterials which include UV, spICP-MS, TEM, TGA, and FFF.

4.1.3.3.1. UV-Visible Spectroscopy

A single beam Varian Cary 50 UV-Vis Spectrometer was used for attaining optical properties of the synthesized AuNPs capped with *Aloe Vera* extract and NiNPs capped with *honey* extract at a wavelength range of 200 nm to 800 nm. During this procedure, a blank and a sample solution were placed separately in a glass cuvette, which was then placed into the radiation path within the spectrometer.

4.1.3.3.2. Single Particle Inductively Coupled Plasma- Mass Spectrometry

The characteristics (particle size, particle size distribution, and concentration) of the synthesized nanomaterials were determined using the spICP-MS. The apparatus was operated in single-particle mode using the Syngistix Nano module software. Single-particle mode analysis allowed the differentiation between the nanoparticle analyte and the dissolved while assessing agglomeration of the nanoparticles in the process of measuring the nanoparticle size and size distribution.

4.1.3.3.3. Transmission Emission Microscopy

The morphology of the nanoparticles was studied using a JEM 2100 equipped with a LaB_6 emitter (MAX OXFORD instrument. A transmission emission microscope was used for optical microscopic viewing of the nanoparticles at an acceleration voltage of

200 kV. The samples were prepared in ethanol and sonicated for 45 min before the microscopic analysis.

4.1.3.3.4. Thermogravimetric Analysis

The thermal stability of the nanomaterials was studied using the STAR^{e} system of TGA/DSC 1 SF/1346 model thermogravimetric analysis. Nitrogen gas was utilized to purge the system and the TGA was calibrated using indium standards. The mass loss of the sample was observed as the temperature was increased from 0 ^{o}C to 1000 ^{o}C.

4.1.3.3.5. Field-Flow Fractionation

To separate the nanoparticle mixtures into individual components, an Asymmetric Field-Flow Fractionation (AF4) was used. The nanoparticles were suspended in 0.2% NovaChem during the particle size characterization. The AF4 separates the particles and the sample molecules according to their hydrodynamic size/ molecular weight.

4.1.3.4. Preparation of NTM standard, supporting electrolyte and spiked samples

0.5 mM standard solution of NTM was prepared by weighing an equivalent amount in a 5.0 mL volumetric flask and diluted using 20% methanol. 1.0 M phosphate buffer was prepared by dissolving an equivalent amount of sodium dihydrogen orthophosphate and di-sodium hydrogen phosphate in 1 L of deionized water. 4 mL of HCl was used to adjust 200 mL of buffer to optimum pH 2.0, the adjusted buffer was stored at 4 °C. The spiked NTM samples (1120 µg L^{-1}, 1870 µg L^{-1}, 2610 µg $L^{-1,}$ and 2980 µg L^{-1}) were prepared with Fanta orange cool drink, red grape juice, and apple juice. The spiked samples were prepared by the direct dissolution of the adjusted phosphate buffer in a 10 mL volumetric flask with the real samples mentioned above.

Red grape, Fanta orange soft drink, and apple juice were used after being diluted with deionized water and adjusted to the relevant pH using 1.0 M HCl.

4.1.3.5. Preparation of carboxylesterase enzyme and alcohol oxidase enzyme solution.

An oxidase solution from Pichia pastoris was diluted using a 50 mM phosphate buffer at pH 7.5 to make a 100 mL solution. An esterase solution from porcine liver – lyophilized was diluted using a 50 mM phosphate buffer at pH 7.5 to make a 100 mL solution.

4.1.3.6. Preparation and fabrication of CaE/AuNPs/MWCNTs modified GCE

A bare glassy carbon electrode was polished with ≤ 3 µm alumina slurry and then rinsed with deionized distilled water followed by electrochemical cleaning by cycling at a potential range of -1.0 to +0.20 V for 30 cycles in an acidified deionized distilled water to remove any physisorbed or chemisorbed materials from the surface of the electrode (Bathinapatla *et al.* 2015a). 0.3 g of MWCNTs was added to 3.0 mL of dimethylformamide followed by 2.0 mL of biosynthesized AuNPs to prepare a paste of AuNPs/MWCNTs. The mixture was sonicated for 30 min at 60 °C until a black dispersion of AuNPs/MWCNTs was obtained. 5.0 µL of the nanocomposite paste was coated on the GCE and 0.2 µL of the CaE prepared in 50 mM phosphate buffer was immobilized on the GCE modified AuNPs/MWCNTs. The fabricated electrode was oven-dried at 35 ℃ for 15 min. After cooling to room temperature, the modified electrode was ready for use.

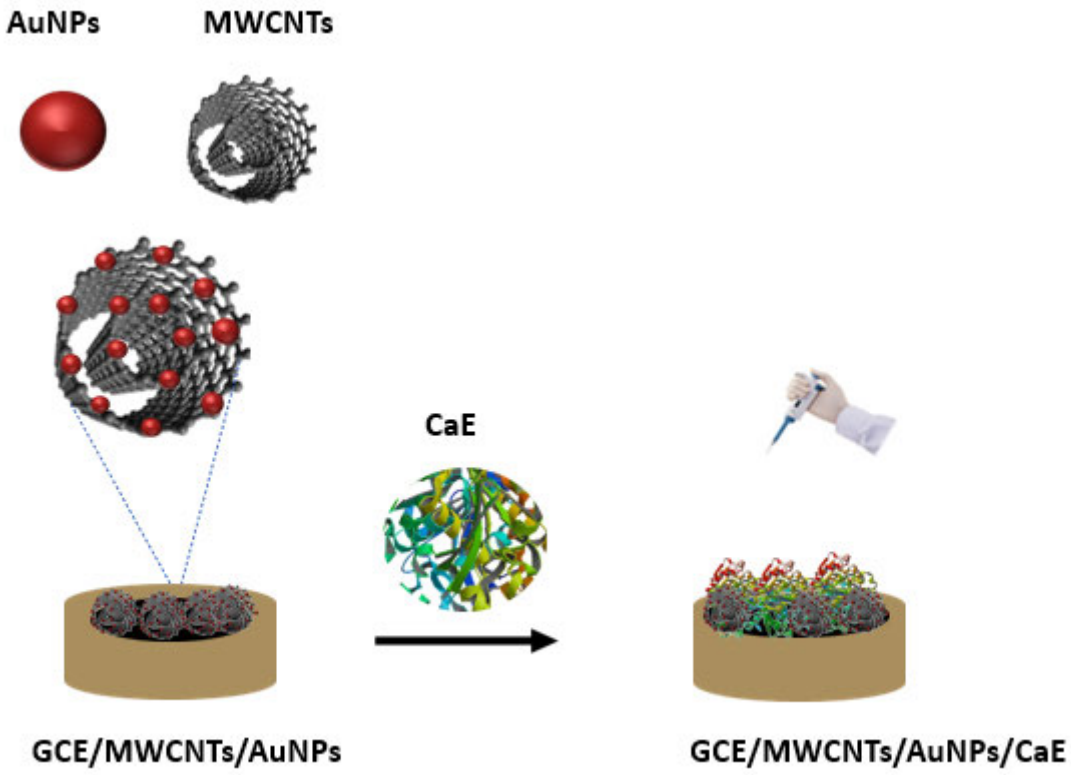

Figure 4-3: A schematic representation of the fabrication of the CaE/AuNPs/MWCNTs modified GCE for the detection of NTM was redrawn from *(Yan et al. 2020).*

4.1.3.7. Preparation and fabrication of AOx/NiNPs/GO modified GCE

3 mL of graphene oxide, 2 mL of capped NiNPs, and 2 mL of the oxidase solution were mixed until a brownish dispersion of AOx/NiNPs/GO called a nanocomposite paste was obtained. A bare glassy carbon electrode was polished carefully with ≤ 3 µm alumina slurry and then rinsed with distilled water followed by electrochemical cleaning by cycling at a potential range of -1.0 to +0.20 V for 30 cycles in acidified distilled water. Thereafter, the GCE was coated with 5.0 µL of nanocomposite paste and oven-dried at 35 °C for 15 mins. The modified electrode was cooled at room temperature and was ready for use.

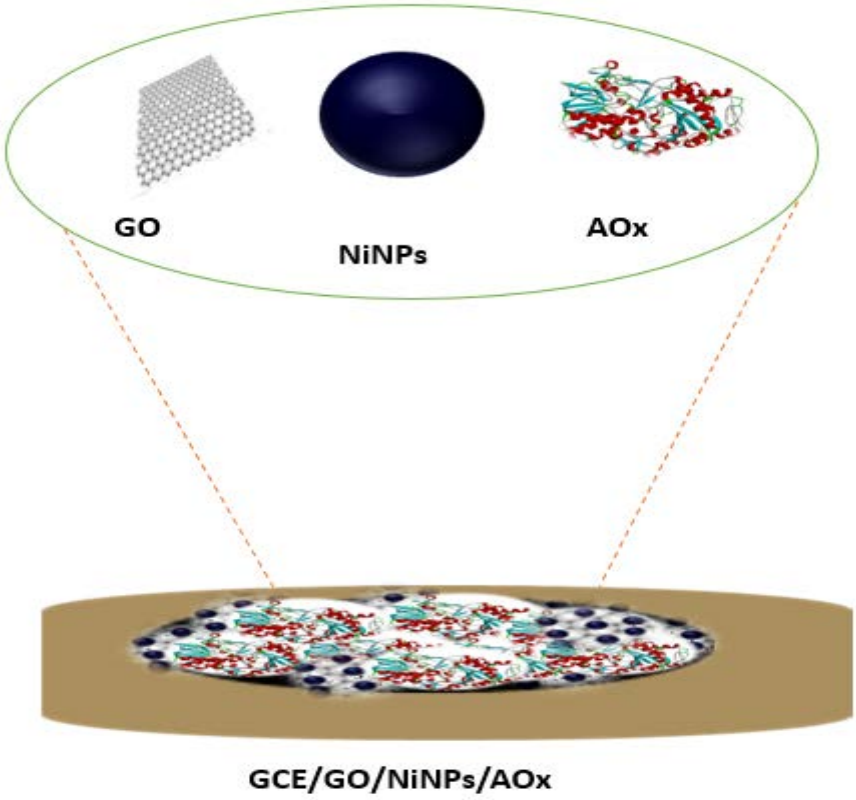

Figure 4-4: A schematic representation of the fabrication of the AOx/NiNPs/GO modified GCE for the detection of NTM was drawn from *(Yan et al. 2020)*.

4.1.3.8. Electrochemical detection with CaE/AuNPs/MWCNTs modified GCE and AOx/NiNPs/GO modified GCE

10 mL of the phosphate buffer was added into the electrochemical cell in which the bare GCE or the modified electrode was submerged before the electrochemical detections. 10 cyclic sweeps were applied to attain a low background current. 20 µL of the analyte solution was added into the electrochemical cell, and a pre-concentration potential of 1.3 V was applied to the working electrode, while the solution was stirred at 400 rpm during the deposition process. After the pre-concentration stage, stirring was stopped and the solution equilibrated for 5 s. The raw data of voltammograms were then recorded by scanning the potential towards the positive

direction using differential pulse or linear sweep potential at the scanning rate of 0.1 Vs^{-1} (Bathinapatla *et al.* 2015a).

4.2. Computational Methods

4.2.1. Template selection

The two proteins were extracted from the RCSB Protein database (Hasenpusch, Bornscheuer, and Langel 2011) and were modelled by homology modelling using Chimera software as an interface to the modeller software 9.1 (Takeda-Shitaka *et al.* 2005).

4.2.2. Computational protocols

The structures of Carboxylesterase from the porcine liver and Alcohol oxidase from Pichia pastoris obtained from the protein database (PDB IDs: 5FV4 and 5HSA, respectively) showed discontinuity in the structural coordinates. Hence the structures of the two proteins had to be minimized and remodelled. Density functional theory (DFT) calculations on the 3D structure of NTM geometrically optimized at the B3LPY level using the 6-311+G basis sets were implemented using Gaussian 09 (Frisch et al 2016). The nanomaterial-based structures such as gold nanoclusters, nickel nanoclusters, multiwalled carbon nanotubes, and graphene oxide were formulated using the Gauss view program present in Material Studio (MS) (Reyes *et al.* 2011). B3LPY level of theory using $DMOI^3$ module of MS was used to perform DFT calculations. Chimera software and AutoDock Vina (Wang *et al.* 2016) was used to dock the described proteins along with the optimized structure of NTM. AutoDock executes the prediction of the bound conformation based on the free energy force field

coupled with the Lamarckian Genetic Algorithm (Morris *et al.* 2009). CDOCKER module and Chemistry at Harvard Macromolecular Mechanics (CHARMM) (Parthasarathy, TV and Wellness 2019) were used to validate the docking scores based on the docking algorithm (Vanommeslaeghe *et al.* 2010).

4.2.3. Adsorption studies using molecular modeling

Adsorption locator and Forcite modules in Materials Studio (MS) were used to carry out adsorption studies (Kirkpatrick, Gelatt and Vecchi 1983; Bunte and Sun 2000). The nanomaterials were geometrically optimized with Forcite Module with the Condensed-phase Optimized Molecular Potentials for Atomistic Simulation Studies (COMPASS) forcefields to get the energy of minimized structures. (Ulicny and Kozar 2018).

4.2.4. Construction of nanoclusters

The MWCNTs, GO, nickel nanoparticles (Ni), and the gold nanoparticles (Au) were constructed using the Build option conforming to the standard library of parameters of the Material Studio (MS) software package developed by BIOVIA (Ulicny and Kozar 2018). For observing the feasibility of the nanostructures, and energy minimization for each was performed followed by a geometry optimization using the Forcite module with an ultrafine-COMPASS force field (Sun 1998). The convergence criteria for the maximum values of energy alteration, force, stress, and displacement were set at 2x 10^{-5} kcal mol^{-1}, 0.001 kcal $(molÅ)^{-1}$, 0.001 GPa, and 10^{-5} Å.

CHAPTER 5: RESULTS AND DISCUSSIONS

This chapter provides experimental outcomes obtained using the CaE/AuNPs/MWCNTs modified GCE and AOx/NiNPS/GO GCE. This chapter is divided into 2 sections (Sensor 1 and Sensor 2). Computational work was carried out to get a better understanding of the conformational profile of the NTM-CaE enzyme and NTM-AOx enzyme. Furthermore, the interaction studies were helpful to get a better understanding of the interactions between the enzymes, nanomaterials, and NTM. HOMO-LUMO calculations were executed to assess the redox ability of NTM.

5.1. Sensor 1: Detection of NTM using CaE/AuNPs/ MWCNTs modified GCE

5.1.1. Characterization of *aloe vera*-capped AuNPs

A UV-Vis spectrum monitored the reduction of Au(III) to Au(0). There was a single SPR peak at 550 nm which confirmed the shape of biosynthesized AuNPs as spherical and monodispersed in an aqueous solution (Malarkodi *et al.* 2013; Yadav 2018) as displayed in Figure 5-1A(i).

Precise size distribution was obtained using the AF4 in combination with the MALS detector. The AF4-MALS technique analyses the radius of gyration, (r_g), and the average geometric diameter (D_{geo}) of the nanoparticles over the whole elution time. It is shown in Figure 5-1A(ii) that a separation peak of the biosynthesized AuNPs has an elution time between 13 to 19 min. The size distribution curve of the biosynthesized AuNPs reveals the uniform distribution of the AuNPs. The calculated r_g and D_h for the biosynthesized AuNPs corresponding to a sphere fit formalism in MALS were 36.9 nm and 95.22 nm respectively using the formula:

$$D_{geo} = \frac{rg}{0.775} \; x \; 2 \qquad \textbf{[Eqn 5.1]}$$

The single-particle inductively coupled plasma-mass spectroscopy (spICP-MS) is a specific model of the ICP-MS operation, which enables the detection of single particles. The spICP-MS mode was used to determine the average particle size and distribution of the biosynthesized AuNPs. The intensity of the pulse created by a single particle as a function of the number of atoms in a nanoparticulate is illustrated in Figure 5-1A(iii). The results suggested that the maximum intensity signals were observed between 50 to 65 nm, resulting in average particle size of 61 nm. The spICP-MS and AF4/MALS gave information about the particle size and distribution of the whole sample, TEM determined the size, chemistry, and morphology of a single particle. The TEM image of MWCNTs demonstrated the hollow cylindrically shape as illustrated in Figure 5-1A(iv).

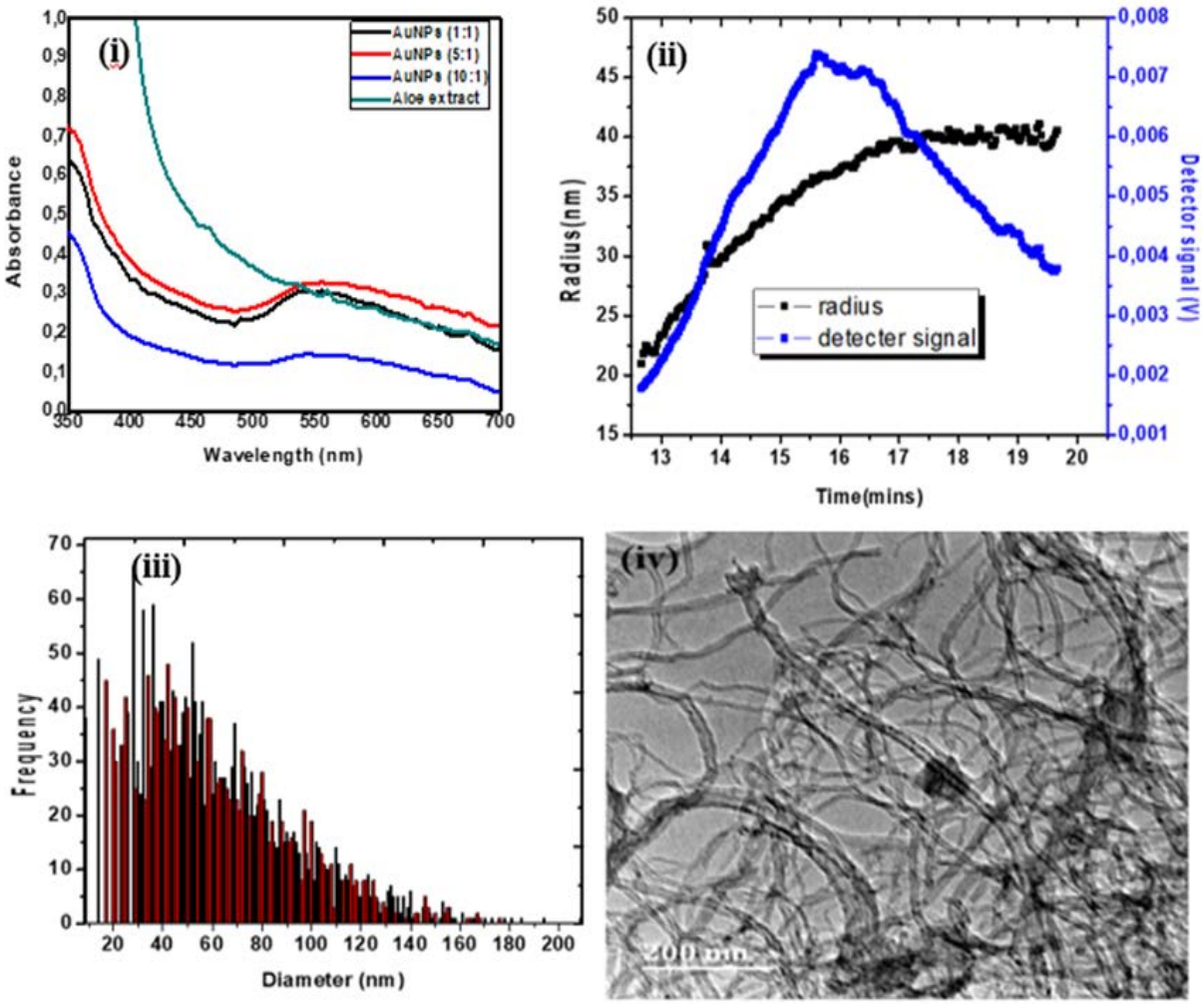

Figure 5-1A: (i) UV-Vis spectrum of the biosynthesized AuNPs showing a broad absorption peak at a wavelength of 540 nm, (ii) Hydrodynamic size characterization and particle size distribution of biosynthesized AuNPs with AF4-MALS, (iii) Average size determination of biosynthesized AuNPs with spICP-MS, (iv) TEM images of MWCNTs biosynthesized AuNPs using aloe vera extract.

The TEM images of the *aloe vera*-derived AuNPs (Figure 5-1B(i)) showed the distribution and morphology of the biosynthesized AuNPs. An HR-TEM image (Figure 5-1B(ii)) of the *aloe vera*-capped AuNPs (10 nm magnification) resulted in the clear visualization of lattice fringes on the surface of the biosynthesized AuNPs. The lattice fringes portrayed a spacing of 0.238 nm which corresponded to the spacing between (1 1 1) plane of the face-centred cubic lattice of Au indicating the highly crystalline nature of the *aloe vera*-capped AuNPs (Kanchi *et al.* 2018). The outcomes demonstrated that the particles are spherical in size and are monodispersed with an

average particle size of 40 nm, in agreement with the narrow size distribution shown in Figure 5-1A(iii) (Chen *et al.* 2006). Figure 5-1B(iii) shows the decoration of biosynthesized AuNPs onto the MWCNTs and reduce AuNPs aggregation, thus improving uniform attachment around the surface of the MWCNTs.

Thermogravimetric analysis (TGA) was executed to assess the thermal stability of the *aloe vera*-capped AuNPs. The TGA curve displayed in Figure 5-1B(iv) shows a 67% weight loss at a temperature range of 25 ^{o}C and 50 ^{o}C due to the bioorganic compounds like proteins and enzymes present on the surface of the extract (Aljabali *et al.* 2018). Then finally, the thermal stability of the sample was observed at the temperature in the range of 330 ^{o}C and 600 ^{o}C.

The *aloe vera-capped* AuNPs were assimilated with MWCNTs to form a nanocomposite to modify the GCE and for the immobilization of CaE to enhance the electrochemical signalling when detecting trace levels of NTM in beverage samples.

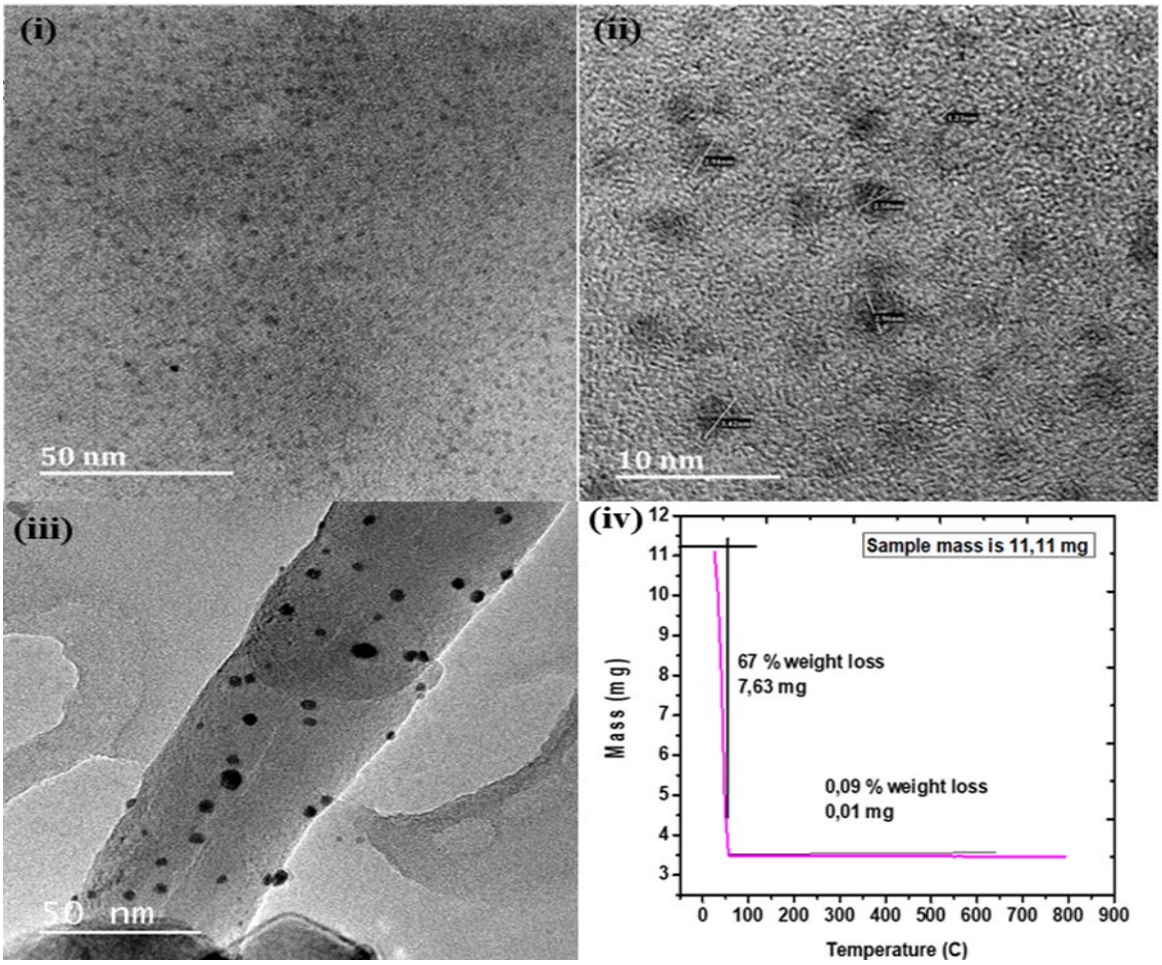

Figure 5-1B: (ii) TEM images of biosynthesized AuNPs using aloe-vera extract; (ii) AuNPs with fringes; (iii) HR-TEM images of biosynthesized AuNPs decorated MWCNTs, and (iv) TGA curve of biosynthesized in a nitrogen atmosphere at a temperature range of 0°C to 600°C.

5.1.2. Electrochemical characterization of the enzymatic biosensor and the behavior of NTM to CaE/AuNPs/MWCNTs modified GCE

CaE was used in the fabrication of GCE using MWCNTs decorated with *aloe vera*-capped AuNPs. MWCNTs were utilized to facilitate the rapid transfer of electrons, to facilitate high surface activity and catalytic efficiency (Fujigaya *et al.* 2008; Vellaichamy *et al.* 2018) while dimethylformamide (DMF) was utilized as a dispersing reagent for the MWCNTs (Balgobind *et al.* 2016; Jiang and Lee 2018). The aloe vera-capped AuNPs were decorated onto the MWCNTs to generate electro-catalytic sites and the CaE was added to increase the detection limits and sensitivity of the biosensor.

The fabricated enzymatic biosensor was characterized by cyclic voltammetry (CV) and the Randles-Sevcik equation (Eqn 3.5) was used to acquire the areas of the bare electrode and the CaE/AuNPs/MWCNTs modified electrode.

The surface areas of the bare GCE and the CaE/AuNPs/MWCNTs modified GCE was determined to be 0.310 cm^{-2} and 0.998 cm^{-2}, respectively. Current-potential responses were measured to evaluate the electrochemical performance of CaE/AuNPs/ MWCNTs/GCE towards the determination of NTM. Figure 5-2A shows a significant enhancement in current responses after modifying with the nanocomposite and immobilizing with CaE. That confirmed that a larger surface area provided by the composite of the nanomaterials allowed more NTM molecules to be oxidized according to the mechanism shown in Scheme 5-1. In this mechanism, NTM undergoes fragmentation to form dimethylbutyl-L-aspartic acid and phenylalanine involving a single proton transfer during the quasi-reversible process. The beginning of dissociation due to acid hydrolysis is shown by the anodic peak at 1.4V in Figure 5-2A as NTM is oxidized on the surface of the CaE/AuNPs/MWCNTs modified GCE resulting in dimethylbutyl-L-aspartic acid and phenylalanine. Furthermore, there was an intense reversible peak at -0.4 V due to the contribution of methanol when a reversible reaction took place.

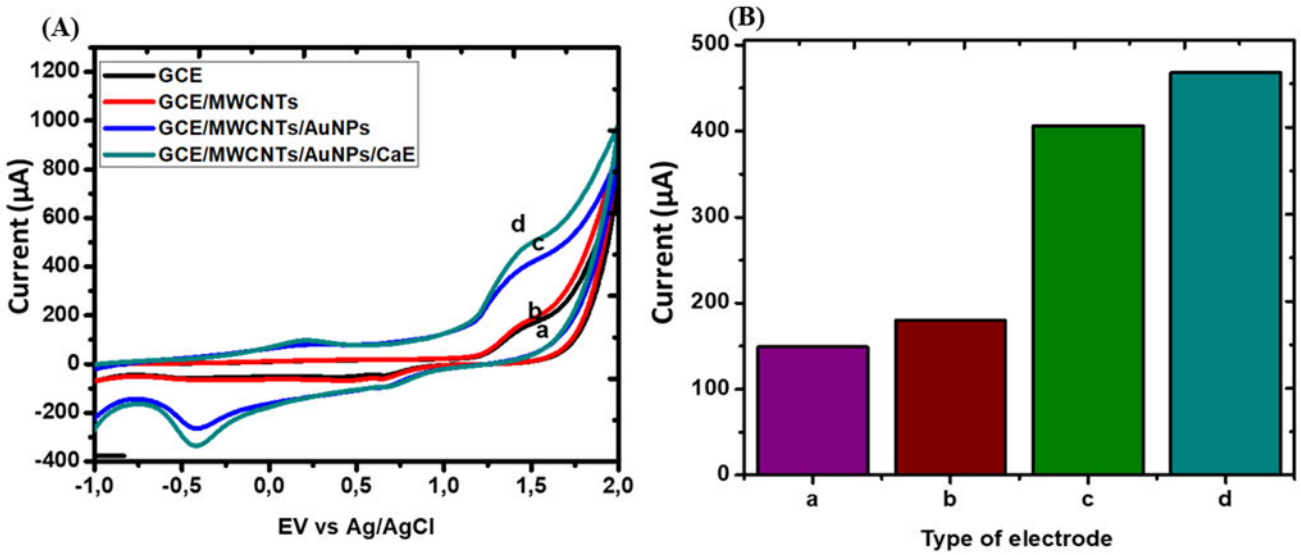

Figure 5-2: (A) Cyclic voltammograms of 0.5 mM NTM at (a) bare GCE, (b) MWCNTs/GCE, (c) AuNPs/MWCNTs/GCE, and (d) CaE/AuNPs/MWCNTs modified GCE. (B) A bar graph displaying the current responses of (a) a bare GCE, (b) MWCNTs/GCE, (c) AuNPs/MWCNTs/GCE and (d) CaE/AuNPs/MWCNTs modified GCE.

A comparative peak current response for the electrodes displayed using a bar graph Figure 5-2B, confirms the catalytic effect of carboxylesterase for the electrochemical oxidation of NTM, due to a 33.33 % amplification of peak signal.

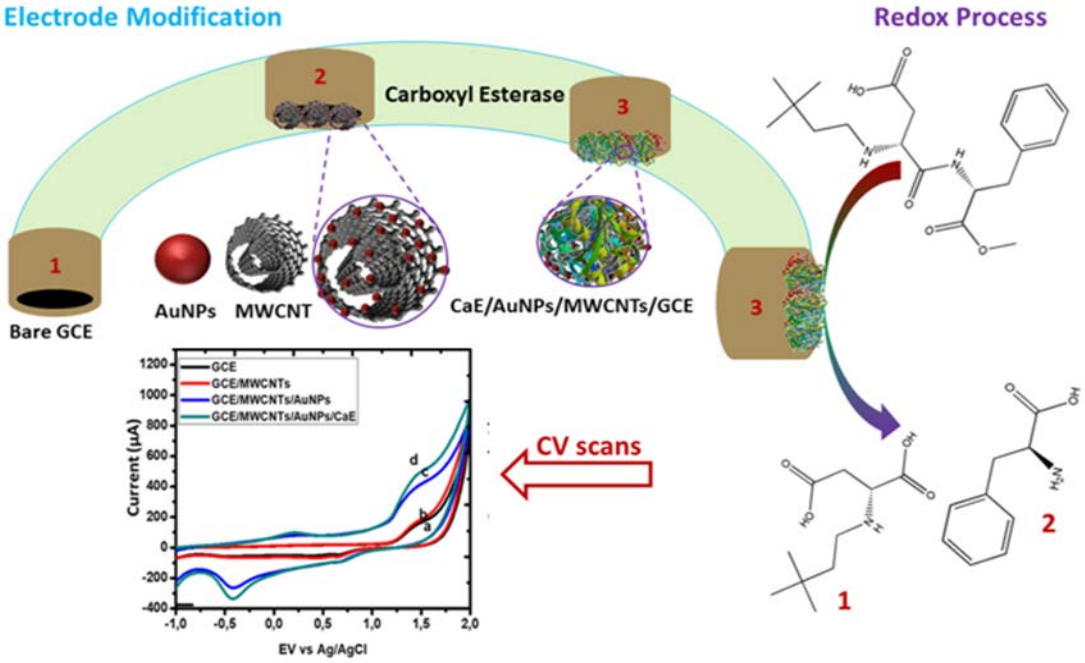

Scheme 5-1: A schematic representation of electro-oxidation of NTM at CaE/AuNPs/MWCNTs modified GCE.

The outcomes from the electrochemical characterization of CaE/AuNPs/MWCNTs modified GCE demonstrated an irreversible mechanism for the oxidation of NTM. The higher anodic peak current was observed with a modified electrode compared to the bare electrode; however, it is necessary to optimize the different experimental parameters including pH, scan rate, and deposition time of the electrochemical oxidation procedure.

5.1.3. Effects of pH, scan rate, and deposition time on the peak potentials and peak currents

The effect of pH was evaluated on the anodic peak potentials and peak currents of NTM using the CV in a buffer solution containing 0.5 mM NTM at a range of 2.0 to 7.0. Figure 5-3A displays the electrochemical behaviour of NTM on the bare GCE at the range of pHs. The anodic peak currents decreased with the increase in pH. This indicated that the peak current responses for the determination of NTM using the CaE/AuNPs/MWCNTs modified GCE were pH-dependent. A higher peak current was observed at pH 2.0, hence it was selected as the optimum pH for the detection of NTM. The scan rate was optimized ranging from 0.01 to 0.21 V s^{-1} to observe its effect on the anodic peak potential and the peak currents as illustrated by the cyclic voltammograms (CV) ranging from 0.01 to 0.21 V s^{-1} in Figure 5-3B. The anodic peak current increased with an increase in scan rates up to 0.21 Vs^{-1} on the modified electrodes and the bare GCE. Figure 5-3C illustrates the effect of deposition time on peak potentials and currents at a range of 30 s to 150 s. The anodic peak current increased with an increase in deposition time on the modified electrodes. Even though the maximum peak for the bare and modified electrodes was observed at 150 s, the deposition time of the 30 s was chosen as an optimum.

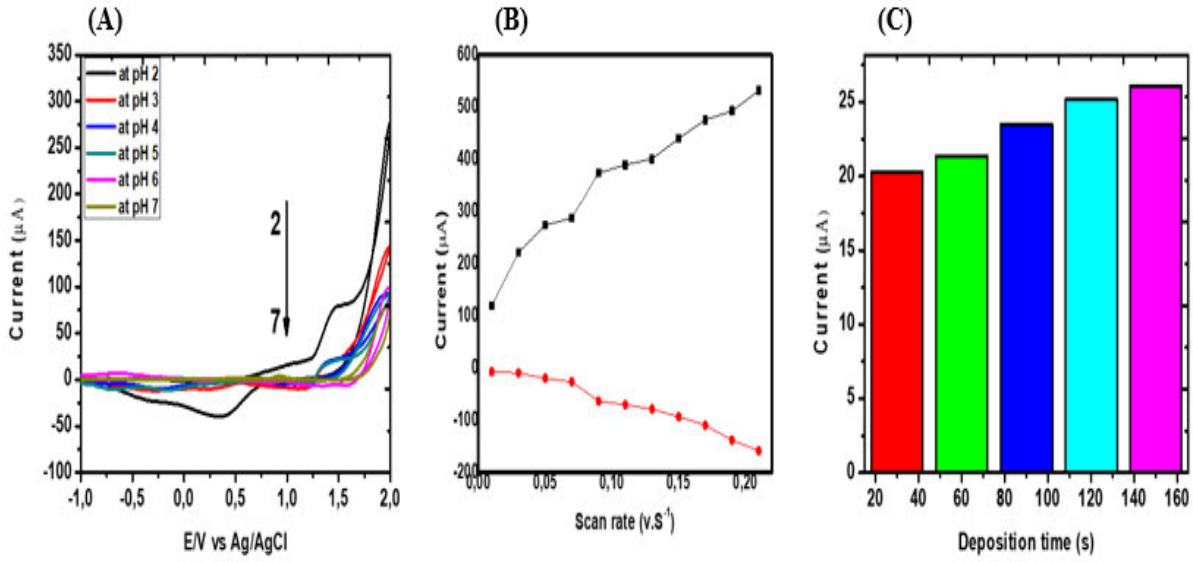

Figure 5-3: (A) Current responses were observed with respect to change in pH with 0.5 mM NTM, (B) Plots of the scan rate from 0.1 V.s -1 are displayed to show current responses, (C) A bar graph shows the effect of deposition time on peak current at the 30 s and 150 s.

5.1.4. DPV technique for quantitative detection of NTM

Differential pulse voltammetry (DPV) has proven to yield better peak separations; hence, it was used for the sensitive detection of NTM using the nanocomposite CaE/AuNPs/MWCNT modified GCE in the presence of a PSB (pH 2.0). A fixed anodic peak was obtained at the modified GCE indicating a better absorption of methanol and oxidation of NTM on the CaE/AuNPs/MWCNTs modified GCE as illustrated in Figure 5-6A.

The DPV signals for the different concentrations of NTM using CaE/AuNPs/MWCNTs modified GCE in 0.1 M PSB (pH 2.0) shows a linear relationship between the anodic peak and the concentrations of NTM observed in the concentration ranging from 1120 µg L^{-1} to 3340 µg L^{-1}. The calibration curve of I_{pa} = 53.18 x + 89.44 as displayed in Figure 5-6B was linear with R^2 of 0.9829 with a limit of detection (LOD) of 27 µg L^{-1} and a limit of quantification (LOQ) of 83 µg L^{-1}. These outcomes revealed that the

developed electrochemical enzymatic sensor is efficient and suitable for the determination of NTM in soft drink samples.

5.1.5. Stability, recovery, accuracy, and precision studies

In this work, the stability of the CaE/AuNPs/MWCNTs modified GCE was studied in a PSB (pH 2.0) by determining the responses in 0.5 mM NTM for 10 runs using the same coating on the electrode. The developed biosensor maintained 90%, 88%, 85%, 50% of the original response after run 1-4 respectively, however, there was a sudden drop in current and a shift of the anodic peak of NTM after the 5^{th} run, hence the developed biosensor was stable up to 4 runs on the same day with the same coating on the electrode. The precision, accuracy, and recovery were measured by analyzing three different concentrations of standard NTM ranging from 1120 µg L^{-1} to 2610 µg L^{-1} in three measurements in one day. In Table 5-1, we show that the range of values for the % RSD and relative error were 0.81 to 1.04 and -1.0 to -3.6 respectively. The percentage recoveries of NTM using the modified electrode ranged from 96% to 99%. These outcomes demonstrated that the developed enzymatic sensor showed higher accuracy and precision, hence this confirmed its suitability for the analysis of NTM in real beverage samples.

Table 5-1: Analytical parameters in the terms of precision, stability, accuracy, and recovery obtained for the detection of NTM using CaE/AuNPs/MWCNTs modified GCE.

Stability	**NTM**	**NTM**	**Analytical parameters**		
Peak response[a] (I_{pa})	**Added** (µg/L)	**Found** (µg/L)	**Relative error[b]**	**Recovery** (%)	**RSD[c]** (%)
147	1120	1080	-3.6	96	1.04
188	1870	1850	-1.0	99	0.81
225	2610	2550	-2.3	98	0.88

[a] Average of three measurements, [b] relative error = (DPV value – added value/ added value) x 100, [c] relative standard deviation for the three measurements.

5.1.6 Real samples studies

This biosensor was employed for the detection of NTM in the real beverage samples. The beverage samples were spiked with these different concentrations of standard NTM solution and then the CaE/AuNPs/MWCNTs modified GCE was used to measure the total amount of NTM under optimum conditions. By comparing the responses of three different concentrations for apple juice, Fanta orange, and red grape juice, the relative standard deviation (RSD) of the measurements (n=3) was calculated to be at the range of 0.80 to 1.47, 1.60 to 1.97, and 2.03 to 2.48, respectively. This suggested that this modified electrode is highly reproducible. The recovery was between 89% to 99% suggesting that the determination of NTM using the modified electrode was effective and sensitive. These outcomes describe that the enzymatic biosensor has the capability of determining NTM in soft drink samples as illustrated in Table 5-2.

Table 5-2: Corresponding results for the detection of NTM in spiked beverage samples analyzed using the CaE/AuNPs/MWCNTs modified GCE.

Sample	Added NTM (µg/L)	Recovery (%)	RSD [a] (%)	Relative error [b]
APPLE JUICE				
Spiked sample 1	1870	91	1.31	-8.56
Spiked sample 2	2610	99	0.80	-0.77
Spiked sample 3	2980	92	1.47	-7.05
FANTA ORANGE				
Spiked sample 1	1120	98	1.68	-1.79
Spiked sample 2	1870	93	1.97	-7.49
Spiked sample 3	2610	95	1.60	-5.63
RED GRAPE JUICE				
Spiked sample 1	1870	89	2.48	-10.70
Spiked sample 2	2610	91	2.16	-8.05
Spiked sample 3	2980	95	2.03	-4.36

[a] Average of three measurements, [b] relative error = (DPV value – added value/ added value) x 100.

5.1.7. Effect of interferents on the detection of NTM

Possible interferent compounds such as sucralose, glucose, and ascorbic acid were added together with 0.5 mM NTM standard solution to test the selectivity of CaE/AuNPs/MWCNTs modified GCE nanocomposite. The DPV was employed to carry out this study and the outcomes revealed that the glucose and ascorbic acid anodic peak potentials were observed at -0.7 V, and 0.2 V respectively as shown in Appendix 3A. Nevertheless, the presence of the above-mentioned interferents did not affect the detection of NTM. These results confirm that the CaE immobilized on the surface of the GCE modified with AuNPs/MWCNTs has shown selectivity and

sensitivity in the sensing of NTM, due to selective interaction of CaE with the analyte in conjunction with the high surface area of the *aloe vera*- capped AuNPs.

5.1.8 Stability of the electrode for detection of NTM in real samples

The stability of the CaE/AuNPs/MWCNTs modified GCE was studied in the phosphate buffer (pH 2) by determining the responses in three different concentrations of NTM in apple juice, Fanta orange, and red grape juice at a range of 10 runs using the same coating on the electrode. The voltammograms in Appendix 1A (Figures 1A, B, and C) showed that there was a shift in the anodic peak and a sudden drop of current due to the saturation of the electrode. Figures 5-4A, 5-4B, and 5-4C show that the initial response diminished rapidly, however, the electrode was stable enough to run three runs for the three different concentrations as mentioned below. the surface of the electrode started fouling due to the residues of NTM so that made the transfer of electrons to be difficult during the fourth run. Electrode fouling is the passivation of the electrode surface by the adsorption of non-electroactive species. This leads to a decreasing biosensor response over time (Geise *et al.* 1991). The electrode should be polished before the fourth determination, as the residues of NTM on the surface of the electrode will influence the fourth measurement. To find similar NTM oxidation peak currents, it is necessary to polish the surface of the electrode with ≤ 3 μm alumina slurry and then rinse with deionized distilled water after the third run.

Figure 5-4A (i, ii, and iii) displays the responses of apple juice samples at a concentration of 1.87 ppm, 2.61 ppm, and 2.98 ppm of NTM respectively.

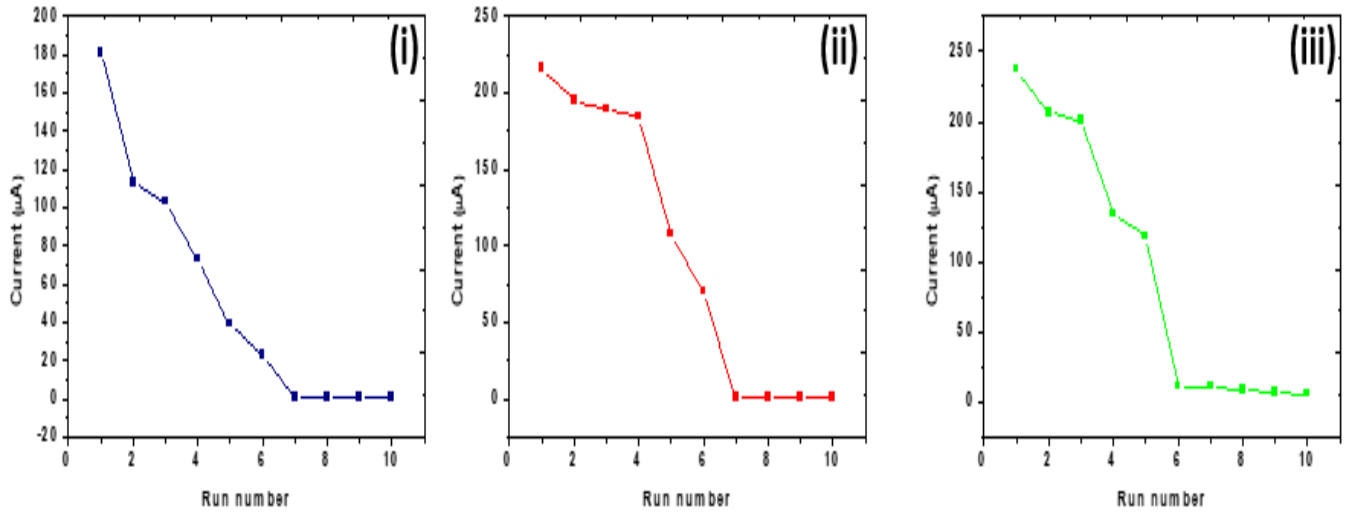

Figure 5-4A: Line graphs displaying the response of NTM in apple juice sample (i)1.87 ppm; (ii) 2.61 ppm (iii) 2.98 ppm.

Figure 5-4B (i, ii, and iii) displays the responses of Fanta orange samples at a concentration of 1.12 ppm, 1.87 ppm, and 2.61 ppm of NTM respectively.

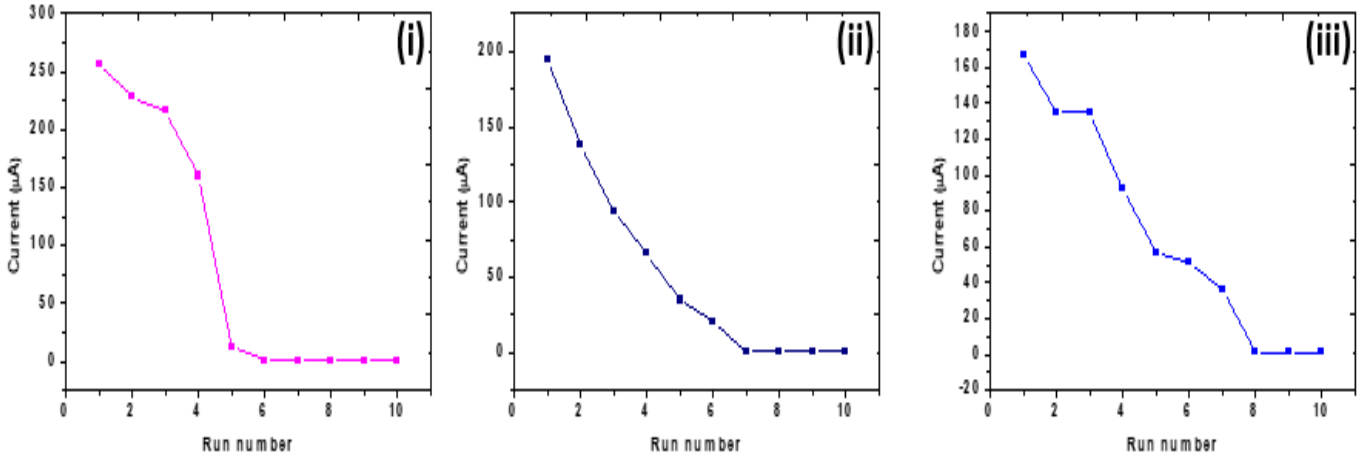

Figure 5-4B: Line graphs displaying the response of NTM in Fanta orange sample (i)1.12 ppm; (ii) 1.87 ppm (iii) 2.61 ppm.

Figure 5-4C (i, ii, and iii) displays the responses of red grape juice samples at a concentration of 1.87 ppm, 2.61 ppm, and 2.98 ppm of NTM respectively.

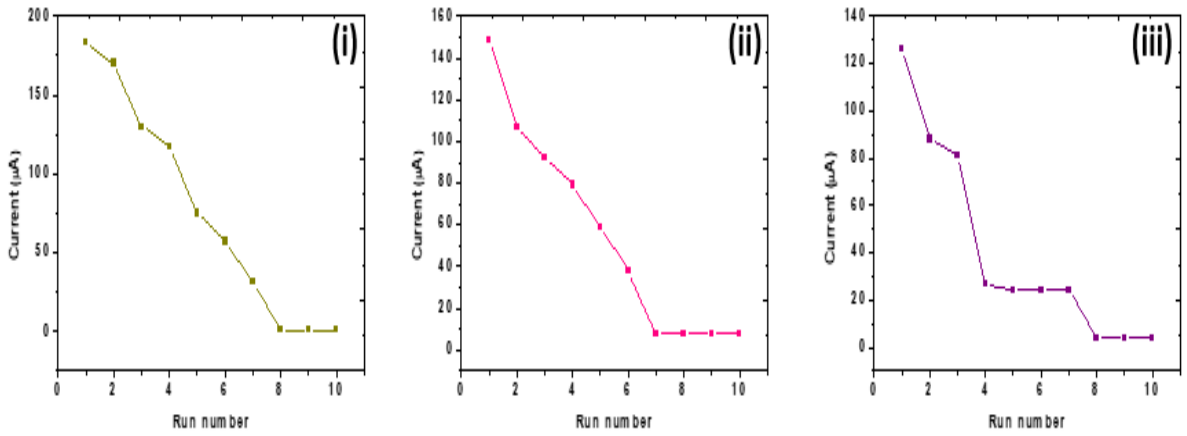

Figure 5-4C: Line graphs displaying the response of NTM in red grapes juice sample (i)1.87 ppm; (ii) 2.61 ppm (iii) 2.98 ppm.

In this study, computational tools were employed for a better understanding of the interaction of the nanomaterials with the surface modification of the electrode surface, and the outcomes are exhibited below.

5.1.9. Computational section

5.1.9.1. Homology modeling

Pig liver esterase (PEG) is a trimer, derived from human carboxylesterase (hCaE). This enzyme is used as a biocatalyst in organic synthesis processes. The crystal structure of the carboxylesterase enzyme was obtained from the RCSB Protein Data Bank (5fV4) (Hasenpusch, Bornscheuer and Langel 2011) in a complex form. It was revealed that the protein has 6 segments however in this study Segment A (an active

site of the enzyme) was chosen and it gave a docking score of -6.9 when it was docked using Chimera software as an interface to the modeler software.

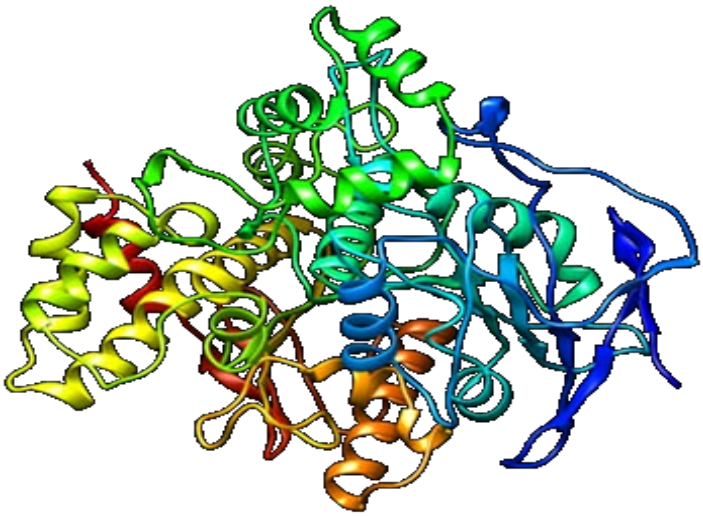

Figure 5-5: A structure of segment A of the described protein.

5.1.9.2. HOMO-LUMO DFT calculations

The highest energy level that is possessed by electrons capable of donating electrons is referred to as the highest occupied molecular orbital (HOMO). The lowest energy that is not occupied by electrons capable of accepting electrons is referred to as the lowest unoccupied molecular orbital (LUMO) (Kavitha, Sundaraganesan and Sebastian 2010). A small energy gap is normally associated with a high chemical reactivity, low kinetic stability, and these molecules are known as "fine molecules" (Orbitals 1976). The HOMO-LUMO calculations performed at the B3LYP 6-311+G level of theory along with the 3D optimized structure of NTM, with an overall energy value -79.4 x 10^4 kcal mol^{-1} are illustrated in Figure 5-6C. The calculated energy values of HOMO and LUMO are -0.32541 eV and 0.14077 eV, respectively. The value of the HOMO-LUMO energy gap is -0.46618 eV as shown in Figure 5-6C. The loosely bound electrons in the HOMO of NTM presented a charge density restricted mainly on the

carboxyl functional group while on the contrary, LUMO was centred upon the amide functional group. Molecular orbitals (MO) energies are used to predict the most reactive position in conjugated systems and to explain different types of chemical reactions (Choudhary *et al.* 2013). It is understood that electron transfer from the HOMO in a molecule is linked to the capability of a molecule to undergo a redox reaction and the electrons will flow to the LUMO throughout the reduction process. Using the DFT, we were able to locate the density of the electrons in the NTM and to verify the active site of NTM based on electron density maps shown in Figure 5-6D(ii). It was expected that the functional groups identified by DFT calculations would agree with the redox mechanism and the extent of HOMO-LUMO band gaps of NTM, indicating the redox ability of NTM. When a reduction process takes place as illustrated in Scheme 5-1 and 5-2, the electrons moved from HOMO to LUMO hence by locating the density of the electrons in NTM the DFT calculations were used to predict the active site of NTM based on the electron density maps. This is demonstrated by the data summarized in Table 5-3 and 5-6, with the corresponding HOMO–LUMO obtained using 6-311+G basis sets displayed in Figure 5-6C.

5.1.9.3. Docking and interaction studies

Scheme 5-1 displays a reversible reduction reaction whereby NTM undergoes oxidation on the surface of CaE/AuNPs/MWCNTs modified GCE, leading to the formation of dimethylbutyl-L-aspartic acid and phenylalanine with the electron density in agreement with the redox mechanism. The chemical interaction between the NTM and CaE was studied as shown in Appendix 2A (adsorbate-substrate system) by docking and interaction studies as displayed in Figure 5-6D(i). The hydrophobic map of the NTM-CaE enzyme complex showed the presence of hydrogen bonds with LEU

249 residue the most favourable, because of a stronger hydrogen bonding with (-CH) NTM followed by GLY251 as illustrated in Figure 5-6D(ii). The outcomes confirmed that the CaE enzyme facilitated the electron transfer from NTM ligand, hence enhancing the biosensing response.

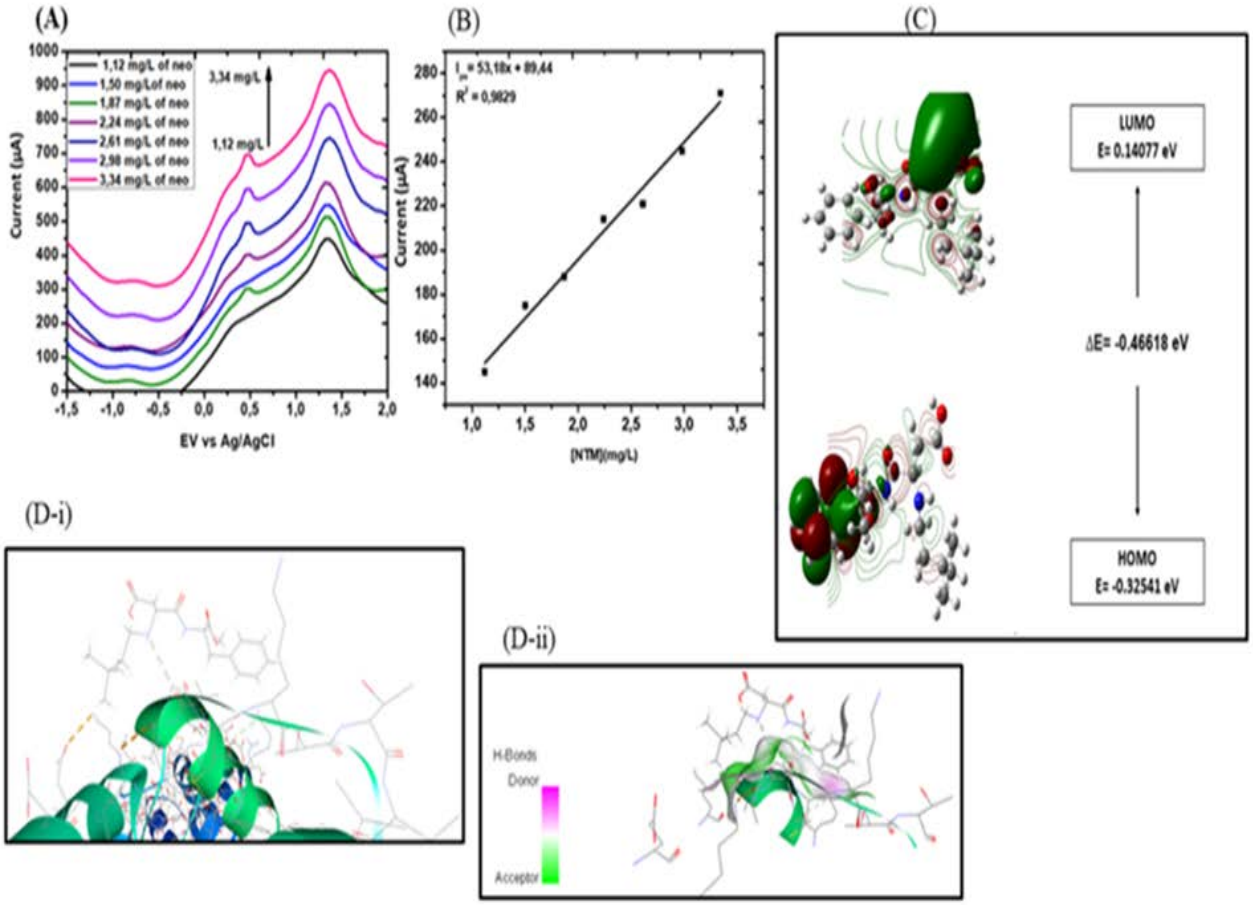

Figure 5-6: (A) DPV responses for NTM at CaE/AuNPs/MWCNTs modified GCE at different concentrations ranging from 1.12 to 3.34 mg/L, (B) Calibration curve showing linear dependence of the peak currents versus concentration of NTM, (C) Molecular orbital surfaces and energy levels for the HOMO and LUMO of NTM computed at DFT level 6-311+G (d,p) basis set (D-i) Molecular docking studies of NTM and CaE complex, and (D-ii) Hydrophobic map of the NTM-CaE enzyme.

5.1.9.4. Computational adsorption studies

We measured the adsorption energies of the adsorbate-substrate system as shown in Appendix 2A for the layers to mimic the electrochemical layers (Scheme 5-1). The

energy values for the minimized structures along with the adsorption energies (Figure 5-7A, B, and C) based on the adsorption locator (AL) are presented in Table 5-3. The calculated adsorption energies are all negative, signifies stabilization, and an exothermic adsorption process with the more negative value indicating stronger adsorption energy (Binder 2006).

Our results indicate that (NTM/CaE/AuNPs/MWCNTs) is the most stabilized layer that is attributed to the presence of the high energy CaE enzyme, in agreement with the amplified electrochemical signals depicted in Figure 5-6A.

Table 5-3: Summary of the minimized and adsorption energies using AL.

Systems	**Minimized energy** **kcal mol^{-1}**	**Adsorption energy** **kcal mol^{-1}**
AuNPs cluster	30 x 10^{-3}	
NTM (NTM)	45.45	
MWCNTs	30.145 x 10^{8}	
CaE	39.360 x 10^{8}	-
*AuNPs/MWCNTs	30.145 x 10^{8}	-65.420
$^{\#}$NTM/CaE	39.386 x 10^{3}	-1.254 x 10^{3}
$^{\$}$NTM/CaE/AuNPs/MWCNTs	30. 450 x 10^{8}	-37.262 x 10^{3}

***Layer 1; # Layer 2; $Layer 3.**

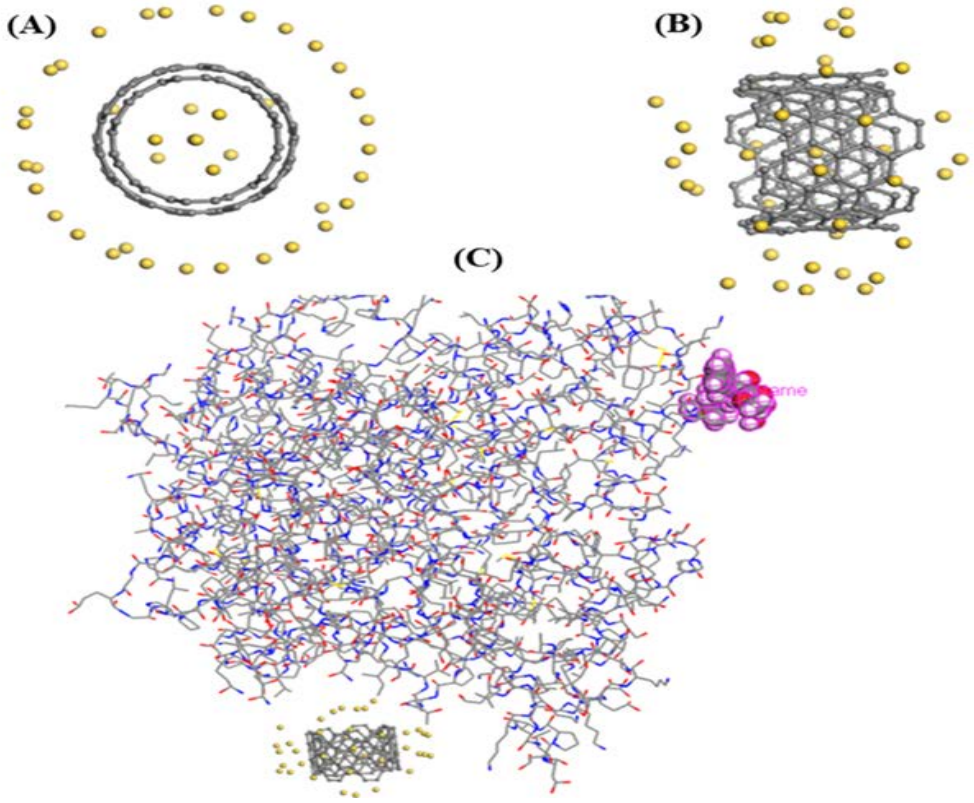

Figure 5-7: Optimized structures of MWCNTs AND AuNPs (A) Front view, (B) Side view, and (C) Layer-by-Layer adsorption of NTM-CaE/AuNPs/MWCNTs. The C and Au atoms are denoted in grey and yellow, respectively. The NTM is highlighted in purple.

5.1.10. Conclusions

For this study, a new enzymatic biosensor for the detection of NTM in beverage samples has been developed. This work showed that *aloe vera* extracts can reduce $AuCl_3$ into AuNPs and have advantages over other extracts due to their availability. The *aloe vera*-capped AuNPs were integrated into the MWCNTs to improve the electrochemical sensing of NTM. The UV-Vis spectrophotometer was employed to monitor the reduction of Au in terms of absorption, while the AF4-MALS showed how the particles were distributed in the nanoparticulate. The DPV and CV outcomes revealed that the CaE/AuNPs/MWCNTs modified GCE nanocomposite exhibited efficient electrocatalytic oxidation for NTM with high selectivity and high stability.

Calibration curves were obtained under optimum conditions using DPV. Moreover, the computational tools assisted in the understanding of the electronic properties of NTM; the mechanism of the bio-molecular interaction, and adsorption of CaE with MWCNTs decorated with the biosynthesized AuNPs. The latter supported the layer-by-layer experimental strategy employed in this work.

Finally, the capability of the developed electrochemical enzymatic biosensor was tested on NTM beverage samples, yielding a good analytical performance, and thus providing a promising alternative for sensing applications in the beverage industry.

5.2. Sensor 2: Detection of NTM using AOx/NiNPs/GO modified GCE

5.2.1. Characterization of biosynthesized NiNPs

In this study, we measured the size distribution using the AF4 in combination with the MALS detector because the AF4-MALS technique can analyze the average geometric diameter (D_{geo}) and the radius of gyration (r_g) of the nanoparticles over the entire elution time. A well-resolved separation peak of the honey-capped NiNPs with an elution time between 9 to 19 min is illustrated in Figure 5-8A(i). The *honey* capped NiNPs showed uniform distribution of the nanoparticles as displayed using a size distribution curve. The r_g and D_h for the biosynthesized NiNPs were calculated corresponding to a sphere fit formalism in MALS, the results were 28.4 nm and 73.3 nm respectively using equation 5.1.

The spICP-MS mode was employed to determine the distribution and the average particle size of the biosynthesized NiNPs because it enables the determination of single particles. A single particle creates a pulse as a function of the number of atoms in a nanoparticulate hence the intensity of the pulse is illustrated in Figure 5-8A(ii). The maximum intensity signals were observed between 55 to 60 nm, resulting in the average particle size of 59 nm. The HR-TEM image of the biosynthesized NiNPs displayed a particle size of 42 nm as illustrated in Figure 5-8A(iii).

A UV-Vis spectrum was used as a confirmatory tool to monitor the reduction of Ni^{+2} to Ni^{+0}. A well-resolved single SPR peak at 380 nm confirmed the shape of biosynthesized NiNPs as spherical and monodispersed in an aqueous solution (Nouneh *et al.* 2011; Pandian, Palanivel and Dhananasekaran 2015) as displayed in

Figure 5-8A(iv). There was an enhanced electrochemical signal because the spherically shaped and monodispersed biosynthesized NiNPs from honey extract had a higher surface area to accommodate more analytes.

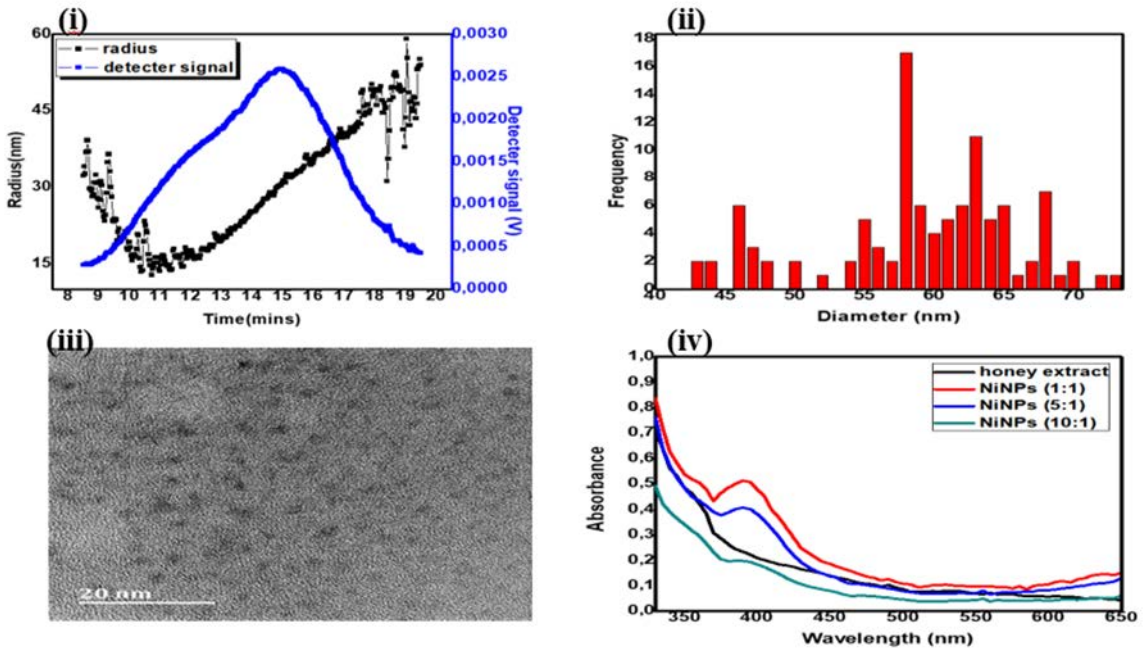

Figure 5-8A: (i) Hydrodynamic size characterization and particle size distribution of biosynthesized NiNPs with AF4-MALS, (ii) Average size determination of biosynthesized NiNPs with spICP-MS, (iii) TEM image of biosynthesized NiNPs using honey extract, and (iv) UV-vis spectrum of the biosynthesized NiNPs showing a broad absorption peak at a wavelength of 380 nm.

Thermogravimetric analysis (TGA) was employed to evaluate the thermal stability of the *honey* capped NiNPs. A TGA plot shown in Figure 5-8B demonstrated that the nanoparticles lost 51.6% weight loss at a temperature range of 25 ^{o}C to 53 ^{o}C and there was 3.7% weight loss due to the decomposition of bioorganic compounds like enzymes and proteins that are found on the surface of the honey solution (Nouneh *et al.* 2011). The thermal stability of the biosynthesized NiNPs was observed at the temperature range of 350 ^{o}C and 450 ^{o}C.

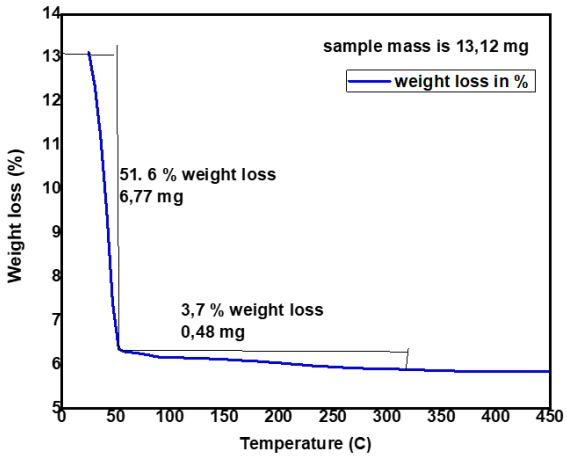

Figure 5-8B: TGA curve biosynthesized NiNPs in a nitrogen atmosphere at a temperature range of 0 ^{o}C to 400 ^{o}C.

5.2.2. Electrochemical behavior of NTM on AOx/NiNPs/GO modified GCE

Alcohol Oxidase (AOx) was used in the modification of GCE using GO anchored with *honey* capped NiNPs. Graphene oxide has inherent properties such as high conductivity and can have an anchoring site (Duan *et al.* 2014; Aljabali *et al.* 2018). The biosynthesized NiNPs were decorated onto the GO to generate electro-catalytic sites and the AOx was introduced to increase the sensitivity with significant detection limits. The biosensor was characterized by cyclic voltammetry (CV) and the areas of the bare electrode and the AOx/NiNPs/GO modified electrode were acquired using the Randles-Sevcik equation (Eqn 3.5).

For the AOx/NiNPs/GO modified GCE, the surface area was determined to be 1.199 cm^{-2}, while the surface area of the bare was determined to be 0.310 cm^{-2}. To evaluate the electrochemical performance of AOx/NiNPs/GO modified GCE towards the detection of NTM, current-potential responses were measured. Figure 5-9A reveals an enhancement in current responses which proves that a larger surface area was

provided by the composite of the nanomaterials however there was a 37% decrease of the oxidation peak current when AOx was introduced on the electrode. The presence of the AOx causes the disturbance of the electron relaying capacity at higher amounts which then allows fewer NTM molecules to be oxidized because there was no sufficient electron transfer between the AOx and the electrode. With the presence of NTM in the working cell, excess AOx could not be incorporated in the GO/NiNPs nanocomposite hence that would block the electron exchange as per the mechanism shown in Scheme 5-2 as NTM breaks into fragmentations to form dimethylbutyl-L-aspartic acid and phenylalanine involving a single proton transfer during the quasi-reversible process. The beginning of dissociation is shown by the anodic peak at 1.5 V in Figure 5-9A as NTM oxidized on the surface of the AOx/NiNPs/GO modified GCE resulting in a dimethylbutyl-L-aspartic acid and phenylalanine. The presence of oxygen which is the co-substrate of the alcohol oxidase reaction results in the oxidation of methanol at 0.5 V.

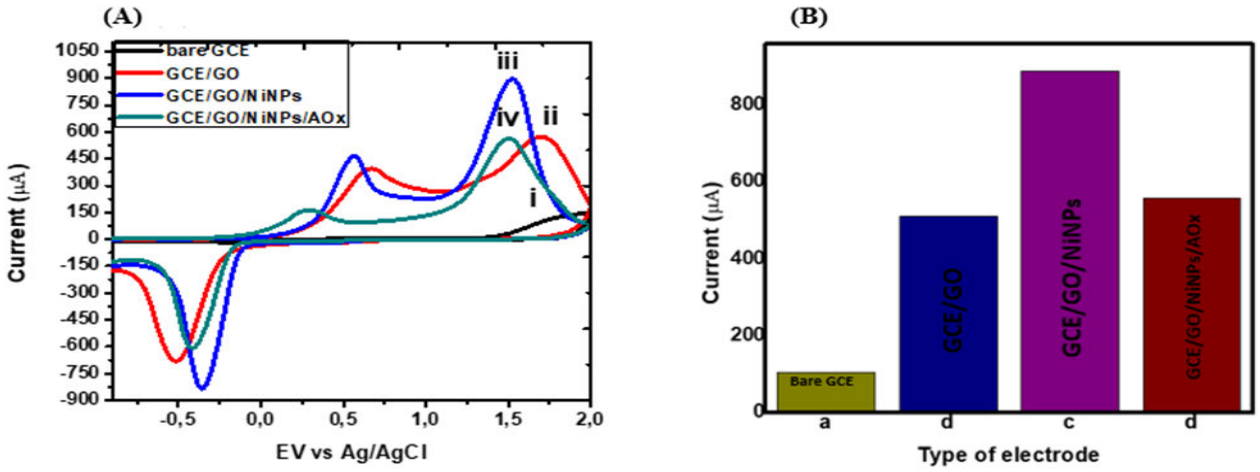

Figure 5-9: (A) Cyclic Voltammograms of 0.5 mM NTM at (i) bare GCE, (ii) GO/GCE, (iii)NiNPs/GO/GCE and (iv) AOx/NiNPs/GO modified GCE and (B) A bar graph displaying the current responses of a (a) bare GCE, (b) GO/GCE, (c) NiNPs/GO/GCE and (d) AOx/NiNPs/GO modified GCE.

A comparative peak current response for the electrodes displayed using a bar graph Figure 5-9B, confirms the catalytic effect of alcohol oxidase for the electrochemical oxidation of NTM, due to an 18.07 % amplification of peak signal.

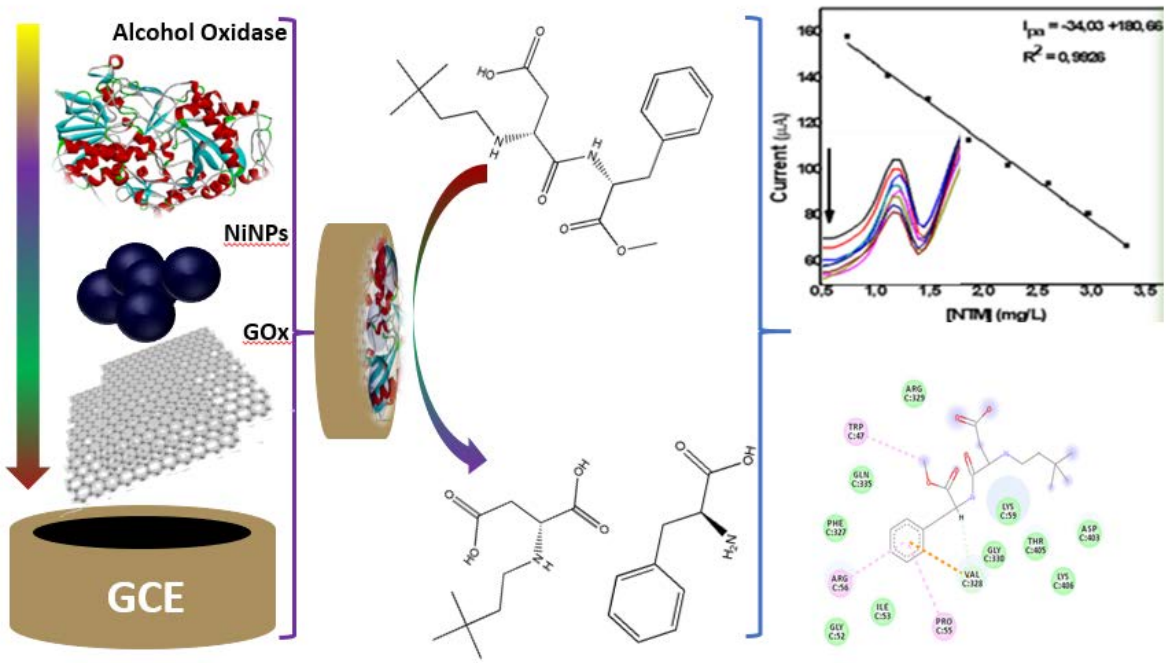

Scheme 5-2: A schematic representation of electro-oxidation of NTM at AOx/NiNPs/GO modified GCE.

An irreversible mechanism for the oxidation of NTM was demonstrated by the electrochemical characterization of AOx/NiNPs/GO modified GCE. The modified electrode displayed a higher anodic peak current as compared to the bare electrode however the electrochemical oxidation process requires optimization of experimental parameters such as deposition time, scan rate, and the pH.

5.2.3. Effects of pH, scan rate, and deposition time on the peak currents and peak potentials

The effect of pH ranging from 2.0 to 7.0 was assessed on the anodic peak currents and peak potentials of NTM using the CV in a phosphate buffer solution containing 0.5

mM NTM. Figure 5-10A shows the electrochemical behavior of NTM on the bare GCE at different pHs. The anodic peak currents decreased with the increase in pH. It was observed that the peak current responses for the detection of NTM using the AOx/NiNPs/GO modified GCE were pH-dependent. The results revealed that the maximum peak current is observed at pH 2.0 and hence it was selected as the optimum pH for the detection of NTM. A decrease in the size of the diffusion layer is a result of a faster scan rate hence the effect of the scan rate on the anodic peak currents and peak potential is illustrated by the CV in Figure 5-10B at a range of 0.01 to 0.21 V s^{-1}. The anodic peak current increased with an increase in scan rates on the modified GCE and the bare GCE. A longer deposition time always leads to a higher current intensity however it can lower the upper range of detection due to fast surface saturation when detecting an analyte at a higher concentration hence a deposition time of the 30s was chosen. Figure 5-10C displays the effect of deposition time on peak potentials and peak currents at the range of 30s to 150s.

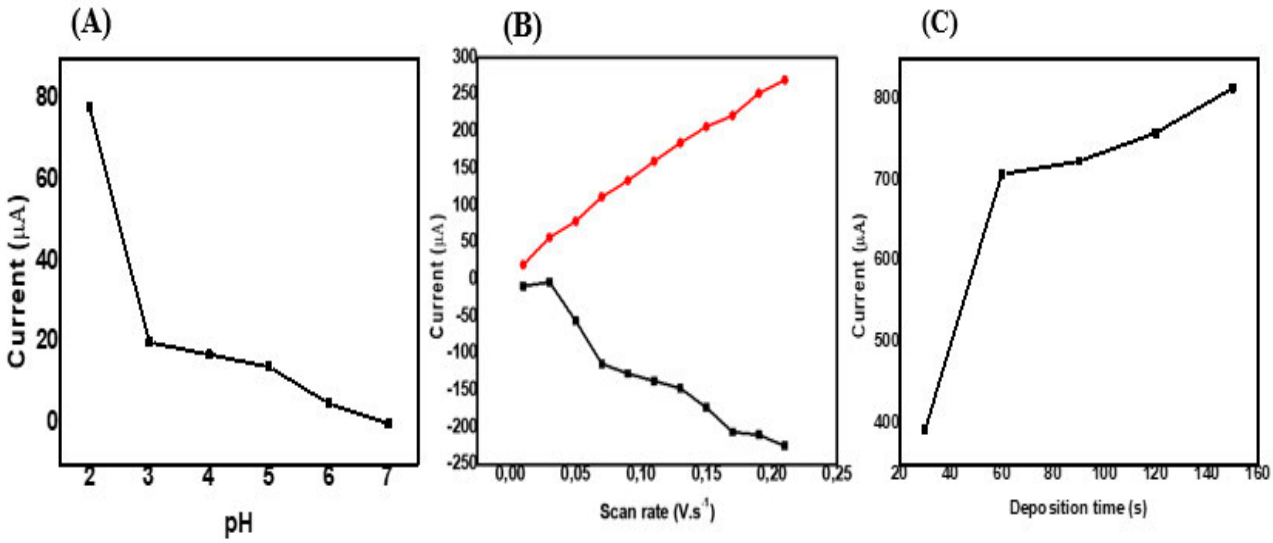

Figure 5-10: (A) Current responses were observed with respect to change in pH with 0.5 mM NTM, (B) Plots of scan rate from 0.01 $V.s^{-1}$ to 0.21 $V.s^{-1}$ are displayed to show current responses; (C) A line graph shows the effect of deposition time on peak current at the 30s to 150s

5.2.4. DPV technique for quantitative detection of NTM

An anodic peak is noticed at the AOx/NiNPs/GO modified GCE confirming oxidation of NTM and better absorption of methanol as illustrated in Figure 5-11A, all this was achieved by using the DPV in the presence of a PSB (pH 2.0). DPV responses for the different concentrations of NTM using AOx/NiNPs/GO modified GCE in 0.1 M PSB (pH 2.0) showed a linear relationship between the anodic peak currents and the concentrations of NTM observed in the concentration ranging from 1120 µg L^{-1} to 3340 µg L^{-1}. The calibration curve of I_{pa} = -34.02 x +180.66 as displayed in Figure 5-11B was linear with R^2 of 0.9926 with a LOD of 15 µg L^{-1} and LOQ of 47 µg L^{-1}.

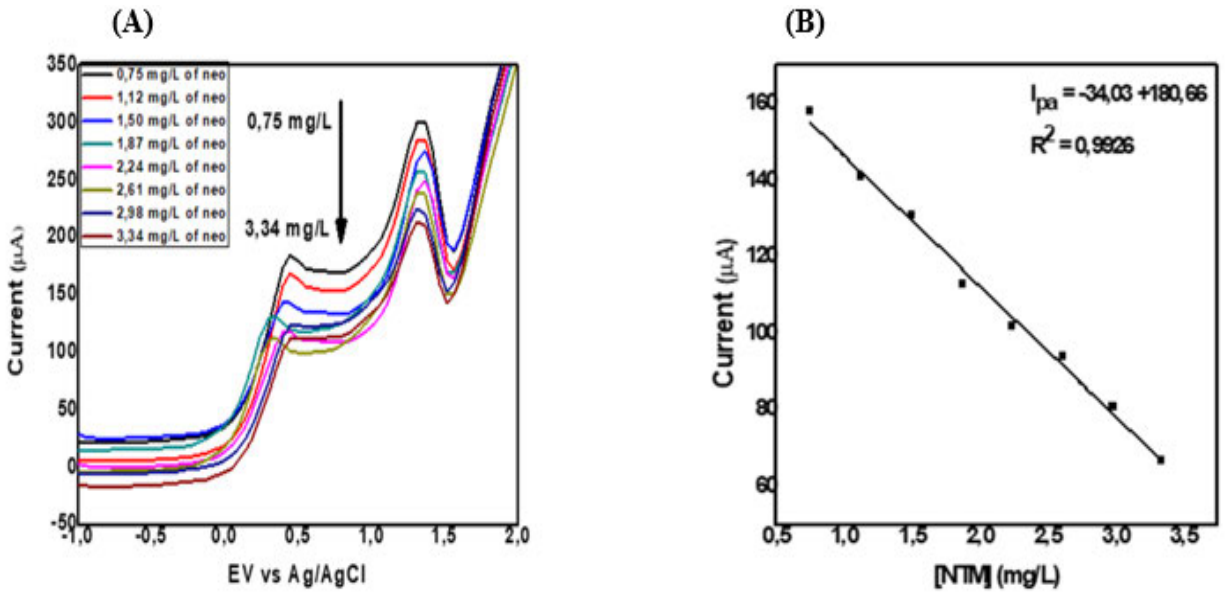

Figure 5-11: (A) DPV responses for NTM at AOx/NiNPs/GO modified GCE at different concentrations ranging from 1.12 to 3.34 mg/L, (B) Calibration curve showing linear dependence of the peak currents versus concentration of NTM.

5.2.5. Stability, recovery, accuracy, and precision studies

In this work, the stability of the AOx/NiNPs/GO modified GCE was assessed in a PSB (pH 2.0) by detecting the responses in 0.5 mM NTM for 10 runs using the same coating on the electrode. The modified electrode maintained 96%, 94%, 83%, 83%, and 68% of the original response after 1-5 runs respectively, but due to the saturation of the electrode, there was a shift in the anodic peak of NTM and a sudden drop in current after the 6th run. These results indicated that the biosensor is stable to run five runs on the same day with the same coating. The accuracy, precision, and recovery were studied by analyzing three different concentrations of standard NTM ranging from 1120 µg L^{-1} to 2610 µg L^{-1} in three measurements in one day. Table 5-4 displays that the range of values for the percentage recoveries of NTM using the modified electrode ranged from 86% to 99%. These outcomes confirmed that the designed sensor showed higher precision and accuracy, proving its suitability for the analysis of NTM in beverage samples.

Table 5-4: Analytical parameters in the terms of precision, stability, accuracy, and recovery obtained for the detection of NTM using AOx/NiNPs/GO modified GCE.

Stability	**NTM**	**NTM**	**Analytical parameters**		
Peak response[a] (I_{pa})	**Added (µg/L)**	**Found (µg/L)**	**Relative error[b]**	**Recovery (%)**	**RSD[c] (%)**
145	1120	1050	-6.3	94	1.82
126	1870	1610	-13.9	86	1.59
93	2610	2580	-1.2	99	1.64

[a] Average of three measurements, [b] relative error = (DPV value – added value/ added value) x 100, [c] relative standard deviation for the three measurements.

5.2.6. Real samples studies

The developed biosensor was used to detect NTM in real beverage samples. Under optimum conditions, three different concentrations of standard NTM solution were selected to spike the samples, and then the AOx/NiNPs/GO modified GCE was employed to detect the total amount of NTM using the DPV. By comparing the responses of three different concentrations for apple juice, Fanta orange, and red grape juice, the relative standard deviation (RSD) of the measurements (n=3) was calculated to be at the range of 1.19 to 1.99, 1.23 to 1.93, and 1.77 to 2.02, respectively. This suggested that this modified electrode is highly reproducible. The recovery was between 84% to 97% suggesting that the determination of NTM using the modified electrode was effective and sensitive. These outcomes revealed that the enzymatic biosensor has the capability in the detection of NTM in real samples as illustrated in Table 5-5.

Table 5-5: Corresponding results for the detection of NTM in spiked beverage samples analyzed using the AOx/NiNPs/GO modified GCE.

Sample	**Added NTM (µg/L)**	**Recovery (%)**	**RSD [a] (%)**	**Relative error [b]**
APPLE JUICE				
Spiked sample 1	1870	89	1.19	-11.0
Spiked sample 2	2610	84	1.99	-16.0
Spiked sample 3	2980	86	1.82	-14.0
FANTA ORANGE				
Spiked sample 1	1120	94	1.23	-3.6
Spiked sample 2	1870	96	1.93	-4.0
Spiked sample 3	2610	97	1.47	-2.3
RED GRAPE JUICE				

Spiked sample 1	1870	94	1.77	-6.0
Spiked sample 2	2610	95	1.68	-5.0
Spiked sample 3	2980	94	2.02	-5.7

[a] Average of three measurements, [b] relative error = (DPV value – added value/ added value) x 100.

5.2.7. Effect of interferents on the detection of NTM

The sensitivity and selectivity of AOx/NiNPs/GO modified GCE was evaluated by adding possible interferent compounds such as ascorbic acid, glucose, and sucrose simultaneously to the 0.5 mM NTM standard solution. This was carried out using the DPV and the results indicated that there were no other anodic peak potentials that were observed except that of NTM at the potential of 1.3 V so this showed that the above-mentioned interferents did not affect the enzymatic biosensor. Thus confirming that the AOx immobilized on the surface of the NiNPS/GO modified GCE has high selectivity and high sensitivity for the detection of NTM, due to selective interaction of AOx with the NTM in conjunction with the large surface area of the honey capped NiNPs.

5.2.8. Stability of the electrode for detection of NTM in real samples

The stability of the AOx/NiNPs/GO modified GCE was studied in the phosphate buffer (pH 2) by determining the responses in three different concentrations of NTM spiked samples at a range of 10 runs using the same coating on the electrode. The results depicted a shift on the anodic peak and a sudden drop of current as the electrode became saturated as illustrated in Appendix 1B (Figure 2A, B, and C). Figures 5-12A, 5-12B, and 5-12C show that the initial response diminished rapidly, however, the

electrode was stable enough to run four runs for the three different concentrations as mentioned below. The surface of the electrode started fouling due to the residues of NTM so which made the transfer of electrons to be difficult during the fifth run. Electrode fouling is the passivation of the electrode surface by the adsorption of none electroactive species. This leads to a decreasing biosensor response over time (Geise *et al.* 1991). The electrode should be polished before the fifth determination, as the residues of NTM on the surface of the electrode will influence the fifth measurement. To find similar NTM oxidation peak currents, it is necessary to polish the surface of the electrode with ≤ 3 µm alumina slurry and then rinse with deionized distilled water after the fourth run.

Figure 5-12A (i, ii, and iii) displays the responses of apple juice samples at a concentration of 1.87 ppm, 2.61 ppm, and 2.98 ppm of NTM respectively.

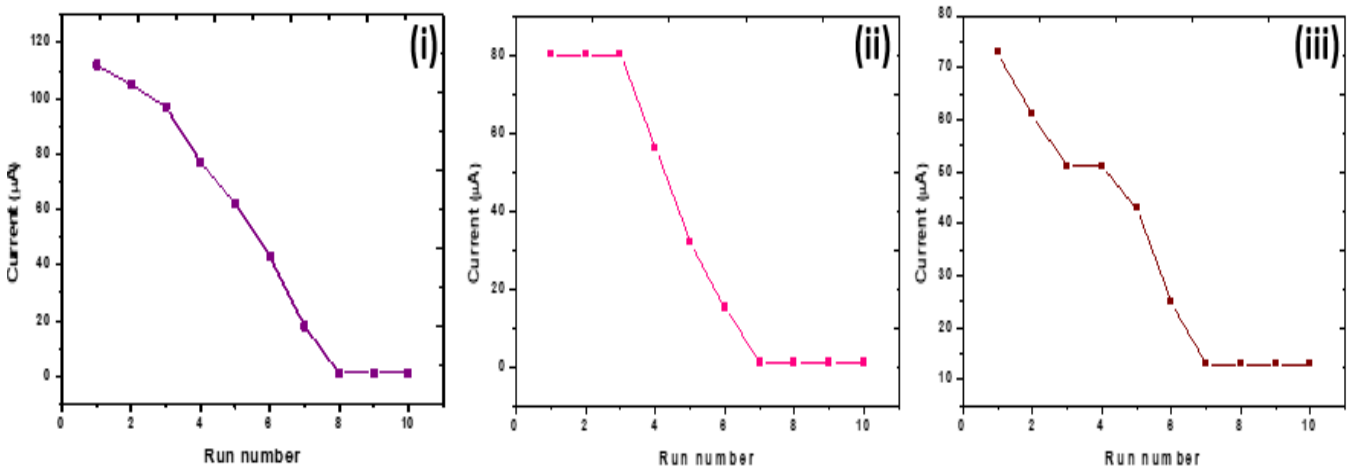

Figure 5-12A: Line graphs displaying the response of NTM in apple juice sample (i)1.87 ppm; (ii) 2.61 ppm (iii) 2.98 ppm.

Figure 5-12B (i, ii, and iii) displays the responses of Fanta orange samples at a concentration of 1.12 ppm, 1.87 ppm, and 2.61 ppm of NTM respectively.

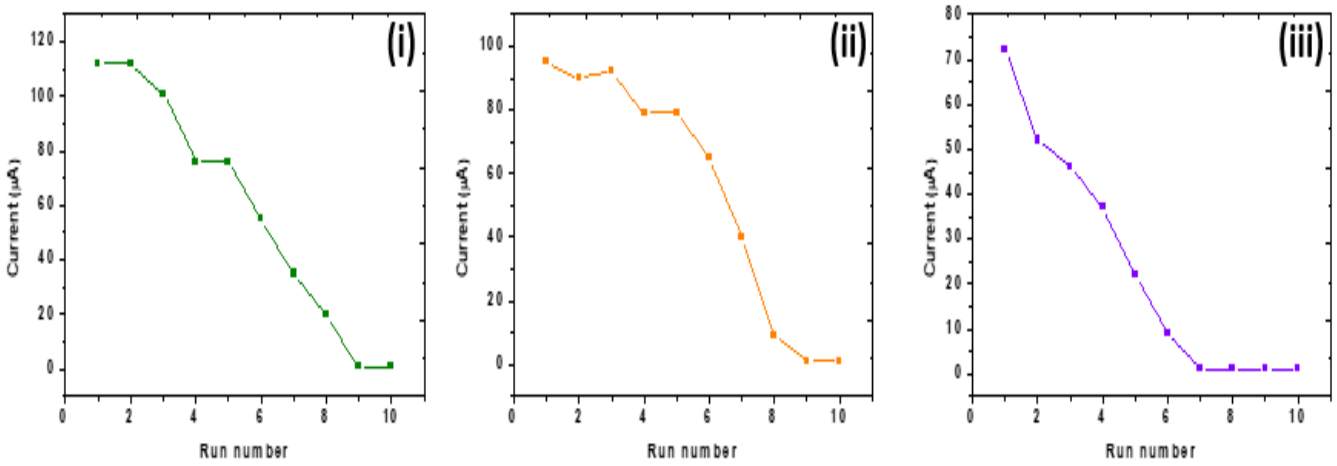

Figure 5-12B: Line graphs displaying the response of NTM in Fanta orange sample (i)1.12 ppm; (ii) 1.87 ppm (iii) 2.61 ppm.

Figure 5-12C (i, ii, and iii) displays the responses of red grape juice samples at a concentration of 1.87 ppm, 2.61 ppm, and 2.98 ppm of NTM respectively.

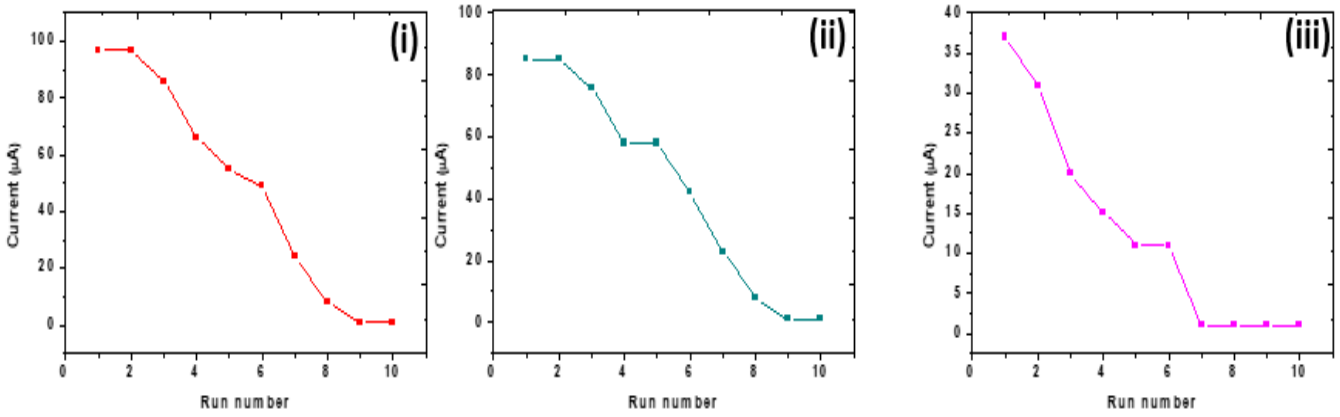

Figure 5-12C: Line graphs displaying the response of NTM in red grapes juice sample (i)1.87 ppm; (ii) 2.61 ppm (iii) 2.98 ppm.

In this work, computational tools were implemented to comprehend the interaction of the nanomaterials with the surface modification of the electrode surface because

computational materials science is gaining widespread recognition in the field of engineered nanomaterials (ENMs). The outcomes are shown below.

5.2.9. Computational section

5.2.9.1. Docking and interaction studies

A reversible reduction reaction is shown in Scheme 5-2 whereby NTM undergoes oxidation on the surface of AOx/NiNPs/GO modified GCE. As a result, there was a formation of dimethylbutyl-L-aspartic acid and phenylalanine with an electron density that agrees with the redox reaction mechanism. Docking and interaction studies were carried out to get further details on the chemical interaction between the NTM and alcohol oxidase as shown in Figure 5-13B. The hydrophobic map of the NTM-AOx enzyme complex showed the presence of hydrogen bonds with TRP 47, ARG 56, PRO 55, and VAL 328 residues because of a stronger hydrogen bonding with (-CH-) NTM-phenyl and H-atom of the carboxylate group as demonstrated in Figure 5-13C. These outcomes confirmed that the AOx enzyme facilitated the electron transfer from NTM ligand, hence enhancing the biosensing response.

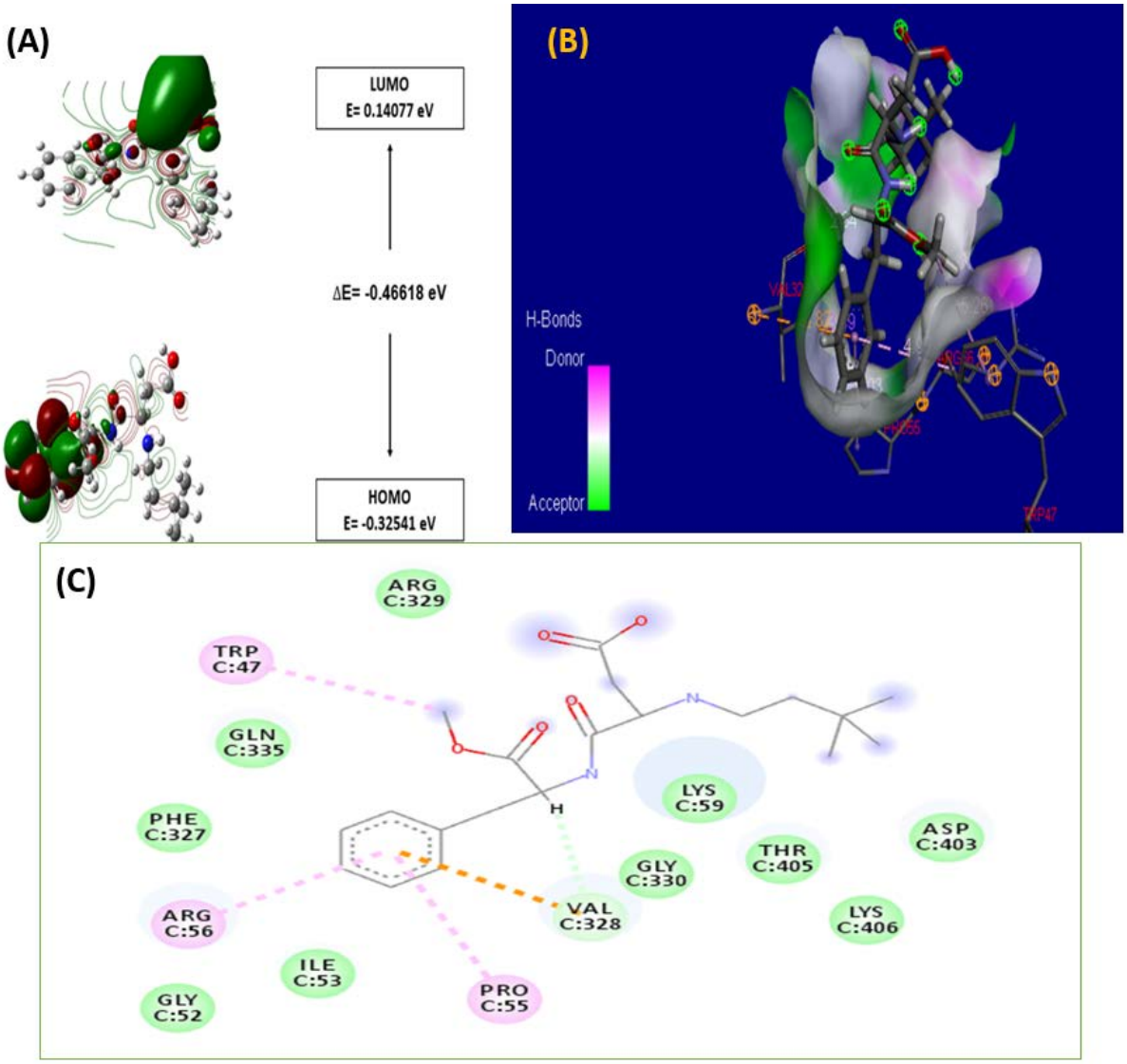

Figure 5-13: (A) Molecular orbital surfaces and energy levels for the HOMO and LUMO of NTM computed at DFT level 6-311+G (d,p) basis set; (B) molecular docking studies of NTM and AOx complex, and (C) hydrophobic map of the NTM-AOx enzyme.

5.2.9.2. Computational adsorption studies

The adsorption energies of the adsorbate-substrate system were measured as depicted in Appendix 2B for the layers to mimic the electrochemical layers (Scheme 5-2). The adsorption energies along with the energy values for the minimized structures (Figure 5-14A, B, and C) based on the adsorption locator (AL) are presented in Table 5-6. The calculated adsorption energies are all negative, signifies

stabilization, and an exothermic adsorption process (Binder 2006) with the more negative value indicating stronger adsorption energy. A decrease in the behavior of the adsorption energy was observed with the increase of the layers of the nanomaterials. All adsorption energy values were negative, this means that the AOx was attracted to the surface of NTM for most of the orientations (Jeon, 1991).

The outcomes indicated that (NTM/AOx/NiNPs/GO) is the most stabilized layer that is attributed to the presence of the high energy AOx enzyme.

Table 4-6: Summary of the minimized and adsorption energies using the AL.

Systems	**Adsorption energy** **kcal mol^{-1}**
GO/NiNPs (Layer 1)	-5.124
GO/NiNPs/AOx (Layer 2)	-26.033
GO/NiNPs/AOx/NTM (Layer 3)	-1253

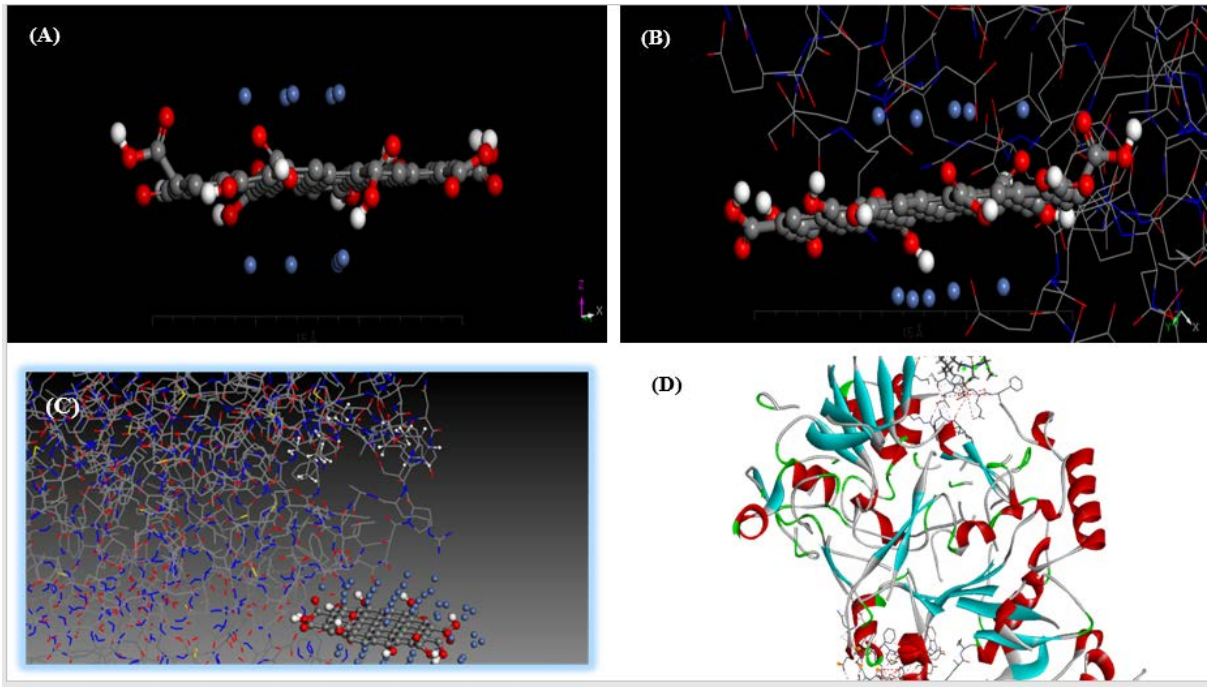

Figure 5-14: (A) Optimized structures of GO and NiNPs, The C, H, O, and Ni atoms are denoted in grey, white, red, and blue respectively. (B) optimized structures of GO, NiNPs, and AOx and (C) Layer-by-layer adsorption of NTM-AOx/NiNPs/GO. (D) Interaction diagram generated using Discovery Studio Visualizer.

5.2.10. Conclusions

A high performance electrochemical enzymatic biosensor was fabricated for the electrochemical enzymatic detection of NTM in beverage samples. The nanomaterials were characterized using TEM to monitor the morphological structure of the nanomaterials. A TGA curve was used to further confirm the mass of decomposition and thermal stability. The sp-ICP-MS and AF4-MALS FFF were used to separate the particles from the sample molecule giving relevant information about the size and hydrodynamic diameter of the nanoparticles. To monitor the reduction of Ni in terms of absorption, the UV-Vis was employed. The DPV and CV were used to study the electrochemical behavior of the developed biosensor. The results revealed that the AOx/NiNPs/GO modified GCE shows satisfactory electrocatalytic oxidation for NTM with high selectivity, high sensitivity, and high stability. We were able to obtain linear

calibration plots using the DPV under optimized conditions. Computational tools were employed to confirm experimental results. The developed electrochemical enzymatic biosensor was tested on real NTM beverage samples providing significant outcomes with lower detection limits hence the AOx/NiNPs/GO modified GCE can serve as an alternative in sensing applications in beverage industries.

CHAPTER 6: A SUMMARY OF CONCLUDING REMARKS AND RECOMMENDATIONS

6.1. A summary of concluding remarks

The purpose of this study was to develop two electrochemical enzymatic biosensors for the detection of NTM in beverages. The first sensor contained a paste of MWCNTs and AuNPs and the second sensor contained a nanocomposite of NiNPs and GO. Both sensors were immobilized with CaE and AOx enzymes respectively, to improve the electrochemical signal of NTM as the analyte. The CV results showed that the CaE/AuNPs/MWCNTs modified GCE and AOx/NiNPs/GO modified GCE with the surface areas of 0.998 cm^{-2} and 1.199 cm^{-2} respectively, has an efficient catalytic effect that amplified the peak signal by 33.3% and 18.0% respectively for the oxidation of NTM. Linear calibration plots of CaE/AuNPs/MWCNTs modified GCE and AOx/NiNPs/GO modified GCE showing an R^2 of 0.9829 and 0.9926 respectively, were obtained under optimized conditions using DPV. Both biosensors were tested for stability, it was observed that CaE/AuNPs/MWCNTs modified GCE was stable to run 1-4 runs using an NTM standard solution and AOx/NiNPs/GO modified GCE was stable to run 1-5 runs using an NTM standard solution. The %RSD of CaE/AuNPs/MWCNTs modified GCE and AOx/NiNPs/GO modified GCE ranged from 0.81 to 1.04 and 1.59 to 1.82, respectively. The % recoveries of CaE/AuNPs/MWCNTs modified GCE and AOx/NiNPs/GO modified GCE ranged from 96% to 99% and 86% to 99%, respectively. The CaE/AuNPs/MWCNTs modified GCE revealed high sensitivity with a LOD of 27 µg L^{-1} and LOQ of 83 µg L^{-1} and the AOx/NiNPs/GO modified GCE revealed high sensitivity with a LOQ of 47 µg L^{-1}.and LOD of

15 µg L^{-1}. Furthermore, the computational methodologies assisted in the understanding of the electronic properties of NTM. NTM showed a HOMO-LUMO energy gap of -0.46618 eV, indicating great potential as an electron donor through DFT calculation studies which is in agreement with the redox mechanism illustrated in Scheme 5-1 and 5-2. Judging from all the results, we can conclude that AOx/NiNPs/GO modified GCE performs better than CaE/AuNPs/MWCNTs modified GCE because it showed a low LOD, a higher R^2. Apart from using the NTM standard solution, the stability of the biosensors was also tested using real samples. CaE/AuNPs/MWCNTs modified GCE was stable enough to run four runs for the three different concentrations while the AOx/NiNPs/GO modified GCE was stable enough to run four runs for the three different concentrations. It appears the AOx/NiNPs/GO modified GCE was more stable than the CaE/AuNPs/MWCNTs modified GCE. This is due to the fouling phenomena. The fouling phenomena depend on the physicochemical nature of the surface such as hydrophobicity and the particle size of the carbon material (Ghanam, Lahcen, and Amine 2017). For the CaE/AuNPs/MWCNTs modified GCE, the MWCNTs have a smaller particle size which implied the easy formation of none electroactive species on the electrode surface thus the fouling was increased. For the AOx/NiNPs/GO modified GCE, the GO has a larger particle size so the formation of none electroactive species on the electrode was not that easy thus the fouling was reduced. Finally, the capability of the developed electrochemical enzymatic biosensors was tested on NTM beverage samples, yielding a good analytical performance, and thus providing a promising alternative for sensing applications in the beverage industry.

6.2 Recommendations for future work

The developed enzymatic biosensors can be evaluated to determine if they can be used to detect other sweeteners leading to significantly lower detection limits. Other nanomaterials can be used together with the CaE and AOx enzymes to prove further improvement of the electrochemical signals during the detection of the analyte. Computational methods can be used to predict the outcomes for the suggested experimental work and be used as a reference for the experimental results.

REFERENCES

ABBOTT, A., EL TTAIB, K., RYDER, K. S. & SMITH, E. 2008. Electrodeposition of nickel using eutectic based ionic liquids. *Transactions of the IMF,* 86**,** 234-240.

ABBOTT, A. P., BALLANTYNE, A., HARRIS, R. C., JUMA, J. A. & RYDER, K. S. 2017. Bright metal coatings from sustainable electrolytes: the effect of molecular additives on electrodeposition of nickel from a deep eutectic solvent. *Physical Chemistry Chemical Physics,* 19**,** 3219-3231.

ALDANA-GONZÁLEZ, J., ROMERO-ROMO, M., ROBLES-PERALTA, J., MORALES-GIL, P., PALACIOS-GONZÁLEZ, E., RAMÍREZ-SILVA, M., MOSTANY, J. & PALOMAR-PARDAVÉ, M. 2018. On the electrochemical formation of nickel nanoparticles onto glassy carbon from a deep eutectic solvent. *Electrochimica Acta,* 276**,** 417-423.

ALDRIDGE, W. 1953. Serum esterases. 2. An enzyme hydrolyzing diethyl p-nitrophenyl phosphate (E 600) and its identity with the A-esterase of mammalian sera. *Biochemical Journal,* 53**,** 117-124.

ALI, M. A., SOLANKI, P. R., SRIVASTAVA, S., SINGH, S., AGRAWAL, V. V., JOHN, R. & MALHOTRA, B. D. 2015. Protein functionalized carbon nanotubes-based smart lab-on-a-chip. *ACS Applied Materials & Interfaces,* 7**,** 5837-5846.

ALI, M. R., RAHMAN, M. Z. & SAHA, S. S. 2014. Electroless and electrolytic deposition of nickel from deep eutectic solvents based on choline chloride. *Indian Journal of Chemical Technology*, 21(2):127-133.

ALIM, S., VEJAYAN, J., YUSOFF, M. M. & KAFI, A. 2018. Recent uses of carbon nanotubes & gold nanoparticles in electrochemistry with application in biosensing: a review. *Biosensors and Bioelectronics,* 121**,** 125-136.

ALJABALI, A. A., AKKAM, Y., AL ZOUBI, M. S., AL-BATAYNEH, K. M., AL-TRAD, B., ABO ALROB, O., ALKILANY, A. M., BENAMARA, M. & EVANS, D. J. 2018. Synthesis of gold nanoparticles using leaf extract of Ziziphus zizyphus and their antimicrobial activity. *Nanomaterials,* 8**,** 174.

ARISTOV, N. & HABEKOST, A. 2015. Cyclic voltammetry-A versatile electrochemical method investigating electron transfer processes. *World Journal of Chemical Education,* 3, 115-119.

AUSTIN, L. A., MACKEY, M. A., DREADEN, E. C. & EL-SAYED, M. A. 2014. The optical, photothermal, and facile surface chemical properties of gold and silver nanoparticles in biodiagnostics, therapy, and drug delivery. *Archives of Toxicology,* 88**,** 1391-1417.

AUTHORITY, E. F. S. 2007. NTM as a sweetener and flavor enhancer-Scientific Opinion of the Panel on Food Additives, Flavourings, Processing Aids, and Materials in Contact with Food. *EFSA Journal,* 5**,** 581.

AVART, S. J., BERNARD, D. W., JEROME, W. G. & GLICK, J. M. 1999. Cholesteryl ester hydrolysis in J774 macrophages occurs in the cytoplasm and lysosomes. *Journal of Lipid Research,* 40**,** 405-414.

AZEVEDO, A. M., PRAZERES, D. M. F., CABRAL, J. M. & FONSECA, L. P. 2005. Ethanol biosensors are based on alcohol oxidase. *Biosensors and Bioelectronics,* 21**,** 235-247.

BAALOUSHA, M., STOLPE, B. & LEAD, J. 2011. Flow field-flow fractionation for the analysis and characterization of natural colloids and manufactured nanoparticles in

environmental systems: a critical review. *Journal of Chromatography A,* 1218**,** 4078-4103.

BALANDIN, A. A., GHOSH, S., BAO, W., CALIZO, I., TEWELDEBRHAN, D., MIAO, F. & LAU, C. N. 2008. Superior thermal conductivity of single-layer graphene. *Nano Letters,* 8**,** 902-907.

BALGOBIND, K., KANCHI, S., SHARMA, D., BISETTY, K. & SABELA, M. I. 2016. Hybrid of ZnONPs/MWCNTs for electrochemical detection of aspartame in food and beverage samples. *Journal of Electroanalytical Chemistry,* 774**,** 51-57.

BARSAN, M. M. & BRETT, C. M. 2008. An alcohol oxidase biosensor using PNR redox mediator at carbon film electrodes. *Talanta,* 74**,** 1505-1510.

BARSAN, M. M., GHICA, M. E. & BRETT, C. M. 2015. Electrochemical sensors and biosensors based on redox polymer/carbon nanotube modified electrodes: a review. *Analytica Chimica Acta,* 881**,** 1-23.

BAŞKAYA, G., YıLDıZ, Y., SAVK, A., OKYAY, T. O., ERIŞ, S., SERT, H. & ŞEN, F. 2017. Rapid, sensitive, and reusable detection of glucose by highly monodisperse nickel nanoparticles decorated functionalized multi-walled carbon nanotubes. *Biosensors and Bioelectronics,* 91**,** 728-733.

BATHINAPATLA, A., KANCHI, S., SINGH, P., SABELA, M. I. & BISETTY, K. 2015. Fabrication of copper nanoparticles decorated multiwalled carbon nanotubes as a high-performance electrochemical sensor for the detection of NTM. *Biosensors and Bioelectronics,* 67**,** 200-207.

BERNE, B. J. & STRAUB, J. E. 1997. Novel methods of sampling phase space in the simulation of biological systems. *Current Opinion in Structural Biology,* 7**,** 181-189.

BESHKAR, F. & SALAVATI-NIASARI, M. J. J. o. N. 2015. Facile synthesis of nickel chromite nanostructures by hydrothermal route for photocatalytic degradation of acid black 1 under visible light. Journal of Nanostructures, 5 (1): 17-23.

BHATTACHARYYA, R., TUDU, B., DAS, S. C., BHATTACHARYYA, N., BANDYOPADHYAY, R. & PRAMANIK, P. 2012. Classification of black tea liquor using cyclic voltammetry. *Journal of Food Engineering,* 109**,** 120-126.

BINDER, H. 2006. Thermodynamics of competitive surface adsorption on DNA microarrays. *Journal of Physics: Condensed Matter,* 18**,** S491.

BLANDEZ, J. F., ESTEVE-ADELL, I., PRIMO, A., ALVARO, M. & GARCÍA, H. 2016. Nickel nanoparticles supported on graphene as catalysts for aldehyde hydrosilylation. *Journal of Molecular Catalysis A: Chemical,* 412**,** 13-19.

BOUŘ, P., 2000. Comparison of Hartree–Fock, and Kohn–Sham determinants as wave functions. Journal of Computational Chemistry, 21(1), pp.8-16.

BUND, A. & ZSCHIPPANG, E. 2007. Nickel electrodeposition from a room temperature eutectic melt. *ECS Transactions,* 3**,** 253.

BUNTE, S. W. & SUN, H. 2000. Molecular modeling of energetic materials: the parameterization and validation of nitrate esters in the COMPASS force field. *The Journal of Physical Chemistry B,* 104**,** 2477-2489.

BURKE, K. 2012. Perspective on density functional theory. *The Journal of Chemical Physics,* 136**,** 150901.

CAI, H., XU, C., HE, P. & FANG, Y. 2001. Colloid Au-enhanced DNA immobilization for the electrochemical detection of sequence-specific DNA. *Journal of Electroanalytical Chemistry,* 510**,** 78-85.

References

CAMPÀS, M., PRIETO-SIMÓN, B. AND MARTY, J.L., 2009, February. A review of the use of genetically engineered enzymes in electrochemical biosensors. In Seminars in cell & developmental biology (Vol. 20, No. 1, pp. 3-9). Academic Press.

CARELLI, D., CENTONZE, D., DE GIGLIO, A., QUINTO, M. & ZAMBONIN, P. G. 2006. An interference-free first-generation alcohol biosensor based on a gold electrode modified by an overoxidised non-conducting polypyrrole film. *Analytica Chimica Acta,* 565**,** 27-35.

CASELY, I. J., ZILLER, J. W., FANG, M., FURCHE, F. & EVANS, W. J. 2011. Facile Bismuth− Oxygen Bond Cleavage, C-H Activation, and Formation of a Monodentate Carbon-Bound Oxyaryl Dianion,(C6H2 t Bu2-3, 5-O-4) 2−. *Journal of the American Chemical Society,* 133**,** 5244-5247.

CHANDRA, S., KUMAR, A. & TOMAR, P. K. 2014. Synthesis of Ni nanoparticles and their characterizations. *Journal of Saudi Chemical Society,* 18**,** 437-442.

CHATTOPADHYAY, S., RAYCHAUDHURI, U. & CHAKRABORTY, R. 2014. Artificial sweeteners–a review. *Journal of Food Science and Technology,* 51**,** 611-621.

CHEN, D.-H. & HSIEH, C.-H. 2002. Synthesis of nickel nanoparticles in aqueous cationic surfactant solutions. *Journal of Materials Chemistry,* 12**,** 2412-2415.

CHEN, H., WANG, Y., WANG, Y., DONG, S. & WANG, E. 2006. One-step preparation and characterization of PDDA-protected gold nanoparticles. *Polymer,* 47**,** 763-766.

CHEN, J., JIANG, Z., ACKERMAN, J. D., YAZDANI, M., HOU, S., NUGEN, S. R. & ROTELLO, V. M. 2015. Electrochemical nanoparticle–enzyme sensors for screening bacterial contamination in drinking water. *Analyst,* 140**,** 4991-4996.

CHOPRA, N., GAVALAS, V.G., BACHAS, L.G., HINDS, B.J. AND BACHAS, L.G., 2007. Functional one-dimensional nanomaterials: applications in nanoscale biosensors. Analytical Letters, 40(11), pp.2067-2096.

CHOUDHARY, N., BEE, S., GUPTA, A. & TANDON, P. 2013. Comparative vibrational spectroscopic studies, HOMO–LUMO and NBO analysis of N-(phenyl)-2, 2-dichloroacetamide, N-(2-chlorophenyl)-2, 2-dichloroacetamide and N-(4-chlorophenyl)-2, 2-dichloroacetamide based on density functional theory. *Computational and Theoretical Chemistry,* 1016**,** 8-21.

CHWALIBOG, A., SAWOSZ, E., HOTOWY, A., SZELIGA, J., MITURA, S., MITURA, K., GRODZIK, M., ORLOWSKI, P. & SOKOLOWSKA, A. 2010. Visualization of interaction between inorganic nanoparticles and bacteria or fungi. *International Journal of Nanomedicine,* 5**,** 1085.

CORAZZARI, I., NISTICÒ, R., TURCI, F., FAGA, M. G., FRANZOSO, F., TABASSO, S. & MAGNACCA, G. 2015. Advanced Physico-chemical characterization of chitosan by means of TGA coupled on-line with FTIR and GCMS: Thermal degradation and water adsorption capacity. *Polymer Degradation and Stability,* 112**,** 1-9.

D'ORAZIO, P. 2003. Biosensors in clinical chemistry. *Clinica Chimica Acta,* 334**,** 41-69.

DAVIES, T. J., HYDE, M. E. & COMPTON, R. G. 2005. Nanotrench arrays reveal insight into graphite electrochemistry. *Angewandte Chemie,* 117**,** 5251-5256.

DE PRADA, A. G.-V., PENA, N., MENA, M., REVIEJO, A. & PINGARRON, J. 2003. Graphite–Teflon composite bienzyme amperometric biosensors for monitoring of alcohols. *Biosensors and Bioelectronics,* 18**,** 1279-1288.

DEB, S., PATRA, H. K., LAHIRI, P., DASGUPTA, A. K., CHAKRABARTI, K. & CHAUDHURI, U. 2011. Multistability in platelets and their response to gold nanoparticles. *Nanomedicine: Nanotechnology, Biology and Medicine,* 7**,** 376-384.

References

DEGUELDRE, C., FAVARGER, P.-Y. & WOLD, S. 2006. Gold colloid analysis by inductively coupled plasma-mass spectrometry in a single particle mode. *Analytica Chimica Acta,* 555**,** 263-268.

DEL CASTILLO, R. M., CALLES, A. G., ESPEJEL-MORALES, R. & HERNANDEZ-CORONADO, H. 2018. Adsorption of CO2 on graphene surface modified with defects. *Computational Condensed Matter,* 16**,** e00315.

DRESSELHAUS, M. S., DRESSELHAUS, G. & EKLUND, P. C. 1996. *Science of fullerenes and carbon nanotubes: their properties and applications*, Elsevier.

DUAN, J., CHEN, S., DAI, S. & QIAO, S. Z. 2014. Shape control of Mn3O4 nanoparticles on nitrogen-doped graphene for enhanced oxygen reduction activity. *Advanced Functional Materials,* 24**,** 2072-2078.

DUBASCOUX, S., LE HECHO, I., HASSELLÖV, M., VON DER KAMMER, F., GAUTIER, M. P. & LESPES, G. 2010. Field-flow fractionation and inductively coupled plasma mass spectrometer coupling: History, development, and applications. *Journal of Analytical Atomic Spectrometry,* 25**,** 613-623.

DUBASCOUX, S., VON DER KAMMER, F., LE HÉCHO, I., GAUTIER, M. P. & LESPES, G. 2008. Optimization of asymmetrical flow field-flow fractionation for environmental nanoparticles separation. *Journal of Chromatography A,* 1206**,** 160-165.

DZYADEVYCH, S.V., ARKHYPOVA, V.N., SOLDATKIN, A.P., EL'SKAYA, A.V., MARTELET, C. AND JAFFREZIC-RENAULT, N., 2008. Amperometric enzyme biosensors: Past, present and future. Irbm, 29(2-3), pp.171-180.

EBY, D. M., SCHAEUBLIN, N. M., FARRINGTON, K. E., HUSSAIN, S. M. & JOHNSON, G. R. 2009. Lysozyme catalyzes the formation of antimicrobial silver nanoparticles. *ACS Nano,* 3**,** 984-994.

EGGINS, B. R. 2008. *Chemical sensors and biosensors*, John Wiley & Sons.

ELSHAFEY, R., TAVARES, A. C., SIAJ, M. & ZOUROB, M. 2013. Electrochemical impedance immunosensor based on gold nanoparticles–protein G for the detection of cancer marker epidermal growth factor receptor in human plasma and brain tissue. *Biosensors and Bioelectronics,* 50**,** 143-149.

ESSÉN, H., 1977. The physics of the born–oppenheimer approximation. International Journal of Quantum Chemistry, 12(4), pp.721-735.

FAN, H., WANG, L., ZHAO, K., LI, N., SHI, Z., GE, Z. & JIN, Z. 2010. Fabrication, mechanical properties, and biocompatibility of graphene-reinforced chitosan composites. *Biomacromolecules,* 11**,** 2345-2351.

FERNANDEZ-FERNANDEZ, A., MANCHANDA, R. & MCGORON, A. J. 2011. Theranostic applications of nanomaterials in cancer: drug delivery, image-guided therapy, and multifunctional platforms. *Applied Biochemistry and Biotechnology,* 165**,** 1628-1651.

FILIPPI, C., UMRIGAR, C.J. AND GONZE, X., 1997. Excitation energies from density functional perturbation theory. The Journal of chemical physics, 107(23), pp.9994-10002.

FRATODDI, I., VENDITTI, I., CAMETTI, C. & RUSSO, M. V. 2015. How toxic are gold nanoparticles? The state-of-the-art. *Nano Research,* 8**,** 1771-1799.

FRISCH MJ, T. G., Schlegel HB, Scuseria GE, Robb MA,, Cheeseman JR, M. J., Vreven T, Kudin KN, Burant, JC, M. J., Iyengar SS, Tomasi J, Barone V, Mennucci B,Cossi M, Scalmani G, Rega N, Petersson GA, Nakatsuji H, Hada, M, E. M., Toyota K, Fukuda R, Hasegawa J, Ishida M,, Nakajima T, H. Y., Kitao O, Nakai H, Klene M, Li X, Knox, JE, H. H., Cross JB, Bakken V, Adamo C, Jaramillo J,, Gomperts R, S. R., Yazyev O, Austin AJ, Cammi R,, Pomelli C, O. J., Ayala PY, Morokuma K, Voth GA,, Salvador P, D. J., Zakrzewski VG,

Dapprich S, Daniels, AD, S. M., Farkas O, Malick DK, Rabuck AD, Raghavachari, K, F. J., Ortiz JV, Cui Q, Baboul AG, Clifford S,, Cioslowski J, S. B., Liu G, Liashenko A, Piskorz P,, Komaromi I, M. R., Fox DJ, Keith T, Al-Laham MA, Peng, CY, N. A., Challacombe M, Gill PMW, Johnson B, and Chen W, W. M., Gonzalez C, Pople JA. 2004. http://www.gaussian.com/g_misc/g03/citation_g03.htm. Gaussian Inc, Wallingford, CT,

FUJIGAYA, T., MORIMOTO, T., NIIDOME, Y. & NAKASHIMA, N. 2008. NIR Laser-Driven Reversible Volume Phase Transition of Single-Walled Carbon Nanotube/Poly (N-isopropylacrylamide) Composite Gels. *Advanced Materials,* 20**,** 3610-3614.

GADHE, A., SONAWANE, S. S. & VARMA, M. N. 2015. Enhancement effect of hematite and nickel nanoparticles on biohydrogen production from dairy wastewater. *International Journal of Hydrogen Energy,* 40**,** 4502-4511.

GANESANA, M., ISTARNBOULIE, G., MARTY, J.-L., NOGUER, T. & ANDREESCU, S. 2011. Site-specific immobilization of a (His) 6-tagged acetylcholinesterase on nickel nanoparticles for highly sensitive toxicity biosensors. *Biosensors and Bioelectronics,* 30**,** 43-48.

GANESHKUMAR, M., SASTRY, T. P., KUMAR, M. S., DINESH, M. G., KANNAPPAN, S. & SUGUNA, L. 2012. Sun light-mediated synthesis of gold nanoparticles as carrier for 6-mercaptopurine: Preparation, characterization, and toxicity studies in zebrafish embryo model. *Materials Research Bulletin,* 47**,** 2113-2119.

GEIM, A. K. & NOVOSELOV, K. S. 2010. The rise of graphene. *Nanoscience and Technology: a Collection of Reviews from Nature Journals.* World Scientific.

GEISE, R.J., ADAMS, J.M., BARONE, N.J. AND YACYNYCH, A.M., 1991. Electropolymerized films to prevent interferences and electrode fouling in biosensors. Biosensors and Bioelectronics, 6(2), pp.151-160.

GEORGAKILAS, V., TIWARI, J. N., KEMP, K. C., PERMAN, J. A., BOURLINOS, A. B., KIM, K. S. & ZBORIL, R. 2016. Noncovalent functionalization of graphene and graphene oxide for energy materials, biosensing, catalytic, and biomedical applications. *Chemical Reviews,* 116**,** 5464-5519.

GHANAM, A., LAHCEN, A.A., AND AMINE, A., 2017. Electroanalytical determination of Bisphenol A: Investigation of electrode surface fouling using various carbon materials. Journal of Electroanalytical Chemistry, 789, pp.58-66.

GIRAUDET, S. & ZHU, Z. 2011. Hydrogen adsorption in nitrogen-enriched ordered mesoporous carbons doped with nickel nanoparticles. *Carbon,* 49**,** 398-405.

GÓMEZ-NAVARRO, C., MEYER, J. C., SUNDARAM, R. S., CHUVILIN, A., KURASCH, S., BURGHARD, M., KERN, K. & KAISER, U. 2010. Atomic structure of reduced graphene oxide. *Nano Letters,* 10**,** 1144-1148.

GORTON, L., LINDGREN, A., LARSSON, T., MUNTEANU, F.D., RUZGAS, T., AND GAZARYAN, I., 1999. Direct electron transfer between heme-containing enzymes and electrodes as basis for third-generation biosensors. Analytica Chimica Acta, 400(1-3), pp.91-108.

GRZELCZAK, M., PÉREZ-JUSTE, J., MULVANEY, P. & LIZ-MARZÁN, L. M. 2008. Shape control in gold nanoparticle synthesis. *Chemical Society Reviews,* 37**,** 1783-1791.

GÜLCE, H., GÜLCE, A., KAVANOZ, M., COŞKUN, H. & YıLDıZ, A. 2002. A new amperometric enzyme electrode for alcohol determination. *Biosensors and Bioelectronics,* 17**,** 517-521.

References

GUO, H., HUANG, Z., ZHENG, Y. & WENG, S. 2015. Electrodeposition of nickel nanoparticles modified glassy carbon electrode for nonenzymatic glucose biosensing. *International Journal of Electrochemical Science,* 10**,** 10703-10712.

GUO, K., HANSEN, V. F., LI, H. & YU, Z. 2018. Monodispersed nickel and cobalt nanoparticles in desulfurization of thiophene for in-situ upgrading of heavy crude oil. *Fuel,* 211**,** 697-703.

HABERMÜLLER, K., MOSBACH, M. AND SCHUHMANN, W., 2000. Electron-transfer mechanisms in amperometric biosensors. Fresenius' journal of analytical chemistry, 366(6-7), pp.560-568.

HÄMMERLE, M., HILGERT, K., HORN, M. A. & MOOS, R. 2011. Analysis of volatile alcohols in apple juices by an electrochemical biosensor measuring in the headspace above the liquid. *Sensors and Actuators B: Chemical,* 158**,** 313-318.

HARUYAMA, T. 2003. Micro-and nanobiotechnology for biosensing cellular responses. *Advanced Drug Delivery Reviews,* 55**,** 393-401.

HASANZADEH, M., SHADJOU, N., ESKANDANI, M., SOLEYMANI, J., JAFARI, F., AND DE LA GUARDIA, M., 2014. Dendrimer-encapsulated and cored metal nanoparticles for electrochemical nanobiosensing. TrAC Trends in Analytical Chemistry, 53, pp.137-149.

HASENPUSCH, D., BORNSCHEUER, U. T. & LANGEL, W. 2011. Simulation on the structure of pig liver esterase. *Journal of Molecular Modeling,* 17**,** 1493-1506.

HEMALATHA, M., SURIYANARAYANAN, N. & PRABAHAR, S. 2014. Nanoscale synthesis and optical features of nickel nanoparticles. *Optik,* 125**,** 1962-1966.

HERNÁNDEZ-SIERRA, J. F., RUIZ, F., PENA, D. C. C., MARTÍNEZ-GUTIÉRREZ, F., MARTÍNEZ, A. E., GUILLÉN, A. D. J. P., TAPIA-PÉREZ, H. & CASTAÑÓN, G. M. 2008. The antimicrobial sensitivity of Streptococcus mutans to nanoparticles of silver, zinc oxide, and gold. *Nanomedicine: Nanotechnology, Biology and Medicine,* 4**,** 237-240.

HERNÁNDEZ-SANTOS, D., GONZÁLEZ-GARCÍA, M. B. & GARCÍA, A. C. 2002. Metal-nanoparticles based electroanalysis. *Electroanalysis: An International Journal Devoted to Fundamental and Practical Aspects of Electroanalysis,* 14**,** 1225-1235.

HOHENBERG, P. & KOHN, W. 1964. Inhomogeneous electron gas. *Physical Review,* 136**,** B864.

IZYUMSKAYA, N., TAHIRA, A., IBUPOTO, Z.H., LEWINSKI, N., AVRUTIN, V., ÖZGÜR, Ü., TOPSAKAL, E., WILLANDER, M. AND MORKOÇ, H., 2017. electrochemical biosensors based on ZnO nanostructures. ECS Journal of Solid State Science and Technology, 6(8), p.Q84.

JACKSON, R. M., GABB, H. A. & STERNBERG, M. J. 1998. Rapid refinement of protein interfaces incorporating solvation: application to the docking problem. *Journal of Molecular Biology,* 276**,** 265-285.

JAIN, K. K. 2003. Nanodiagnostics: application of nanotechnology in molecular diagnostics. *Expert Review of Molecular Diagnostics,* 3**,** 153-161.

JAMORSKI, C., CASIDA, M.E. AND SALAHUB, D.R., 1996. Dynamic polarizabilities and excitation spectra from a molecular implementation of time-dependent density-functional response theory: N2 as a case study. The Journal of chemical physics, 104(13), pp.5134-5147.

JANG, H. D., KIM, S. K., CHANG, H., ROH, K.-M., CHOI, J.-W. & HUANG, J. 2012. A glucose biosensor based on TiO2–graphene composite. *Biosensors and Bioelectronics,* 38**,** 184-188.

References

JEON, S.I., LEE, J.H., ANDRADE, J.D. AND DE GENNES, P., 1991. Protein—surface interactions in the presence of polyethylene oxide: I. Simplified theory. *Journal Of Colloid And Interface Science*, 142(1), pp.149-158.

JIANG, H. & LEE, E.-C. 2018. Highly selective, reusable electrochemical impedimetric DNA sensors based on carbon nanotube/polymer composite electrode without surface modification. *Biosensors and Bioelectronics,* 118**,** 16-22.

JIANRONG, C., YUQING, M., NONGYUE, H., XIAOHUA, W. & SIJIAO, L. 2004. Nanotechnology and biosensors. *Biotechnology Advances,* 22**,** 505-518.

JOHANSSON, K., JÖNSSON-PETTERSSON, G., GORTON, L., MARKO-VARGA, G. & CSÖREGI, E. 1993. A reagentless amperometric biosensor for alcohol detection in column liquid chromatography based on co-immobilized peroxidase and alcohol oxidase in carbon paste. *Journal of Biotechnology,* 31**,** 301-316.

JOSHI, R., ALWARAPPAN, S., YOSHIMURA, M., SAHAJWALLA, V. & NISHINA, Y. 2015. Graphene oxide: the new membrane material. *Applied Materials Today,* 1**,** 1-12.

KAITTANIS, C., NATH, S. & PEREZ, J. M. 2008. Rapid nanoparticle-mediated monitoring of bacterial metabolic activity and assessment of antimicrobial susceptibility in blood with magnetic relaxation. *PLoS One,* 3**,** e3253.

KAMAL, T., KHAN, S. B. & ASIRI, A. M. 2016. Nickel nanoparticles-chitosan composite coated cellulose filter paper: an efficient and easily recoverable dip-catalyst for pollutants degradation. *Environmental Pollution,* 218**,** 625-633.

KANCHI, S., KUMAR, G., LO, A.-Y., TSENG, C.-M., CHEN, S.-K., LIN, C.-Y. & CHIN, T.-S. 2018. Exploitation of de-oiled jatropha waste for gold nanoparticles synthesis: a green approach. *Arabian Journal of Chemistry,* 11**,** 247-255.

KANG, S., PARK, J. B., LEE, T.-J., RYU, S., BHANG, S. H., LA, W.-G., NOH, M.-K., HONG, B. H. & KIM, B.-S. 2015. Covalent conjugation of mechanically stiff graphene oxide flakes to three-dimensional collagen scaffolds for osteogenic differentiation of human mesenchymal stem cells. *Carbon,* 83**,** 162-172.

KASHID, S. B., RAUT, R. W. & MALGHE, Y. S. 2016. Microwave assisted synthesis of nickel nanostructures by hydrazine reduction route: Effect of solvent and capping agent on morphology and magnetic properties. *Materials Chemistry and Physics,* 170**,** 24-31.

KAVITHA, E., SUNDARAGANESAN, N. & SEBASTIAN, S. 2010. Molecular structure, vibrational spectroscopic and HOMO, LUMO studies of 4-nitroaniline by density functional method. *Indian Journal of Pure and Applied Physics*, 20-30.

KIM, T.-H., SHAH, S., YANG, L., YIN, P. T., HOSSAIN, M. K., CONLEY, B., CHOI, J.-W. & LEE, K.-B. 2015. Controlling differentiation of adipose-derived stem cells using combinatorial graphene hybrid-pattern arrays. *ACS Nano,* 9**,** 3780-3790.

KIRKPATRICK, S., GELATT, C. D. & VECCHI, M. P. 1983. Optimization by simulated annealing. *Science,* 220**,** 671-680.

KOHN, W. & SHAM, L. J. 1965. Self-consistent equations including exchange and correlation effects. *Physical Review,* 140**,** A1133.

KONDRATYUK, N. D. & PISAREV, V. V. 2019. Calculation of viscosities of branched alkanes from 0.1 to 1000 MPa by molecular dynamics methods using COMPASS force field. *Fluid Phase Equilibria,* 498**,** 151-159.

KONG, F.-Y., ZHANG, J.-W., LI, R.-F., WANG, Z.-X., WANG, W.-J. & WANG, W. 2017. Unique roles of gold nanoparticles in drug delivery, targeting and imaging applications. *Molecules,* 22**,** 1445.

References

KRISHNA, R., CAMPIÑA, J. M., FERNANDES, P. M., VENTURA, J., TITUS, E. & SILVA, A. F. 2016. Reduced graphene oxide-nickel nanoparticles/biopolymer composite films for the sub-millimolar detection of glucose. *Analyst,* 141**,** 4151-4161.

KROGER, M., MEISTER, K. & KAVA, R. 2006. Low-calorie sweeteners and other sugar substitutes: a review of the safety issues. *Comprehensive Reviews in Food Science and Food Safety,* 5**,** 35-47.

KUILA, T., BOSE, S., MISHRA, A. K., KHANRA, P., KIM, N. H. & LEE, J. H. 2012. Chemical functionalization of graphene and its applications. *Progress in Materials Science,* 57**,** 1061-1105.

KUMAR, H. AND NEELAM, R., 2016. Enzyme-based electrochemical biosensors for food safety: A review. Nanobiosensors in Disease Diagnosis, 5, pp.29-39.

LABORDA, F., JIMÉNEZ-LAMANA, J., BOLEA, E. & CASTILLO, J. R. 2013. Critical considerations for the determination of nanoparticle number concentrations, size and number size distributions by single particle ICP-MS. *Journal of Analytical Atomic Spectrometry,* 28**,** 1220-1232.

LATA, S., BATRA, B., KUMAR, P. & PUNDIR, C. 2013. Construction of an amperometric d-amino acid biosensor based on d-amino acid oxidase/carboxylated mutliwalled carbon nanotube/copper nanoparticles/polyalinine modified gold electrode. *Analytical Biochemistry,* 437**,** 1-9.

LEE, C., WEI, X., KYSAR, J. W. & HONE, J. 2008. Measurement of the elastic properties and intrinsic strength of monolayer graphene. *Science,* 321**,** 385-388.

LEE, C.-A. & TSAI, Y.-C. 2009. Preparation of multiwalled carbon nanotube-chitosan-alcohol dehydrogenase nanobiocomposite for amperometric detection of ethanol. *Sensors and Actuators B: Chemical,* 138**,** 518-523.

LEE, J., CHATTERJEE, D. K., LEE, M. H. & KRISHNAN, S. 2014. Gold nanoparticles in breast cancer treatment: promise and potential pitfalls. *Cancer Letters,* 347**,** 46-53.

LEKSRISOMPONG, P., GERARD, P., LOPETCHARAT, K. & DRAKE, M. 2012. Bitter taste inhibiting agents for whey protein hydrolysate and whey protein hydrolysate beverages. *Journal of Food Science,* 77**,** S282-S287.

LI, Z., YOUNG, R.J., WANG, R., YANG, F., HAO, L., JIAO, W. AND LIU, W., 2013. The role of functional groups on graphene oxide in epoxy nanocomposites. Polymer, 54(21), pp.5821-5829.

LIANG, B., LI, L., TANG, X., LANG, Q., WANG, H., LI, F., SHI, J., SHEN, W., PALCHETTI, I. & MASCINI, M. 2013. Microbial surface display of glucose dehydrogenase for amperometric glucose biosensor. *Biosensors and Bioelectronics,* 45**,** 19-24.

LIN, M., SONG, P., ZHOU, G., ZUO, X., ALDALBAHI, A., LOU, X., SHI, J. & FAN, C. 2016. Electrochemical detection of nucleic acids, proteins, small molecules and cells using a DNA-nanostructure-based universal biosensing platform. *Nature Protocols,* 11**,** 1244-1263.

LIU, X., SUI, Y., MENG, C. & HAN, Y. 2014. Tuning the reactivity of Ru nanoparticles by defect engineering of the reduced graphene oxide support. *RSC Advances,* 4**,** 22230-22240.

MAHMOUD, K. A., HRAPOVIC, S. & LUONG, J. H. 2008. Picomolar detection of protease using peptide/single walled carbon nanotube/gold nanoparticle-modified electrode. *ACS Nano,* 2**,** 1051-1057.

MALARKODI, C., RAJESHKUMAR, S., VANAJA, M., PAULKUMAR, K., GNANAJOBITHA, G. & ANNADURAI, G. 2013. Eco-friendly synthesis and characterization of gold

nanoparticles using Klebsiella pneumoniae. *Journal of Nanostructure in Chemistry,* 3**,** 30.

MANZETTI, S., MCCULLOCH, D. R., HERINGTON, A. C. & VAN DER SPOEL, D. 2003. Modeling of enzyme–substrate complexes for the metalloproteases MMP-3, ADAM-9 and ADAM-10. *Journal of Computer-aided Molecular Design,* 17**,** 551-565.

MERNISSI CHERIGUI, E. A., SENTOSUN, K., BOUCKENOOGE, P., VANROMPAY, H., BALS, S., TERRYN, H. & USTARROZ, J. 2017. Comprehensive study of the electrodeposition of nickel nanostructures from deep eutectic solvents: self-limiting growth by electrolysis of residual water. *The Journal of Physical Chemistry C,* 121**,** 9337-9347.

MESSAUD, F.A., SANDERSON, R.D., RUNYON, J.R., OTTE, T., PASCH, H. AND WILLIAMS, S.K.R., 2009. An overview on field-flow fractionation techniques and their applications in the separation and characterization of polymers. Progress in Polymer Science, 34(4), pp.351-368.

MEYER, J. C., GEIM, A. K., KATSNELSON, M. I., NOVOSELOV, K. S., BOOTH, T. J. & ROTH, S. 2007. The structure of suspended graphene sheets. *Nature,* 446**,** 60-63.

MOON, J. B. & HOWE, W. J. 1991. Computer design of bioactive molecules: A method for receptor-based de novo ligand design. *Proteins: Structure, Function, and Bioinformatics,* 11**,** 314-328.

MORRIS, G. M., HUEY, R., LINDSTROM, W., SANNER, M. F., BELEW, R. K., GOODSELL, D. S. & OLSON, A. J. 2009. AutoDock4 and AutoDockTools4: Automated docking with selective receptor flexibility. *Journal of Computational Chemistry,* 30**,** 2785-2791.

MUBARAKALI, D., THAJUDDIN, N., JEGANATHAN, K. & GUNASEKARAN, M. 2011. Plant extract mediated synthesis of silver and gold nanoparticles and its antibacterial activity against clinically isolated pathogens. *Colloids and Surfaces B: Biointerfaces,* 85**,** 360-365.

MUÑETON ARBOLEDA, D., SANTILLÁN, J. M., MENDOZA HERRERA, L. J., VAN RAAP, M. B. F. N., MENDOZA ZELIS, P., MURACA, D., SCHINCA, D. C. & SCAFFARDI, L. B. 2015. Synthesis of Ni nanoparticles by femtosecond laser ablation in liquids: structure and sizing. *The Journal of Physical Chemistry C,* 119**,** 13184-13193.

MURALIKRISHNA, T., PATTANAYAK, M. AND NAYAK, P.L., 2014. Green synthesis of gold nanoparticles using (aloe vera) aqueous extract. World Journal of Nano Science & Technology, 3(2), pp.45-51.

MUSAMEH, M. M., GAO, Y., HICKEY, M. & KYRATZIS, I. L. 2012. Application of carbon nanotubes in the extraction and electrochemical detection of organophosphate pesticides: a review. *Analytical Letters,* 45**,** 783-803.

NISHIBATA, Y. & ITAI, A. 1993. Confirmation of usefulness of a structure construction program based on three-dimensional receptor structure for rational lead generation. *Journal of Medicinal Chemistry,* 36**,** 2921-2928.

NOUNEH, K., OYAMA, M., DIAZ, R., ABD-LEFDIL, M., KITYK, I. & BOUSMINA, M. 2011. Nanoscale synthesis and optical features of metallic nickel nanoparticles by wet chemical approaches. *Journal of Alloys and Compounds,* 509**,** 5882-5886.

NOVOSELOV, K. S., GEIM, A. K., MOROZOV, S. V., JIANG, D., KATSNELSON, M. I., GRIGORIEVA, I., DUBONOS, S., FIRSOV & AA 2005. Two-dimensional gas of massless Dirac fermions in graphene. *Nature,* 438**,** 197-200.

NOVOSELOV, K. S., GEIM, A. K., MOROZOV, S. V., JIANG, D., ZHANG, Y., DUBONOS, S. V., GRIGORIEVA, I. V. & FIRSOV, A. A. 2004. Electric field effect in atomically thin carbon films. *Science,* 306**,** 666-669.

References

NOVOSELOV, K. S., JIANG, D., SCHEDIN, F., BOOTH, T., KHOTKEVICH, V., MOROZOV, S. & GEIM, A. K. 2005. Two-dimensional atomic crystals. *Proceedings of the National Academy of Sciences,* 102**,** 10451-10453.

OLIVEIRA, J. P., PRADO, A. R., KEIJOK, W. J., ANTUNES, P. W. P., YAPUCHURA, E. R. & GUIMARÃES, M. C. C. 2019. Impact of conjugation strategies for targeting of antibodies in gold nanoparticles for ultrasensitive detection of 17β-estradiol. *Scientific Reports,* 9**,** 1-8.

OLLIS, D. L., CHEAH, E., CYGLER, M., DIJKSTRA, B., FROLOW, F., FRANKEN, S. M., HAREL, M., REMINGTON, S. J., SILMAN, I. & SCHRAG, J. 1992. The α/β hydrolase fold. *Protein Engineering, Design and Selection,* 5**,** 197-211.

ORBITALS, I. F. F. 1976. Organic Chemical Reactions John Wiley and Sons. *New York*.

PAGADALA, N. S., SYED, K. & TUSZYNSKI, J. 2017. Software for molecular docking: a review. *Biophysical Reviews,* 9**,** 91-102.

PANÁČEK, A., KOLÁŘ, M., VEČEŘOVÁ, R., PRUCEK, R., SOUKUPOVA, J., KRYŠTOF, V., HAMAL, P., ZBOŘIL, R. & KVÍTEK, L. 2009. Antifungal activity of silver nanoparticles against Candida spp. *Biomaterials,* 30**,** 6333-6340.

PARK, J., KIM, B., HAN, J., OH, J., PARK, S., RYU, S., JUNG, S., SHIN, J.-Y., LEE, B. S. & HONG, B. H. 2015. Graphene oxide flakes as a cellular adhesive: prevention of reactive oxygen species mediated death of implanted cells for cardiac repair. *ACS Nano,* 9**,** 4987-4999.

PARK, S., CHIBLI, H., WONG, J. & NADEAU, J. L. 2011. Antimicrobial activity and cellular toxicity of nanoparticle–polymyxin B conjugates. *Nanotechnology,* 22**,** 185101.

PARTHASARATHY, V. AND TV, A.K., 2019. Screening of potential GCMS derived antimigraine compound from the leaves of Abrus precatorius Linn to target "calcitonin gene related peptide" receptor using in silico analysis. Food Science and Human Wellness, 8(1), pp.34-39.

PATEL, N., MEIER, S., CAMMANN, K. & CHEMNITIUS, G.-C. 2001. Screen-printed biosensors using different alcohol oxidases. *Sensors and Actuators B: Chemical,* 75**,** 101-110.

PAVLIDIS, I. V., VORHABEN, T., TSOUFIS, T., RUDOLF, P., BORNSCHEUER, U. T., GOURNIS, D. & STAMATIS, H. 2012. Development of effective nanobiocatalytic systems through the immobilization of hydrolases on functionalized carbon-based nanomaterials. *Bioresource Technology,* 115**,** 164-171.

PAVIA, D.L., LAMPMAN, G.M., KRIZ, G.S. AND VYVYAN, J.A., 2008. Introduction to spectroscopy. Cengage Learning.

PEPINO, M. Y. 2015. Metabolic effects of non-nutritive sweeteners. *Physiology & Behavior,* 152**,** 450-455.

PERDEW, J. P., PARR, R. G., LEVY, M. & BALDUZ JR, J. L. 1982. Density-functional theory for fractional particle number: derivative discontinuities of the energy. *Physical Review Letters,* 49**,** 1691.

POPOV, V. N. 2004. Curvature effects on the structural, electronic, and optical properties of isolated single-walled carbon nanotubes within a symmetry-adapted non-orthogonal tight-binding model. *New Journal of Physics,* 6**,** 17.

PUROHIT, V. & MISHRA, S. 2018. The truth about artificial sweeteners–are they good for diabetics? : Elsevier.

PYRZ, W. D. & BUTTREY, D. J. 2008. Particle size determination using TEM: a discussion of image acquisition and analysis for the novice microscopist. *Langmuir,* 24**,** 11350-11360.

References

RAHMAN, M., AHAMMAD, A.J., JIN, J.H., AHN, S.J. AND LEE, J.J., 2010. A comprehensive review of glucose biosensors based on nanostructured metal-oxides. Sensors, 10(5), pp.4855-4886.

RAJ, C. R. & BEHERA, S. 2005. Mediatorless voltammetric oxidation of NADH and sensing of ethanol. *Biosensors and Bioelectronics,* 21**,** 949-956.

RANGELOVA, V., TSANKOVA, D. & DIMCHEVA, N. 2010. Soft computing techniques in modelling the influence of pH. and temperature on dopamine biosensor. *Intelligent and Biosensors,* 99.

RAPAPORT, D.C., 2004. The art of molecular dynamics simulation. Cambridge university press.

RAWAL, R., CHAUHAN, N., TOMAR, M. & GUPTA, V. 2017. A contrivance based on electrochemical integration of graphene oxide nanoparticles/nickel nanoparticles for bilirubin biosensing. *Biochemical Engineering Journal,* 125**,** 238-245.

RAY, S., MOHAN, R., SINGH, J. K., SAMANTARAY, M. K., SHAIKH, M. M., PANDA, D. & GHOSH, P. 2007. Anticancer and antimicrobial metallopharmaceutical agents based on palladium, gold, and silver N-heterocyclic carbene complexes. *Journal of the American Chemical Society,* 129**,** 15042-15053.

RAZUMIEN, J., GUREVIČIEN, V., LAURINAVIČIUS, V. & GRAŽULEVIČIUS, J. 2001. Amperometric detection of glucose and ethanol in beverages using flow cell and immobilised on screen-printed carbon electrode PQQ-dependent glucose or alcohol dehydrogenases. *Sensors and Actuators B: Chemical,* 78**,** 243-248.

REYES, O.J., PATEL, S.J. AND MANNAN, M.S., 2011. Quantitative structure property relationship studies for predicting dust explosibility characteristics (K st, P max) of organic chemical dusts. Industrial & engineering chemistry research, 50(4), pp.2373-2379.

RIVAS, G.A., RUBIANES, M.D., RODRIGUEZ, M.C., FERREYRA, N.F., LUQUE, G.L., PEDANO, M.L., MISCORIA, S.A. AND PARRADO, C., 2007. Carbon nanotubes for electrochemical biosensing. Talanta, 74(3), pp.291-307.

ROCCHITTA, G., SPANU, A., BABUDIERI, S., LATTE, G., MADEDDU, G., GALLERI, G., NUVOLI, S., BAGELLA, P., DEMARTIS, M. I. & FIORE, V. 2016. Enzyme biosensors for biomedical applications: Strategies for safeguarding analytical performances in biological fluids. *Sensors,* 16**,** 780.

ROTSTEIN, S. H. & MURCKO, M. A. 1993. GenStar: a method for de novo drug design. *Journal of Computer-aided Molecular Design,* 7**,** 23-43.

SAGUI, C. & DARDEN, T. A. 1999. Molecular dynamics simulations of biomolecules: long-range electrostatic effects. *Annual Review of Biophysics and Biomolecular Structure,* 28**,** 155-179.

SATOH, T. & HOSOKAWA, M. 1998. The mammalian carboxylesterases: from molecules to functions. *Annual Review of Pharmacology and Toxicology,* 38**,** 257-288.

SCHELLER, F. AND SCHUBERT, F., 1991. Biosensors. Elsevier.

SCHERNHAMMER, E. S., BERTRAND, K. A., BIRMANN, B. M., SAMPSON, L., WILLETT, W. C. & FESKANICH, D. 2012. Consumption of artificial sweetener–and sugar-containing soda and risk of lymphoma and leukemia in men and women. *The American Journal of Clinical Nutrition,* 96**,** 1419-1428.

SECCHI, O., ZINELLU, M., SPISSU, Y., PIRISINU, M., BAZZU, G., MIGHELI, R., DESOLE, M. S., O'NEILL, R. D., SERRA, P. A. & ROCCHITTA, G. 2013. Further in-vitro characterization of an implantable biosensor for ethanol monitoring in the brain. *Sensors,* 13**,** 9522-9535.

References

SHAH, S., YIN, P. T., UEHARA, T. M., CHUENG, S. T. D., YANG, L. & LEE, K. B. 2014. Guiding stem cell differentiation into oligodendrocytes using graphene-nanofiber hybrid scaffolds. *Advanced Materials,* 26**,** 3673-3680.

SHANKAR, S. S., RAI, A., AHMAD, A. & SASTRY, M. 2004. Rapid synthesis of Au, Ag, and bimetallic Au core–Ag shell nanoparticles using Neem (Azadirachta indica) leaf broth. *Journal of Colloid and Interface Science,* 275**,** 496-502.

SHAREL, P., LIU, D., LAZENBY, R. A., SLOAN, J., VIDOTTI, M., UNWIN, P. R. & MACPHERSON, J. V. 2016. Electrodeposition of nickel hydroxide nanoparticles on carbon nanotube electrodes: correlation of particle crystallography with electrocatalytic properties. *J. Phys. Chem. C,* 120**,** 16059-16068.

SHKOTOVA, L. V., SOLDATKIN, A. P., GONCHAR, M. V., SCHUHMANN, W. & DZYADEVYCH, S. V. 2006. Amperometric biosensor for ethanol detection based on alcohol oxidase immobilised within electrochemically deposited Resydrol film. *Materials Science and Engineering: C,* 26**,** 411-414.

SINGH, V., JOUNG, D., ZHAI, L., DAS, S., KHONDAKER, S. I. & SEAL, S. 2011. Graphene based materials: past, present, and future. *Progress in Materials Science,* 56**,** 1178-1271.

SUN, H. 1998. COMPASS: an ab initio force-field optimized for condensed-phase applications overview with details on alkane and benzene compounds. *The Journal of Physical Chemistry B,* 102**,** 7338-7364.

SVENSSON, K., BÜLOW, L., KRIZ, D. & KROOK, M. 2005. Investigation and evaluation of a method for determination of ethanol with the SIRE® Biosensor P100, using alcohol dehydrogenase as recognition element. *Biosensors and Bioelectronics,* 21**,** 705-711.

SWITHERS, S. E. 2013. Artificial sweeteners produce the counterintuitive effect of inducing metabolic derangements. *Trends in Endocrinology & Metabolism,* 24**,** 431-441.

TAKEDA-SHITAKA, M., TERASHI, G., TAKAYA, D., KANOU, K., IWADATE, M. AND UMEYAMA, H., 2005. Protein structure prediction in CASP6 using CHIMERA and FAMS. PROTEINS: Structure, Function, and Bioinformatics, 61(S7), pp.122-127.

TAMBURRI, E., ANGJELLARI, M., TOMELLINI, M., GAY, S., REINA, G., LAVECCHIA, T., BARBINI, P., PASQUALI, M. & ORLANDUCCI, S. 2015. Electrochemical growth of nickel nanoparticles on carbon nanotubes fibers: Kinetic modeling and implications for an easy to handle platform for gas sensing device. *Electrochimica Acta,* 157**,** 115-124.

THOMAS, L. The effect of the orbital velocity of the electrons in heavy atoms on their stopping of α-particles. Mathematical Proceedings of the Cambridge Philosophical Society, 1927. Cambridge University Press, 713-716.

THOMAS, L. T. & UMEDA, K. 1957. Atomic scattering factors calculated from the TFD atomic model. *The Journal of Chemical Physics,* 26**,** 293-303.

THOMAS, O. E. & ADEGOKE, O. A. 2015. Toxicity of food colours and additives: A review. *African Journal of Pharmacy and Pharmacology,* 9**,** 900-914.

TIWARI, J. N., VIJ, V., KEMP, K. C. & KIM, K. S. 2016. Engineered carbon-nanomaterial-based electrochemical sensors for biomolecules. *ACS Nano,* 10**,** 46-80.

TURNER, A., KARUBE, I. AND WILSON, G.S., 1987. Biosensors: fundamentals and applications. Oxford university press.

TURNER, A.P., 2013. Biosensors: sense and sensibility. Chemical Society Reviews, 42(8), pp.3184-3196.

TRIVEDI, U., LAKSHMINARAYANA, D., KOTHARI, I., PATEL, P. & PANCHAL, C. 2009. Amperometric fructose biosensor based on fructose dehydrogenase enzyme. *Sensors and Actuators B: Chemical,* 136**,** 45-51.

References

ULICNY, J. & KOZAR, T. Roadmap for Computer-Aided Modeling of Theranostics and Related Nanosystems. EPJ Web of Conferences, 2018. EDP Sciences, 05017.

ÜNVEREN, E. E., MONKUL, B. Ö., SARıOĞLAN, Ş., KARADEMIR, N. & ALPER, E. 2017. Solid amine sorbents for CO2 capture by chemical adsorption: A review. *Petroleum,* 3**,** 37-50.

URCEZINO, A. S., DOS SANTOS, L. P., CASCIANO, P. N., CORREIA, A. N. & LIMA-NETO, P. D. 2017. Electrodeposition study of Ni coatings on copper from choline chloride-based deep eutectic solvents. *Journal of the Brazilian Chemical Society,* 28**,** 1193-1203.

VANOMMESLAEGHE, K., HATCHER, E., ACHARYA, C., KUNDU, S., ZHONG, S., SHIM, J., DARIAN, E., GUVENCH, O., LOPES, P. & VOROBYOV, I. 2010. CHARMM general force field: A force field for drug-like molecules compatible with the CHARMM all-atom additive biological force fields. *Journal of Computational Chemistry,* 31**,** 671-690.

VELLAICHAMY, B., PERIAKARUPPAN, P., ARUMUGAM, R., SELLAMUTHU, K. & NAGULAN, B. 2018. A novel photocatalytically active mesoporous metal-free PPy grafted MWCNT nanocomposite. *Journal of Colloid and Interface Science,* 514**,** 376-385.

VIJAYAKUMAR, A., CSÖREGI, E., HELLER, A. & GORTON, L. 1996. Alcohol biosensors based on coupled oxidase-peroxidase systems. *Analytica Chimica Acta,* 327**,** 223-234.

VO-DINH, T. & CULLUM, B. 2000. Biosensors and biochips: advances in biological and medical diagnostics. *Fresenius' Journal of Analytical Chemistry,* 366**,** 540-551.

VO-DINH, T., CULLUM, B. M. & STOKES, D. L. 2001. Nanosensors and biochips: frontiers in biomolecular diagnostics. *Sensors and Actuators B: Chemical,* 74**,** 2-11.

VON BARTH, U. & HEDIN, L. 1972. A local exchange-correlation potential for the spin polarized case. i. *Journal of Physics C: Solid State Physics,* 5**,** 1629.

WANG, J. AND LIN, Y. J. T. T. I. A. C. 2008. Functionalized carbon nanotubes and nanofibers for biosensing applications. 27 (7): 619-626.

WANG, Z., SUN, H., YAO, X., LI, D., XU, L., LI, Y., TIAN, S. AND HOU, T., 2016. Comprehensive evaluation of ten docking programs on a diverse set of protein–ligand complexes: the prediction accuracy of sampling power and scoring power. Physical Chemistry Chemical Physics, 18(18), pp.12964-12975.

WHEELOCK, C. E., SEVERSON, T. F. & HAMMOCK, B. D. 2001. Synthesis of new carboxylesterase inhibitors and evaluation of potency and water solubility. *Chemical Research in Toxicology,* 14**,** 1563-1572.

WILSON, M. S. 2005. Electrochemical immunosensors for the simultaneous detection of two tumor markers. *Analytical Chemistry,* 77**,** 1496-1502.

Wilson, G.S. and Hu, Y., 2000. Enzyme-based biosensors for in vivo measurements. Chemical Reviews, 100(7), pp.2693-2704.

WU, Z. G., MUNOZ, M. & MONTERO, O. 2010. The synthesis of nickel nanoparticles by hydrazine reduction. *Advanced Powder Technology,* 21**,** 165-168.

Wujcik, E.K. and Monty, C.N., 2013. Nanotechnology for implantable sensors: carbon nanotubes and graphene in medicine. Wiley Interdisciplinary Reviews: Nanomedicine and Nanobiotechnology, 5(3), pp.233-249.

XU, C., YUAN, R.-S. AND WANG, X. J. N. C. M. 2014. Selective reduction of graphene oxide. Macromolecules, 29 (1): 61-66.

XU, F. 1997. Effects of redox potential and hydroxide inhibition on the pH activity profile of fungal laccases. *Journal of Biological Chemistry,* 272**,** 924-928.

YADAV, J. 2018. Synthesis and Characterization of Gold Nanoparticles. *International Journal on Future Revolution in Computer Science & Communication Engineering,* 4**,** 220-230.

References

YAN, F., CHEN, J., JIN, Q., ZHOU, H., SAILJOI, A., LIU, J. AND TANG, W., 2020. Fast one-step fabrication of a vertically-ordered mesoporous silica-nanochannel film on graphene for direct and sensitive detection of doxorubicin in human whole blood. Journal of Materials Chemistry C, 8(21), pp.7113-7119.

YAN, J.A. AND CHOU, M.Y., 2010. Oxidation functional groups on graphene: Structural and electronic properties. Physical review B, 82(12), p.125403.

YANG, D.-J. & CHEN, B. 2009. Simultaneous determination of nonnutritive sweeteners in foods by HPLC/ESI-MS. *Journal of Agricultural and Food Chemistry,* 57**,** 3022-3027.

YANG, J., KIM, S.-E., CHO, M., YOO, I.-K., CHOE, W.-S. & LEE, Y. 2014. Highly sensitive and selective determination of bisphenol-A using peptide-modified gold electrode. *Biosensors and Bioelectronics,* 61**,** 38-44.

YANG, L., FAN, S., DENG, G., LI, Y., RAN, X., ZHAO, H. & LI, C.-P. 2015. Bridged β-cyclodextrin-functionalized MWCNT with higher supramolecular recognition capability: The simultaneous electrochemical determination of three phenols. *Biosensors and Bioelectronics,* 68**,** 617-625.

YILDIZ, H. B. & TOPPARE, L. 2006. Biosensing approach for alcohol determination using immobilized alcohol oxidase. *Biosensors and Bioelectronics,* 21**,** 2306-2310.

YUAN, H., QI, F., ZHAO, N., WAN, P., ZHANG, B., XIONG, H., LIAO, B. AND OUYANG, X., 2020. Graphene oxide decorated with titanium nanoparticles to reinforce the anti-corrosion performance of epoxy coating. Coatings, 10(2), p.129.

ZHANG, G., LI, J., ZHANG, G. & ZHAO, L. 2015. Room-temperature synthesis of Ni nanoparticles as the absorbent used for sewage treatment. *Advances in Materials Science and Engineering,* 2015.

ZHANG, M. & GORSKI, W. 2011. Amperometric Ethanol Biosensors Based on Chitosan-NAD+-Alcohol Dehydrogenase Films. *Electroanalysis,* 23**,** 1856-1862.

ZHANG, Y., TAN, Y.-W., STORMER, H. L. & KIM, P. 2005. Experimental observation of the quantum Hall effect and Berry's phase in graphene. *Nature,* 438**,** 201-204.

ZHAO, L., LI, Q., SU, Y., YUE, Q. & GAO, B. 2017. A novel Enteromorpha based hydrogel for copper and nickel nanoparticle preparation and their use in hydrogen production as catalysts. *International Journal of Hydrogen Energy,* 42**,** 6746-6756.

ZHAO, X., ZHANG, Q., CHEN, D. & LU, P. 2010. Enhanced mechanical properties of graphene-based poly (vinyl alcohol) composites. *Macromolecules,* 43**,** 2357-2363.

ZYGLER, A., WASIK, A. & NAMIEŚNIK, J. 2009. Analytical methodologies for determination of artificial sweeteners in foodstuffs. *TrAC Trends in Analytical Chemistry,* 28**,** 1082-1102.

APPENDICES

Appendix 1A: Voltammograms displaying the stability of the MWCNTs/AuNPs/CaE modified electrode for the detection of NTM.

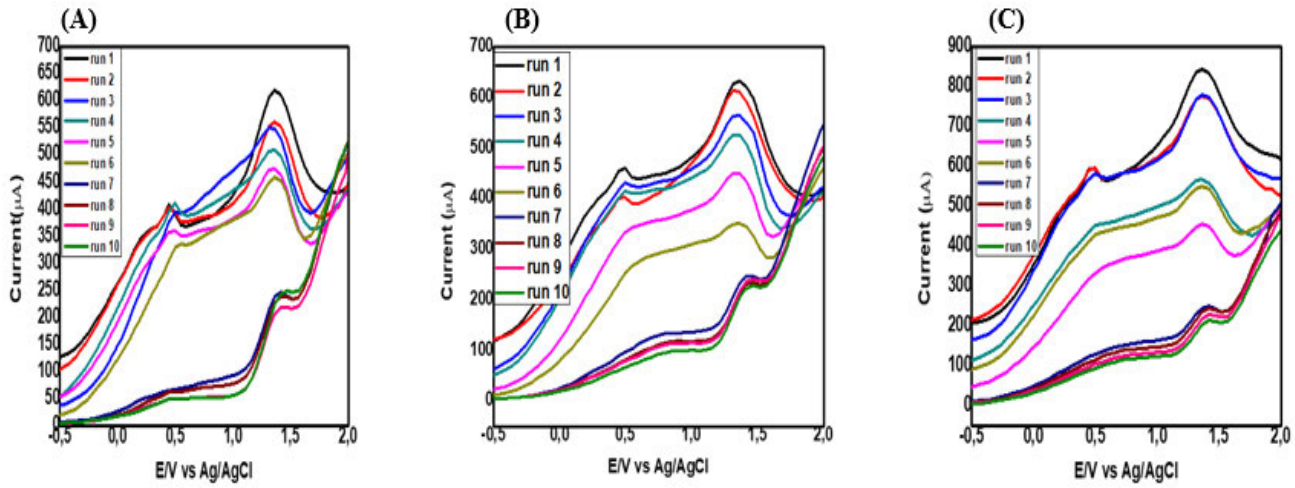

Figure 1A: Voltammograms displaying the response on (A) 1.87 ppm of NTM in apple juice sample; (B) 2.61 ppm of NTM in apple juice sample; (C) 2.98 ppm of NTM in apple juice sample.

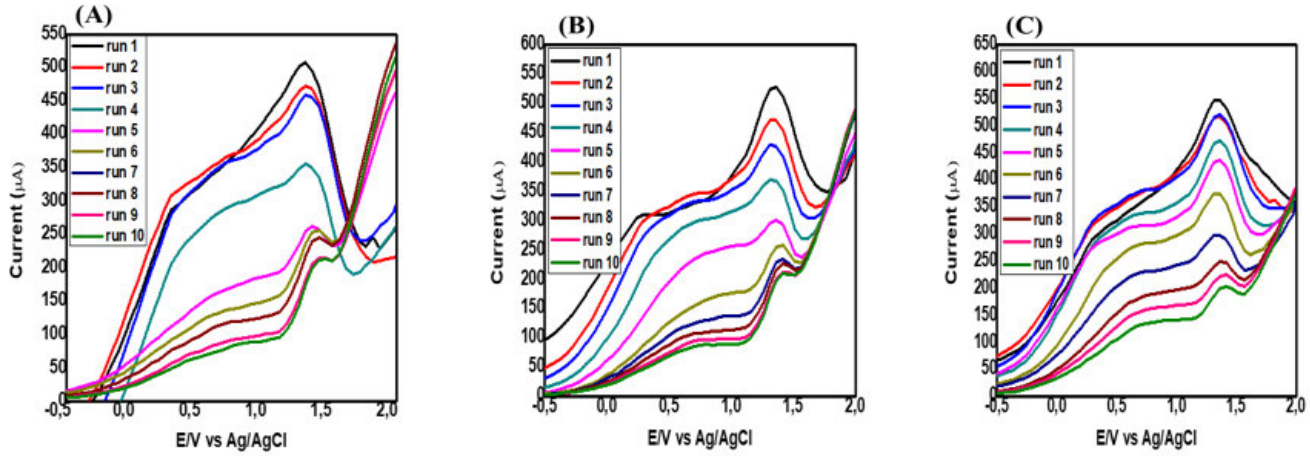

Figure 1B: Voltammograms displaying the response on (A) 1.12 ppm of NTM in Fanta orange sample; (B) 1.87 ppm of NTM in Fanta orange sample; (C) 2.61 ppm of NTM in Fanta orange sample

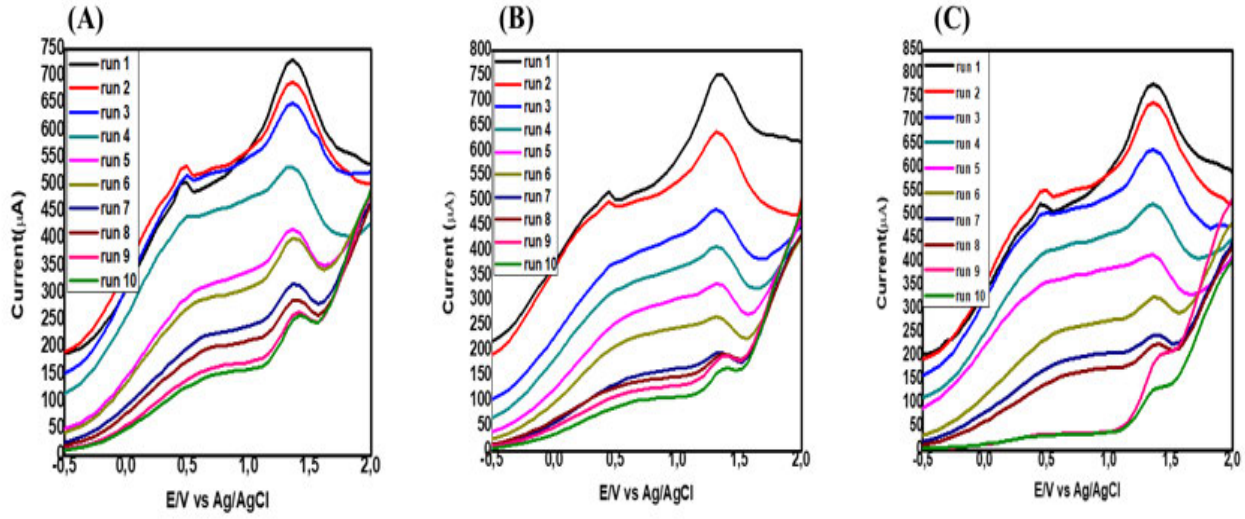

Figure 1C: Voltammograms displaying the response on (A) 1.87 ppm of NTM in red grape juice sample; (B) 2.61 ppm of NTM in red grape juice sample; (C) 2.98 ppm of NTM in red grape juice sample

Appendix 1B: Voltammograms displaying the stability of the GO/NiNPs/AOx modified electrode for the detection of NTM.

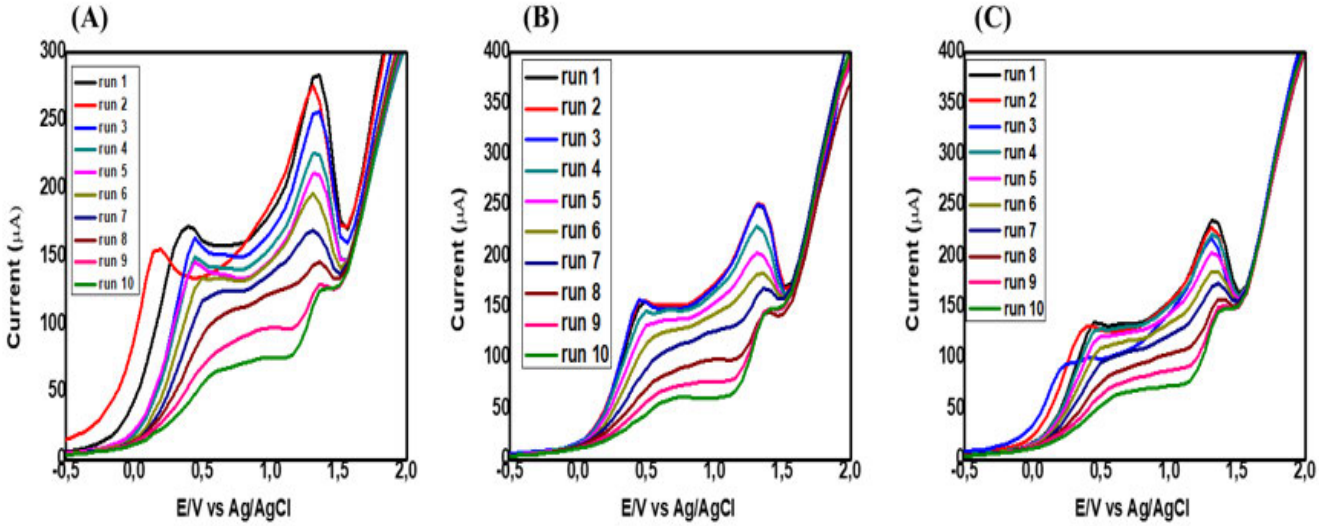

Figure 2A: Voltammograms displaying the response on (A) 1.87 ppm of NTM in apple juice sample; (B) 2.61 ppm of NTM in apple juice sample; (C) 2.98 ppm of NTM in apple juice sample.

Appendix

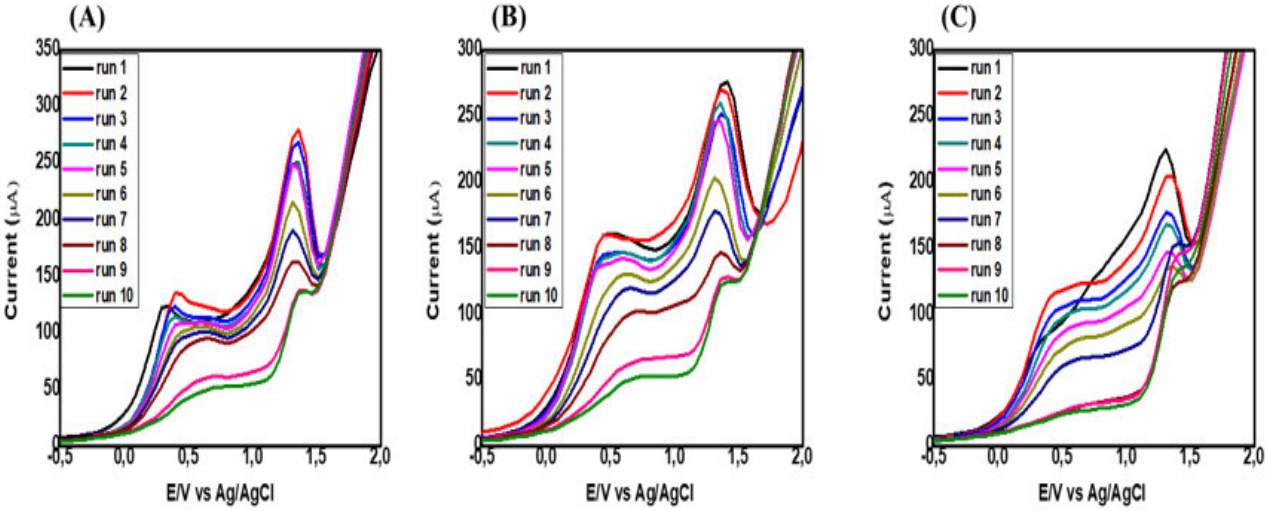

Figure 2B: Voltammograms displaying responses on (A) 1.12 ppm of NTM in Fanta orange sample; (B) 1.87 ppm of NTM in Fanta orange sample; (C) 2.61 ppm of NTM in Fanta orange sample.

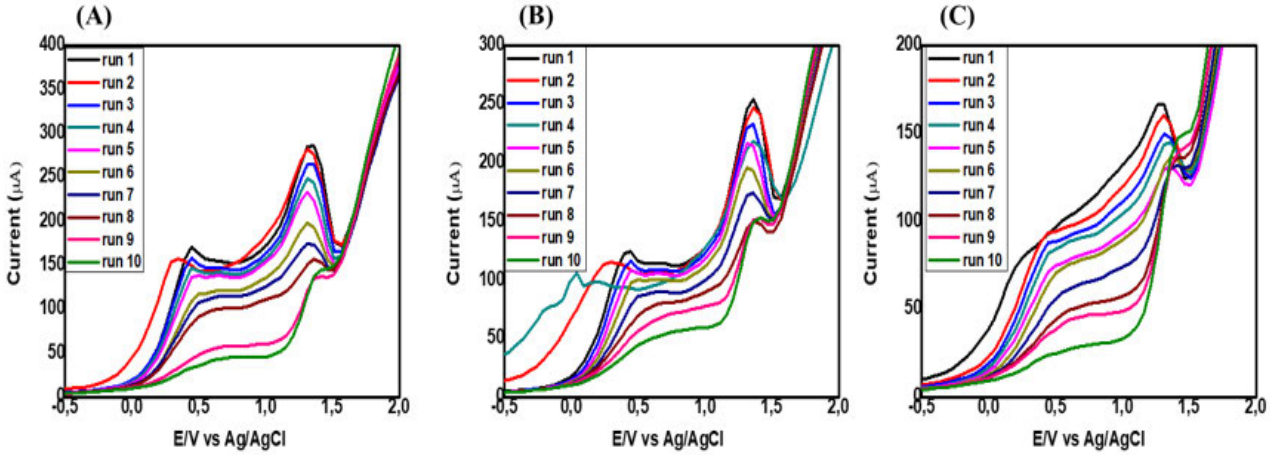

Figure 2C: Voltammograms displaying a response on (A) 1.87 ppm of NTM in red grape juice sample; (B) 2.61 ppm of NTM in red grape juice sample; (C) 2.98 ppm of NTM in red grape juice sample.

Appendix 2A: Table: Substrate-absorbate systems.

System	Substrate	Adsorbate
Layer I	MWCNTs	AuNPs
Layer II	CaE	NTM
Layer III	MWCNTs/AuNPs	NTM/CaE

Appendix 2B: Table: Substrate-absorbate systems.

System	Substrate	Adsorbate
Layer I	GO	NiNPs
Layer II	GO/NiNPs	AOx
Layer III	GO/NiNPs/AOx	NTM

Appendix 3: Effect of interferents on the detection of NTM

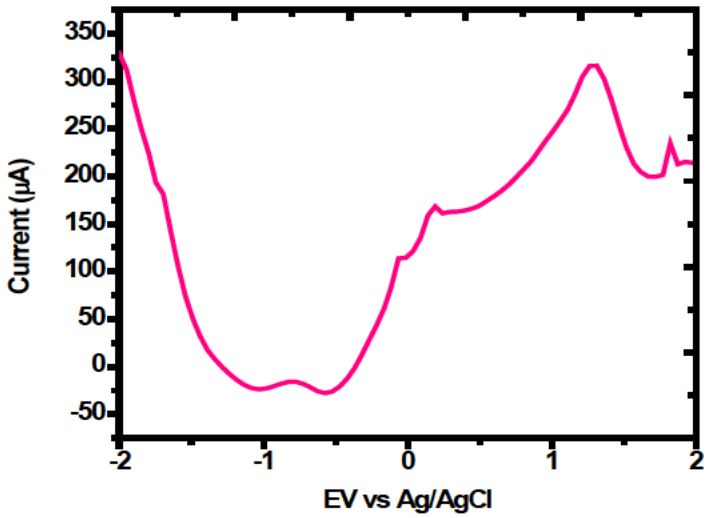

Figure 3A: A voltammogram displaying the effect of interferents on the CaE/AuNPs/ MWCNTs modified GCE.

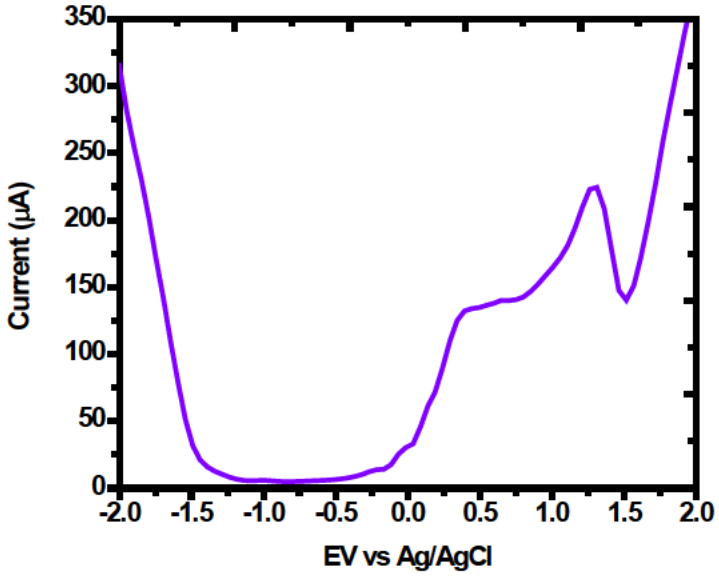

Figure 3B: A voltammogram displaying the effect of interferents on the AOx/NiNPs/ GO modified GCE.